Investigations into novel metal-incorporated THPP photosensitisers for Photodynamic Therapy efficiency against HT-29 Colorectal Adenocarcinoma cells

Dissertation

by

Bongumusa Zami Ntshingila

(2300324)

Submitted in fulfilment of the requirements for the degree

Degree of Master of Science by research only

In

Molecular and Cell Biology

in the Faculty of Science, University of the Witwatersrand, Johannesburg, South Africa

Supervisor: Prof. M.J. Cronjé

21 October 2022

DECLARATION

I declare that this dissertation is my own, unaided work. It is being submitted for the Degree of Master of Science at the University of the Witwatersrand, Johannesburg. It has not been submitted before for any degree or examination at any other University.

_____

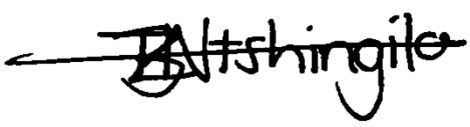

B.Z. Ntshingila

__21___day of __October__2022____at___Midrand___

ABSTRACT

Background: Colorectal cancer is one of the most lethal cancers globally, requiring urgent attention. Research is moving away from current conventional anti-cancer therapeutics with highly toxic side effects that diminish the long-term quality of life towards targeted therapies that only deal with the tumour. Photodynamic therapy has gained attraction as a minimally invasive and tumour-selective phototherapy that utilises a photosensitising agent, oxygen, and specific light irradiance to produce reactive oxygen species and induce tumour cytotoxicity. **Aim:** Our study aimed at investigating the coordination of Pd(II) and Cu(II) metals into the free base H_2THPP core for photosensitiser efficiency in PDT when targeting colorectal cancer cells. **Methods:** Pd(II)-THPP and Cu(II)-THPP were synthesised and characterised using UV-Vis and ^{1}H NMR spectroscopy. Successful coordination of these metals led to the treatment of cultured HT-29 colorectal adenocarcinoma with the photosensitisers to investigate dark and irradiation toxicity. The cells were then subjected to Pd(II)- and Cu(II)-THPP PDT to determine IC_{50} and IC_{80} concentrations. Cellular homeostatic conditions and potential stress were investigated using alamarBlue, Trypan Blue, ATP and LDH assays. ROS production, mode of cell death and cell cycle were assessed using flow cytometric analyses. **Results:** Pd(II)- and Cu(II)-THPP presented no toxicity in the dark nor irradiation toxicity. However, Cu(II)-THPP PDT had a stimulatory effect in HT-29 colorectal cancer and was discontinued, while Pd(II)-THPP IC_{50} and IC_{80} concentrations were determined to be 0.35 µM/mL and 0.9 µM/mL, respectively. Morphological and nuclear apoptotic and necrotic characteristics were observed microscopically and with the Hoechst-33258 stain. PDT produced ROS that disrupted the mitochondrial membrane, reducing cell viability and ATP production dose-dependently. Compromised membranes led to increased LDH release in the medium and phosphatidylserine presentation. Flow cytometric analysis showed induction of apoptosis and necrosis, and the formation of a sub-G1 indicating cell

cycle arrest confirmed cell stress. **Conclusion:** Cu(II)-THPP could not induce cytotoxicity in PDT treated colorectal carcinoma cells but can help gain future insight into the resistive mechanisms set in motion in cancer cells during PDT. On the other hand, Pd (II)-THPP is a potent inducer of cell death when combined with blue light irradiation and can be used in PDT as a substitute therapy to treat colorectal and other cancers.

DEDICATION

Ntombikayise Goodness Ntshingila and Benjamin Dumisani Ntshingila. Emva kukaNkulunkulu niyikho konke empilweni yami. Ngiyanithanda.

ACKNOWLEDGEMENTS

- Prof. Marianne J. Cronjé for the opportunity, her supervision, and her kind encouragement throughout the study. Thank you.
- The University of the Witwatersrand, School of Molecular and Cell Biology, for the opportunity and facilities to complete the degree.
- CSIR National Laser Centre for the provision and upkeep of the diode lasers and CSIR DST-Interbursary Support program for funding the study.
- University of Johannesburg Biochemistry and Chemistry departments. Mr Nwamadi Mutshinyalo and Jackie Mabasa for their assistance with the NMR spectroscopy analyses.
- Colleagues at the MJC lab and MCB school for the emotional and practical support over the years. I treasure all the friendships formed.
- Prof. Mandeep Kaur's lab for the use of their Floid® Imaging Station and Prof. Stephan Weiss for the Flow cytometer.
- God, my Lord and Saviour, for the grace to see this degree to completion.
- My family for being my unwavering pillars of strength and for the financial assistance. Ngiyanithanda boSphepho, Dlabane Mavundla.
- The Girls (Nibaningi) and Precious Mulaudzi for their support and valued friendship.

PREFACE

Ntshingila, B.Z. and Cronjé, M.J. Investigations into novel metal-incorporated THPP photosensitisers for photodynamic therapy efficiency against HT-29 colorectal adenocarcinoma. GradFlash Presentation. *Molecular Biosciences Research Trust Virtual Postgraduate Research Day.* University of the Witwatersrand. 9 December 2021

Ntshingila, B.Z. and Cronjé, M.J. Investigations into novel metal-incorporated THPP photosensitisers for photodynamic therapy efficiency against HT-29 colorectal adenocarcinoma. Oral Presentation. *School of Molecular and Cell Biology Seminar.* University of the Witwatersrand. 15 December 2021

Table of Contents

LIST OF FIGURES

Figure 4.3 A Light microscopy images of HT-29 colorectal adenocarcinoma cells following a) no irradiation, b) 2 J irradiation, c) 4 J irradiation, d) 6J irradiation, e) 8 J irradiation, and f) 10 J irradiation with a 405nm laser at 20X magnification. **B** Viability study of irradiation toxicity 24 hours post-exposure to 405nm blue light diode laser using alamarBlue® dye reduction assay. (n=6, SEM)

Figure 4.4 Sigmoidal polynomial curve plotted after treating HT-29 adenocarcinoma with 0.1 µM, 0.25 µM 0.5 µM 0.75 µM and 1 µM Pd(II)-THPP and 4 J/cm^2 irradiation fluency to obtain IC_{50} and IC_{80} values. (n=6, error bars ±SEM). Mitochondrial activity determined with alamarBlue® reduction dye assay.

Figure 4.5 Sigmoidal polynomial curve determining Cu(II)-THPP IC_{50} and IC_{80}. Mitochondrial activity was measured with alamarBlue® reduction dye assay after treating HT-29 cells with concentrations of Cu(II)-THPP and 4 J/cm^2 irradiation fluency. (n=6, error bars drawn from SEM)

Figure 4.6 Cell morphology images of PDT treated HT-29 adenocarcinoma cells taken with the Floid® Cell Imaging System and cell viability determined using the Trypan Blue dye exclusion assay. (n=3, Mean±SD)

Figure 4.7 Mitochondrial activity of PDT treated HT-29 colorectal adenocarcinoma determined by the alamarBlue® dye reduction assay and the determination of Pd(II)-THPP cytotoxicity using the CytoTox-ONE™ Homogenous Membrane Integrity Assay. (P<0,05* P<0,01** P<0,001 *** n=6, SEM)

Figure 4.8 Confirmation of ROS production in PDT treated cells using the flow cytometric Muse® Oxidative Stress Kit 3 hours post-treatment and ATP quantification using the luminescence CellTiter-Glo™ Cytotoxicity Assay. Caspase 3/7 expression was quantified using the luminescent Caspase-Glo® 3/7 assay. (P<0,05* P<0,001***, ROS activity n=3; histogram single representation, ATP, and Caspase 3/7 n=6. Error bars= SEM).

Figure 4.9 Microscopic visualisation of active mitochondria in PDT treated HT-29 adenocarcinoma labelled with Mitotracker Orange CMTMRos dye and detection

of cytochrome *c* release using anti-cytochrome *c* (ab154476) labelling. Mitotracker Orange-Filter 15 Ex 546/12 nm and Cytochrome *c*- Filter 09 Ex 470/40 nm were used at 400X magnification.

Figure 4.10 Determination of HT-29 colorectal adenocarcinoma cell stress and death stages using flow cytometric Annexin V & Dead cell assay staining 24h post-PDT treatment. (Dot plots are single representation; Percentages; n=3, mean±SEM)

Figure 4.11 Flow cytometric DNA cell cycle analysis of PI-stained HT-29 colorectal adenocarcinoma cells. Histograms are single representations. Pie chart: mean, n=3

Figure 4.12 Nuclear damage determination of Pd(II)-THPP PDT treatment on HT-29 adenocarcinoma using Hoechst-33258 blue fluorescence microscopy. Cell populations included non-treated control cells, 0.9 µM Pd(II)-THPP and 4 J/cm^2 irradiation only treated cells and low 0.35 µM Pd(II)-THPP and high 0.9 µM Pd(II)-THPP PDT cells. Photos were captured using the AxioPlan 2 Imaging light microscope and no. 1 Ex. 365/12 lens filter at 400X magnification

Figure 4.13 Photosensitiser uptake and localisation in HEK-293 cells. Cells were treated with 80 µM Pd(II)-THPP and incubated for 24 hours. Autofluorescence visualisation was done on the Axioplan 2 Imaging light microscope with AxioVision 4.7 software and number 15 (546/12 nm) filter at 400X magnification.

Figure 4.14 Cellular morphology of HEK-293 embryonic kidney cell line with no treatment (Control), treated with PEG2000-PE dissolved in 0.5X PBS (PEG-vehicle), 0.9 µM Pd(II)-THPP only, 4 J/cm^2 only, and PDT treated with low 0.35 µM Pd(II)-THPP and 0.9 µM Pd(II)-THPP doses. Images were taken 24 h post PDT with Floid® Cell Imaging System. Mitochondrial activity was determined using the alamarBlue® reduction dye assay. n=6, error bars are SEM, $p<0.001$***

Figure SR1 UV/Vis absorbance spectra of PEG2000-PE encapsulated H_2THPP, Pd(II)-THPP and Cu(II)-THPP complexes dissolved in 0.5X PBS. Absorbance was recorded on a Jasco V-630 Spectrophotometer.

Figure SR2 Proton NMR spectra of A H_2THPP, B Pd(II)-THPP and C Cu(II)-THPP. H_2THPP was dissolved in deuterated DMSO and run. Pd(II)-acetate and Cu(II)-acetate were reacted with H_2THPP in 99.8% ethanol. 30mg dry powder was dissolved in deuterated DMSO and analysed on a Bruker Ascend 500MHz spectrometer.

LIST OF TABLES

ABBREVIATIONS

ABCG2	ATP binding cassette subfamily G member 2
APC	Adenomatous polyposis coli
Bak	Bcl-2 antagonist/killer 1
Bax	Bcl-2 associated X protein
Bcl-2	B-cell lymphoma 1
Bid	BH3-interacting domain death agonist
Caspase	Cysteine-dependent-aspartate-specific proteases
CIN	Chromosomal instability
CME	Complete mesocolic excision
EGFR	Epidermal growth factor receptor
LC3	Microtubule-associated protein 1A/1B light chain
LDH	Lactate dehydrogenase
HIF	Hypoxia inducible factor
ICI	Immune checkpoint inhibitors
MAPK	Mitogen-activated protein kinase
MLKL	Mixed lineage kinase domain-like proteins
MSI	Microsatellite instability
PI3K	Phosphatidylinositol 3-kinase
RIPK	Receptor interacting protein kinases
THPP	5,10,15,20-tetra(hydroxyphenyl)porphyrins
TNFα	Tumor necrosis factor α
VEGF-A	Vascular endothelial growth factor A
XRCC1	X-ray repair cross completing 1

CHAPTER 1: INTRODUCTION

1.1 INTRODUCTION

The primary cause of global deaths is non-communicable diseases, and cancer is ranked as the first and vital cause of global deaths with increasing incidences and mortality (Bray *et al.*, 2018; Sung *et al.*, 2021). Colorectal cancer (CRC), arising from sessile serrated lesions and adenomas, is a prevalent cause of cancer-related deaths worldwide (Soons *et al*., 2021). CRC is commonly treated with conventional surgery, chemotherapy, and radiation therapies. Although these are successful through early detection, complete remission for cancer in the late stages is low and with painful consequences as chemotherapy and irradiation have toxic side effects and increased chances of drug resistance (Zbakh *et al*., 2020). Novel drugs and treatments are therefore being developed to combat resistance and extended recovery periods.

Photodynamic therapy (PDT) is now accepted worldwide as a clinically approved treatment modality for malignant cells. Its selling advantage is the high specificity and selectivity to targeted tumour cells resulting in minimised surrounding tissue effects. Furthermore, it is researched for its potential in overcoming restrictions of toxic systemic therapies and incomplete radical resections that decrease the opportunity for long-term survival post-surgery (Elekonawo *et al*., 2019), along with the ability to repeat the procedure on the same site if required (Peng *et al*., 2009). The PDT procedure involves the administration of a light-activated, tumour selective photosensitiser (PS) that produces reactive oxygen species (ROS) once irradiated with light of a particular wavelength matching the PS absorption spectrum. The generated ROS of either superoxide anions or singlet oxygen oxidises some biological molecules resulting in tumour destruction (Cogno *et al*., 2020).

PSs, along with oxygen and light, are essential elements of PDT. PSs are being tested for ideal characteristics such as no dark toxicity and the ability to generate significant amounts of ROS to induce cell death (Cogno *et al*., 2020). In addition, it needs to clear quickly from normal tissue to minimise phototoxicity (Abrahamse & Hamblin, 2016). Macrocyclic poly-pyrroles such as porphyrins and their derivatives and tricyclic phenothiazinium salts produce high yields of ROS and are preferred PSs for PDT use (Dos Santos *et al*., 2019). Porphyrins are effectively activated around the blue 400nm Soret band region, but due to Q-bands found up until the 630nm region, red light is used most in external PDT applications (Abrahamse & Hamblin, 2016). Our study utilised 405nm blue light *in vitro* on colorectal cancer, did not produce any irradiation toxicity and was sufficient to induce cytotoxic results after PDT treatment.

Metal-free H_2THPP was used in this study to investigate if Pd(II) and Cu(II) metal insertion into the porphyrin core would improve its PS efficacy during PDT and induce cell death in HT-29 colorectal adenocarcinoma cells. Furthermore, the photosensitiser was tested on a regular HEK-293 kidney cell line to determine the effects of PDT on normal cells.

Cellular uptake, localisation and dark toxicity of Pd(II)- and Cu(II)-THPP PSs were investigated, and both passed the optimisation stages. During the practical determination of IC_{50} and IC_{80} concentrations, Cu(II)-THPP produced stimulatory results instead of inducing cytotoxicity when irradiated and was therefore ruled a non-ideal photosensitiser and discontinued. Pd(II)-THPP, on the other hand, induced cytotoxicity at low concentrations. Pd(II)-THPP PDT significantly reduced cellular homeostasis and induced stress and cytotoxicity within HT-29 colorectal adenocarcinoma. The mode of cell death caused by Pd(II)-THPP determined using flow cytometric methods showed late apoptosis and some necrosis. No significant changes in caspase 3/7 activity were detected. Although cytochrome *c* release was

microscopically observed using fluorescence stain, autophagy was speculated to be another mode of cell death induced by Pd(II)-THPP.

To conclude, Cu(II)-THPP can be used to investigate resistive mechanisms within colorectal cancer cells against PDT treatment to find ways around it. Pd(II)-THPP is an effective photosensitiser and inducer of cell death against colorectal cancer that should be studied further in PDT treatment. PDT can therefore be a better alternative to conventional therapeutics when treating colorectal and other cancer types.

1.2 HYPOTHESIS

Coordination of copper(II) and palladium(II) into the commercial free-base H_2-THPP porphyrin core will result in comparable photodynamic therapy (PDT) efficiencies and cell death induction when targeting HT-29 colorectal adenocarcinoma.

1.3 AIMS

- To evaluate Pd(II)-THPP and Cu(II)-THPP for unwanted dark toxicity and irradiation toxicity at 405nm on colorectal cancer cells.
- To investigate the comparable PDT efficiency of Pd(II)-THPP and Cu(II)- THPP derivatives on colorectal cancer cells.
- To ascertain whether apoptosis or necrosis is induced by phototoxic responses of Pd(II)-THPP and Cu(II)-THPP derivatives.

1.4 STUDY OBJECTIVES

- Determine intracellular localisation of Pd(II)-THPP and Cu(II)-THPP within HT-29 colorectal adenocarcinoma cells.

- Screen dosage ranges for threshold conditions that induce unwanted dark toxicity (Pd(II)-/ Cu(II)-THPP) and light toxicity (Irradiation 405nm).
- Establish THPP-PDT treatment conditions for HT-29 cells by determination of IC_{50} and IC_{80}.
- Determine the effects on cell homeostasis through mitochondrial activity assay (alamarBlue dye reduction assay) and ATP (Celltiter-Glo® Luminescent Cell Viability assay) production mechanisms.
- Confirm cytotoxicity by determination of cellular membrane integrity using CytoTox-ONE™ Homogeneous Membrane Integrity and Trypan Blue dye exclusion assays.
- Determine localisation of active mitochondria using Mitotracker® Orange and cytochrome *c* proteins using the anti-cytochrome *c* antibody (ab154476).
- Determine ROS production using the flow cytometric Muse® Oxidative Stress Kit and upregulation or downregulation of apoptotic proteins (Caspases 3 and 7).
- Detect for cell cycle arrest using flow cytometry and propidium iodide dye.
- Detect for potential cell death using flow cytometry (Muse® Annexin V & Dead Cell kit) and fluorescence microscopy (Hoechst 33258 stain assay).

CHAPTER 2: LITERATURE REVIEW

2.1 CANCER

Cancer is defined as a genetic disorder caused by genomic mutations or epigenetic changes in somatic cells producing oncogenes whose function dominate over tumour suppressor genes (Chakraborty and Rahman, 2012). Hanahan and Weinberg (2000) stated that the mammalian tumorigenesis process involves multiple steps reflecting the alterations within the genes that transform healthy cell tissue into malignant tumours. The eight 'Hallmarks of cancer' (Figure 2.1), as described by Hanahan and Weinberg (2000 & 2011), now provide the solid groundwork in cancer research to describe multiple cancer adaptations within the tumour microenvironment that aid in the development of treatment therapies. They include the cancer possessing independent growth signals, desensitisation to growth suppressor signals, ability to evade apoptosis, increased proliferation, angiogenesis, metastatic ability, tumour cell ability to modify cellular metabolism to fuel proliferation and the evasion of cellular destruction by the immune system. The alteration and instability of the genes and tumour-promoting inflammation hallmarks are of great importance to malignant tumours as they are initiators for developing the main hallmarks (Broertjes, 2015).

2.1.1 THE HALLMARKS:

Growth signal independency

Healthy somatic cells depend on mitogenic growth signals to control proliferation processes. At the same time, tumours have adapted to deregulate standard tissue growth signals and produce their own to grow regardless of the surrounding tissue microenvironment. This independence is achieved by altering cytoplasmic growth signalling processes. Specific growth factor receptors are overexpressed by the

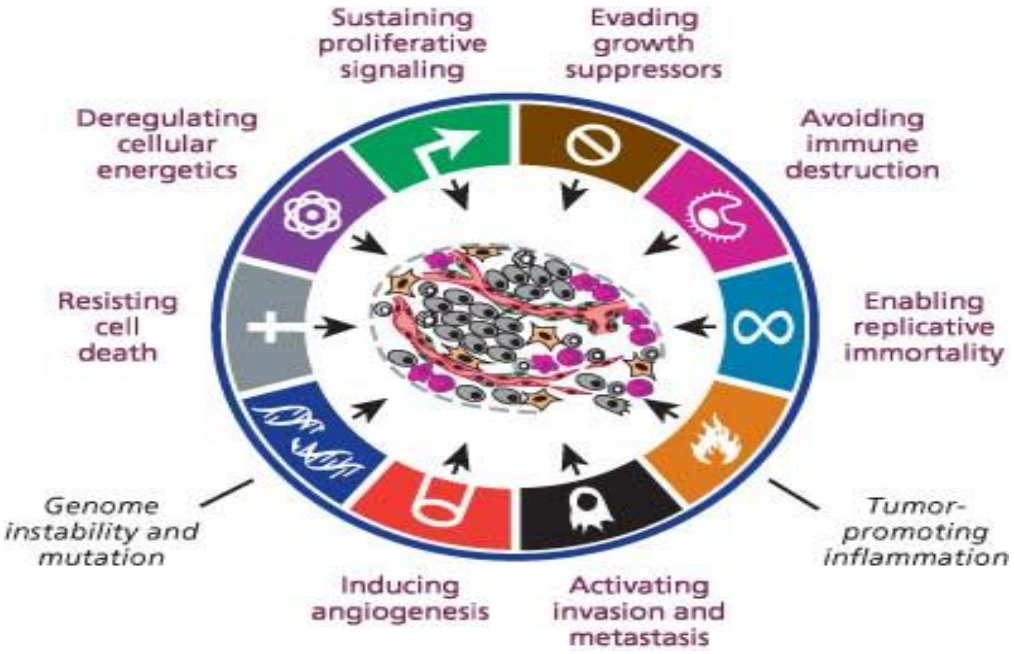

Figure 2.3 Hallmark cancer characteristics as proposed by Hanahan and Weinberg (2011)

tumour, causing even minuscule stimulation to result in proliferation or typically expressed extracellular matrix receptors are exchanged for pro-growth signal receptors. An alteration to the SOS-Ras-Raf-MAPK cascade either by mutation or deregulation can be detrimental to the proliferation process of normal cells (Hanahan and Weinberg, 2000).

Antigrowth signal desensitisation

Healthy tissue cells maintain homeostasis and cellular quiescence by utilising growth stunting signals that force proliferating cells into dormant G_0 states or through the induction of the postmitotic state. Tumour cells disrupt the retinoblastoma (RB) protein's pathway, which generally blocks proliferation and releases E2F transcription factors. E2Fs control the transition from G_1/S to S-phase within the cell cycle, and overexpression can coerce cells into the S-phase (Dimova

& Dyson, 2005) therefore desensitising the cells to growth-inhibitory factors (Hanahan & Weinberg, 2000).

Apoptosis evasion

The evasion of apoptosis has proven to be a prominent characteristic of cancer tumours. Apoptosis is controlled by machinery classed as sensors and effectors which monitor the environmental conditions and relay signals that trigger an apoptotic response accordingly. Cytochrome *c*, the Bcl-2 protein family, p53 tumour suppressor proteins and the caspase proteins all play a role in eliciting an apoptotic response. Cancer tumours evade apoptosis by stimulating an upregulation of the antiapoptotic Bcl-2 proteins with the *myc*-oncogene, which stimulates proliferation or inactivation of p53 tumour suppressor proteins. Tumours also evade apoptosis by manipulating the PI3 K-AKT/PKB signalling pathway (Hanahan & Weinberg, 2000).

Increased proliferation

Somatic cells possess intrinsic mechanisms promoting senescence that need to be dilapidated for the cancer cells to freely proliferate into near-fatal tumours. Malignant cells, therefore, manipulate telomere production by upregulating telomerase expression or through alternative lengthening of telomerase (ATL) activation, increasing replication (Hanahan and Weinberg, 2000).

Angiogenesis

Organs utilise a vasculature network for nutrients and oxygen supply as well as metabolic waste disposal. Developing tumours require angiogenic ability to obtain resource supply. From the evidence presented, this is achieved via the alteration of positive angiogenesis inducers and negative inhibitors, thus activating the

"angiogenic switch" (Hanahan and Folkman, 1996). Vascular endothelial growth factor-A (VEGF-A) upregulation and thrombospondin-1 (TSP-1) control are the recognised vital players of the angiogenic switch (Hanahan and Weinberg, 2011).

Increased metastatic ability

Metastasis is the process where cancer cells dissociate from the primary tumour and travel to distant tissue microenvironments (Gupta & Massagué, 2006). Highly metastatic cells have more genetic alterations than non-metastatic cells. They have been thought to use these genetic alterations to preserve the malignant characteristics of tumours, including the ability to metastasise and invade other tissues (Yokota 2000). For example, proteins such as cell-to-cell adhesion molecules (CAM's) and E-cadherins lose their adhesion function through alterations that affect expression patterns allowing cell migration (Hanahan and Weinberg, 2000). These alterations accumulate as the tumour stages progress (Yokota, 2000). The protein TGFβ (Transforming growth factor β) promotes metastasis by breaking cell-to-cell connections rendering lung capillaries more permeable for infiltration by tumour cells (Yan *et al*., 2010).

Modification of cellular metabolism

As the number of cells increases, concomitant energy metabolism reprogramming occurs to accommodate the abnormal cellular proliferation. A noticeable change is the upregulation of aerobic glycolysis and GLUT1, a glucose transporter protein. Glycolysis, however, was observed to occur within both aerobic and hypoxic conditions in tumours, with the latter upregulating multiple glycolytic pathway enzymes and glycolysis stimulating transcription factors, HIF1 and HIF2 (Hanahan and Weinberg, 2011). This describes the Warburg Effect, whereby cells use glucose to produce lactic acid in an aerobic environment. Cancer cells adapt to hypoxic conditions by using the Warburg effect to produce lactate and use it further to

produce ATP in support of the mitochondrial phosphorylation process (Kim & Dang, 2006). In addition, the increased lactic acid production causes acidosis of the tumour microenvironment, which increases available H^+ ions that alter the connective mechanisms, thus promoting invasiveness (Liberti & Locasale, 2016).

Mechanisms for immune system evasion

The immune system surveillance theory hypothesises that all cells are monitored by the immune system for any abnormalities. However, cancer cells have developed tactics to manoeuvre around surveillance and extermination by the immune system (Ribatti, 2017). Hanahan and Weinberg (2011) concluded that immunocompromised hosts have a higher probability of developing cancer and metastasis than immunocompetent hosts who can eliminate immunogenic cancer cells early. Studies done on premetastatic 4T1 mice showed that TGFβ signalling, both a tumour suppressor and promoter, recruits myeloid Gr-1+CD11b+ (immature monocytes and neutrophils) suppressor cells which are overproduced in tumours advancing metastasis and angiogenesis. The Gr-1+CD11b act by decreasing a critical immune defence cytokine against cancer, IFN-ɣ (Yan *et al.*, 2010; *Yang et al*., 2010).

2.2 COLORECTAL CANCER

2.2.1 INCIDENCE AND MORTALITY

Colorectal cancer is more frequent in developed countries and is linked to diets with higher animal fat intake (Yu & Li, 2006). From global statistical findings, colorectal cancer is ranked third in incidence rates and second in mortality rates when compared to all cancers. The highest incidences were found in European countries, Australia, North America and East Asia (Bray *et al*., 2018). According to CANSA (2018), in South Africa, colorectal cancer ranks second most common cancer in males and third in females. The overall lifetime risk for developing colorectal cancer stands at 0.74 for females and 1.24 for males (Brand *et al*., 2018).

Most cases were found in Caucasian patients leading with 54% diagnoses made. Africans followed at 28%, mixed-race patients were 15% and lastly, the Indian/Asian patients were a low 7% (McCabe *et al*., 2020). New cases are expected to have increased by 30%, and mortality to increase by 40% in 2030 (Magwaza *et al*., 2021). Siegel *et al.* (2021) estimated 149 500 new colorectal cases in the United States of America, and 52 980 related deaths were reported in 2021. Due to the misclassification of rectal cancers in postpartum investigations, mortality numbers are reported as the combined colorectal category instead of separate numbers. The reduced numbers are due to increased early colonoscopy screening and treatment. Developing and underdeveloped countries may fall into underreporting due to a lack of resources. A meagre percentage of African countries have high-quality cancer registries which are not regularly updated. Only South Africa, Malawi, Uganda and Zimbabwe have population-based cited registries but, are not regularly updated (Katsidzira *et al*., 2017). This concludes that colorectal cancer statistics in African or underdeveloped countries are severely underreported. Furthermore, more countries are adopting Westernized culture, which may leave the population susceptible to colorectal cancer. On the other hand, access to quality healthcare is increasing, which ensures early treatment, and decreases mortality (Katsidzira *et al*., 2017).

2.2.2 COMMON RISK FACTORS

Colorectal cancer pathogenesis is a sophisticated phenomenon instigated by lifestyle, diet and genetics (McCabe *et al*., 2020). Diet and nutrition are important factors often overlooked by the population that can initiate or inhibit the multistep tumour progression process. Colorectal cancer dietary and lifestyle-change carcinogens include the excess consumption of processed and red meats. This was found in studies done across the United States and Western countries whose very culture promotes increased meat consumption. The meats contain hemes and N-nitroso compounds associated with an increased risk of colorectal cancer (Vargas & Thompson, 2012). The formation of electrophilic alkyl diazonium ions due to the

spontaneous elimination of an aldehyde by N-nitroso derivatives alkylate the DNA resulting in modified bases. A G-A transition mutation of the 12th codon within the k-ras gene as a consequence of N-Nitroso compound damage can be found in human colon adenocarcinomas (Tricker & Preussmann, 1991).

Excessive alcohol consumption has increased colorectal cancer risk (Vargas & Thompson, 2012). Poynter *et al.* (2009) found that alcohol consumption increased the risks of colorectal cancer primarily in males and affected the rectum more than the colon. The association of colorectal cancer and alcohol consumption has been linked to the alcohol production of reactive oxygen species, which cause DNA abrasions. The DNA base-excision repair enzymes responsible for eliminating these abrasions are controlled by the XRCCI gene, whose polymorphisms were found to play a role in determining colorectal cancer risk. After the analysis of the three polymorphisms, including Arg280His, Arg194Trp and Arg399Gln XRCCI, carriers of the 399Gln alleles have increased risk of colorectal cancer than 399Arg while combination allele carriers had a significantly higher risk (Hong et al., 2005). The studied mechanisms of action of ethanol mostly point to acetaldehyde as the carcinogen in human cancers (Boffetta and Hashibe, 2006). Therefore, a healthier change in the diet into more plant-based diets and lifestyle changes, decreasing alcohol intake and increasing daily exercise can lower the risks of colon cancer.

As in all cancers, genetics contribute to colorectal cancer. Family and personal history of colorectal cancer, history of polyp development in the colon, chronic inflammatory bowel disease and age are also risk factors associated with colorectal cancer (Younis *et al*., 2021). The earliest known genetic mutation to cause colorectal cancer is the adenomatous polyposis coli (APC) tumour suppressor gene, which prompts the hyperproliferation of polyps in the colon. K-*ras* and p53 mutations aid APC in developing colorectal cancer (Behrens, 2005). K-*ras*^{G12D} expressing mice models showed that deleting the *Ink4a/Arf* led to human-

like metastasising carcinomas and proposed the RAS-RAF-MEK signalling as an additional colorectal cancer gatekeeper to APC (Bennecke *et al*., 2010). Loss of chromosomes 5q, 17p and 18q via mitotic recombination have been associated with loss of targeted suppressor genes such as TP53 that account for colorectal carcinomas and adenomas (Fearson and Vogelstein, 1990; Yamamoto *et al*., 1996). Other noteworthy signalling pathways that, when mutation arise within them, cause colorectal cancer are the Notch, *Wnt*/β-catenin/TCF and TGF-β- superfamily signalling (Smith *et al*., 2008). Manne and colleagues (2011), Chowdhury and Roy (2017) and Malki *et al.* (2021) have detailed reviews on the molecular and genetic modifications arising from chromosomal and microsatellite instability (CIN/MSI) and CpG island methylation in sporadic and hereditary pathways of colorectal cancer development.

2.2.3 COLORECTAL CANCER PROGRESSION

CRC progression involves multiple steps of histological and genetic changes. CRC develops from non-malignant pre-neoplastic lesions known as adenomatous polyps to malignant carcinoma (Younis *et al*., 2021). The adenoma-carcinoma sequence illustrated in Figure 2.2 describes the colonic transformation. CRC is initiated by replicative disorders in the normal mucosa, causing hyperproliferation. Adenomatous polyps, which are lesions of epithelial masses, are regarded as malignant when they enter the submucosa. Hyperplastic, hamartomatous and inflammatory polyps and flat or serrated adenomas have malignancy potential (de Leon & Di Gregorio, 2001). Polyps develop during a person's '20s or '30s, and removal can reduce the development into cancer. Sessile serrated polyps are precursor lesions of colorectal carcinomas with mutations in BRAF and DNA repair genes, CpG island methylation and increased MSI. These can develop into severe dysplasia or carcinoma with high metastatic potential in the lymphatic system. Early detection and examination of polyps using endoscopy and colonoscopy improve treatment efficiency. The cloud-like surfaces and unclear margins are two predictive features of malignant sessile serrated polyps detected

through white light endoscopy (Murakami *et al.*, 2018). Pathological examinations of adenocarcinomas found in the polyps are conducted to determine the distance of the tumour from the polyp margins, lesion size, the extent of tumour differentiation and invasion into the vascular and lymphatic systems (Longo, 2016).

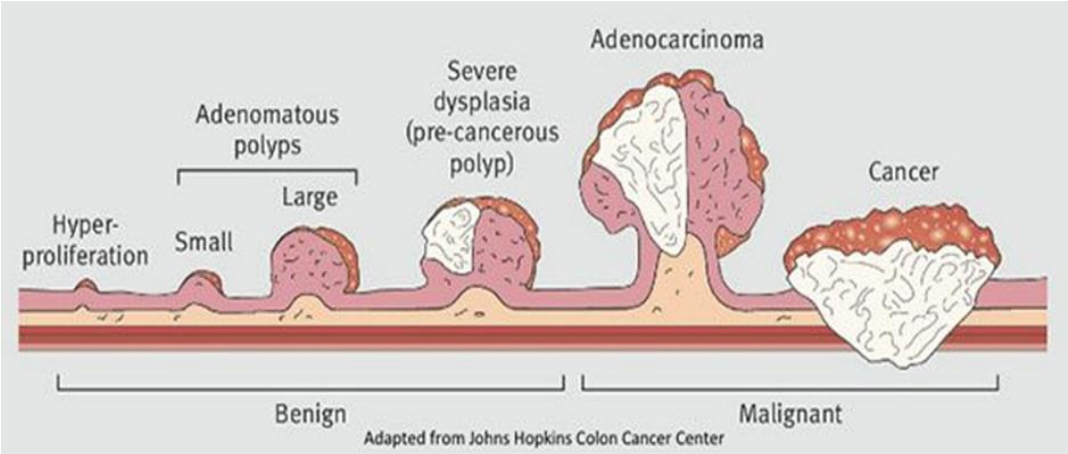

Figure 2.4 Colorectal cancer progression from polyp to cancer (Thrumurthy et al., 2016)

Although colorectal cancer is classified together, rectal and colon cancers have differences in anatomy, embryological origin, and function. Even the metastatic patterns differ due to the proximity of the venous drainage system. Colon cancers will usually first metastasise to the liver and spread until they reach the brain, whereas rectal cancers begin by metastasising to the lungs. However, metastasised colon or rectal cancers are treated in the same manner (Tamas *et al*., 2015). Hong *et al.* (2012) defined colorectal cancer stages which form the basis for the type of treatment administered.

2.3. CURRENT CANCER THERAPIES

2.3.1 SURGERY

Surgical resection is currently the standard treatment for colorectal cancer. When performed in cancer's early stages, this conventional treatment provides long-

standing outcomes with a 65% survival rate in 5 years. However, the survival rate decreases lower than 5% in patients with advanced metastatic lesions, which become unresectable (Shi *et al*., 2019). The complete mesocolic excision (CME) procedure was thought to have better outcomes than conventional surgery, but due to the dissections being close to essential vessels and organs not exposed in conventional surgery such as the superior mesenteric vein, spleen and stomach, and also risk around postoperative sepsis and respiratory failure, the procedure has created concern about a potential increase in morbidity and mortality (Bertelsen *et al*., 2016).

Laparoscopic and robot-assisted surgeries are recently adopted surgical techniques in colorectal cancer appraised for their minimal invasiveness. Laparoscopic surgery involves multiple complicated and delicate steps with the advantage of minimal scarring because of the smaller incision made, minimised bowel handling and exposure of visceral organs leading to minor trauma and quicker gastrointestinal recovery. The operating procedure time is longer, and in a complicated case, however, conversion to open surgery is more common (Lai & Law, 2012). Furthermore, the current limitations include the fulcrum effect, which takes time to perfect, two-dimensional visualisation, restriction of the instrument's degree of motion, amplification of the surgeon's hand tremors and dexterity (Lanfranco *et al*., 2004).

Robotic-assisted surgery was then developed to advance minimally invasive surgery and overcome the limitations of laparoscopic surgery. The Zeus and da Vinci robotic systems are operating wonders that have made technically impractical surgeries possible. Robot-assisted surgery has enhanced dexterity and degrees of freedom, aiding the surgeon's access to tissues. The surgeon's physiological tremors are nearly eliminated through software filters, and there is no fulcrum effect (Lanfranco *et al*., 2004). Robotic-assisted colorectal procedures

have escalated since 2001, whereby Weber *et al.* (2002) performed the first cases of telerobotic-assisted laparoscopic colectomies. A review of meta-analytic and comparative studies for conventional open surgery, laparoscopic surgery and robotic-assisted surgery on rectal cancer by Matsuyama *et al.* (2018) has shown robotic-assisted surgery to be more advantageous with only the cost as the main drawback.

2.3.2 CHEMOTHERAPY

Standard platinum-based chemotherapy includes combinations of cisplatin and gemcitabine or carboplatin and paclitaxel (Zampino *et al.*, 2008). Although highly effective, cisplatin is associated with nephrotoxicity, irreversible ototoxicity and neurotoxic side effects (Viglietta *et al*., 2020).

Chemotherapy has been proven to disrupt gut microbiota which affects the gut-brain axis inducing neurophysiological disorders such as depression, anxiety and other cognitive impairments experienced by cancer survivors (Deleemans *et al*., 2019). Furthermore, long-term side effects of chemotherapy reported by cancer survivors included peripheral neuropathy, premature menopause and andropause in males due to gonadotoxicity of chemotherapeutic agents (Ruddy & Partridge, 2012), cardiomyopathy and sometimes secondary cancers (Nekhlyudov *et al*., 2014). When colorectal carcinomas have advanced, chemotherapy is likely used as a palliative treatment to alleviate tumour-related symptoms and prolong patient life without symptoms rather than a cure (Ragnhammar *et al.,* 2001).

In advanced CRC, the primary chemotherapeutic treatment involves 5-fluorouracil (5-FU) with oxaliplatin and leucovorin (FOLFOX) or oxaliplatin and capecitabine (CAPOX) over a period of 24 weeks (Bettington *et al.*, 2013; Tamas *et al.*, 2015). Adjuvant chemotherapy after surgery dramatically improves the survival of stage

III colon cancer patients. Fluoropyrimidine-based chemotherapy is used to treat stages II and III of rectal cancer (Tamas *et al.*, 2015)

2.3.3 RADIATION

Radiation therapy uses ionising energy to target and puncture cancerous cell DNA, consequently stunting their growth and inhibiting replicative ability, ultimately destroying the cells. Radiation doses vary depending on tumour size, surgery done, and lymph node implication. A significant drawback of radiotherapy is that the neighbouring normal cells are affected by the ionising energy, leading to secondary malignancy due to the DNA damage and mutation of treating the primary tumour. Other side effects when treating colorectal cancer include incontinence, bloody and leaky stools, skin irritation around the treated area, nausea and fatigue (Mohan *et al*., 2019).

Radiotherapy's full effect in colorectal cancer is used in combination before and after surgery or with chemotherapeutic agents and immunotherapy. Radiation is delivered to the tumour site using high-energy rays aimed at the tumour location in external beam radiation or internal radiation using catheters containing radioactive resources (Basker *et al.*, 2012). External beam radiation therapy has been used to treat advanced inoperable colorectal tumours and reduce local recurrence rates (Tam & Wu, 2019). Dosages range from 40-70 Gray units with 1.8-2.0 Gray units per fraction. Using radioprotectors and radiosensitisers aids in lowering the risk of overexposure (Mohan *et al*., 2019).

2.3.4 IMMUNOTHERAPY

Immunotherapy in cancer uses varying treatment modalities that activate the host immune system using immune triggers such as vaccines, transfection agents, cytokines, and cell therapies. Thus, immunotherapy aims to enhance the body's natural defences against malignant tumours. This treatment has been tested on

several different cancers; however, it has shown limited response and works for a few, while other patients showed primary resistance or developed resistance in response to the treatment (Stanculeanu *et al.*, 2016).

Immune checkpoints are found in the coinhibitory signalling pathways that prevent an immune response to specific antigens. Immune checkpoint inhibitors (ICIs) disrupt the coinhibitory signalling pathways and promote the termination of cancer cells through a hyperimmune response. (Zhang & Zhang, 2020). The most studied and used ICI targets are CTLA-4 (cytotoxic T-lymphocyte-associated protein 4), PD-L1 (programmed death-ligand 1) and PD-1s (programmed cell death proteins). These are expressed on T-cells and elicit a specific T-cell immune response by blocking immune checkpoint pathways. (Chae *et al.* 2018; Zhang and Zhang, 2020).

Targeted cancer treatment using monoclonal antibodies (mAbs) is on the rise. Examples of mAbs used in colorectal cancer include Cetuximab IgG1 monoclonal EGFR inhibitors, which are used to suppress tumours because they block EGFR receptors in the PI3K (phosphatidylinositol 3-kinase) and MAPK pathways, thus disrupting cellular proliferation (Bettington *et al.*, 2013). A study done by Cunningham *et al.* (2004) delivered a 17 percent response rate in 121 stage IV colorectal cancer patients. Panitumumab is another anti-EGFR mAb used to treat RAS wild-type advanced colorectal cancer (Modest *et al*., 2019). Bevacizumab is an anti-VEGFA mAb that inhibits VEGFA, prohibiting angiogenesis in tumour growth. The addition of bevacizumab to chemotherapy showed increased survival rates in both metastatic colon and rectal cancer patients (Tamas *et al.*, 2015).

Immunotherapy requires specific immune target study and execution to be successful, requiring more time in research, while chemotherapy and radiation risk

resistance and, because of the non-specificity, kill even healthy tissue in patients. Therefore, a better treatment modality that is specific, minimally invasive, with lower recurrence rates is needed.

2.4 HT-29 COLORECTAL ADENOCARCINOMA CELL LINE

The HT-29 human colon carcinoma cell line was established by Jorgen Fogh in 1964, isolated from a 44-year old Caucasian female patient with a grade II adenocarcinoma in the rectosigmoid colon (von Kleist *et al*., 1975). The cell line was found to have impressive differentiation characteristics which mimic matured intestinal cells (Rousset 1986) and therefore became the most frequently used source for colon cell lines and model for colon cancers (Kawai *et al*., 2002).

2.5 PHOTODYNAMIC THERAPY

Photodynamic therapy, in comparison, is a novel therapeutic modality for cancerous and non-cancerous diseases, with the prospect of being more effective than the current existing therapies. Not only has it treated human diseases, but it has also gained traction for the treatment of viral, bacterial, fungal and parasitic infections (O'Connor *et al*., 2009). It involves a photochemical reaction between molecular oxygen, light, and a photosensitive agent. Although these components prove harmless individually, their combination produces reactive oxygen species (ROS) capable of inducing irreparable cellular damage (Park *et al*., 2021).

2.5.1 BRIEF HISTORY OF PDT AND PHOTOSENSITISERS

PDT was developed from the study of using light's therapeutic properties to treat diseases known as phototherapy. More than a century ago, it was observed that combining certain chemicals with light induced cellular death (Dolmans *et al*., 2003). Oscar Raab (1900), a medical student in Germany, discovered that explicit energy wavelengths killed paramecia when acridine dye was present. The connection between light- and oxygen-dependent reactions was made through

continued research. It was termed the 'Photodynamic action' by von Tappeiner & Jodlbauer (1907) after treating skin tumours with white light and eosin (von Tappeiner and Jesionek, 1903) and later suggested for clinical medicine use.

Further experimentation through the decades testing combinations of light and different reactive chemicals have led to photodynamic therapy as we know it. An earlier example sees W. Hausmann testing the phototoxic effects of the first porphyrin-based photosensitiser (PS), hematoporphyrin on red blood cells and paramecium, confirming cytotoxicity. Furthermore, he tested the effects by injecting mice with hematoporphyrin and light exposure, which led to cutaneous oedema or death depending on the dosage and exposure time (Hausmann 1911). Friedrich Meyer-Betz topically administered 200mg hematoporphyrin on himself, resulting in pain and swelling on the areas of his skin exposed to light (Meyer-Betz 1913). That was the first test of porphyrins done on humans. Schwartz *et al*. (1955) then took the hematoporphyrins, treated them with sulphuric and acetic acids, filtered and neutralised them with sodium acetate. The saline-resolved precipitate that was formed became the hematoporphyrin derivative. Many PSs have since been synthesised and produced to improve photodynamic therapy in the medical industry.

2.5.2 MECHANISM OF ACTION

PDT involves the topical or intravenous administration of a photosensitising agent (PS) and PS activation using light (Visible, UV or near-infrared) irradiation of a specific wavelength. The PS is designed to have minimum to no dark toxicity and to accumulate in diseased or high proliferating tissue selectively. Light exposure is usually done through lasers and is absorbed by PS molecules. Following light absorption, PS molecules become excited and react with the substrates to produce free radicals, or an energy transfer can occur to produce ROS (Figure 2.3) (Park *et al.*, 2021; Josefsen and Boyle, 2008).

2.5.2.1 Type I, Type II, Type III and Type IV photochemical reactions in PDT

The basis of PDT is ROS generation to induce cellular cytotoxicity. When PS molecules absorb light from irradiation, they become activated, moving from the ground to an unstable excited singlet state. The PS loses some of its excess energy directly through heat or the excited triplet state caused by intersystem crossing. PS molecules in the excited triplet state react in what is known as Type-I and Type-II reaction mechanisms (Mroz *et al*., 2011).

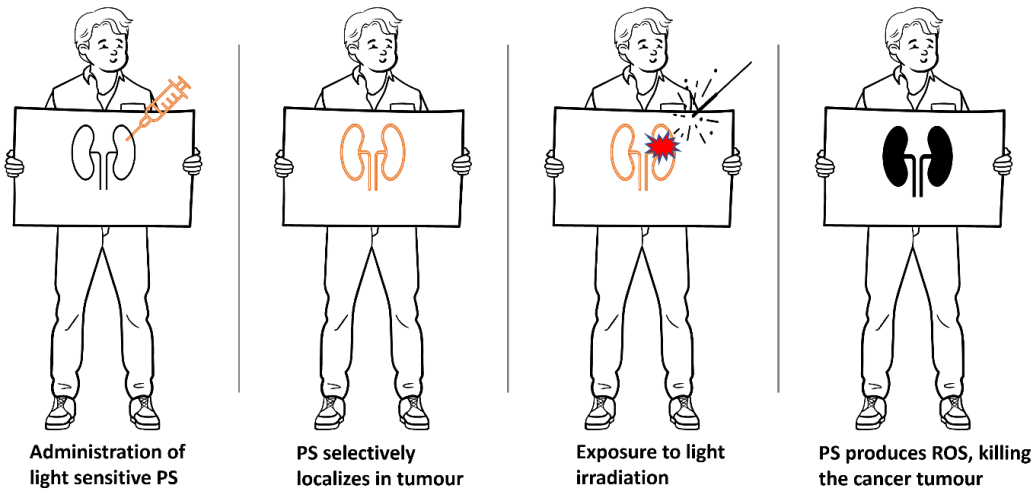

Figure 2.3 Administration of photodynamic therapy in tumours

In Type-I, the excited singlet or triplet states are involved. However, the PS will only react with reducible or oxidisable substrates nearby as the singlet state pathway has a shorter lifetime (nanoseconds). The excited triplet state lifetime is longer (microseconds). Two reactions occur in a Type-I reaction. Firstly, a nearby substrate oxidises the PS to an excited state, producing a radical anion from the PS and a radical cation from the substrate. The radicals immediately react with oxygen to produce superoxide anions ($O_2^{\bullet -}$) that eventually generate hydroxyl radicals ($OH^{\bullet}$) which are highly reactive. The second reaction involves PS reduction by transfer to the hydrogen to excite the PS. The free radicals produced in the

process interact with oxygen to generate reactive peroxides (Josefsen & Boyle, 2008).

Type-II reactions are straightforward because the PS in the excited triplet state reacts with molecular oxygen ($^3O_2$) and undergoes an energy transfer creating high-energy singlet oxygen, which has a short lifespan. The energy transfer also dissipates to low-energy singlet oxygen, which is involved in cytotoxicity. ROS and the high-energy singlet oxygen act upon biological molecules in proximity via redox cascades where ROS are regenerated in fatty acids, lipids, amino acids and DNA to cause cellular damage (Josefsen and Boyle, 2008; Castano *et al*., 2004).

By studying these reactions, PDT effectiveness is highly dependent on oxygen presence; however, through the repeated cascades in Type-I & -II reactions, the oxygen supply can quickly become reduced if not depleted. An allowance for PDT in hypoxic environments had to be thought out. Horne and Cronjé (2017) described a Type III reaction in hypoxic conditions. Lack of oxygen causes the PS molecule to oxidise nearby biological molecules resulting in Type I and Type II-like effects. The difference is the absence of free radical intermediates. Re-excitation of the PS in oxidative cascades can cause the PS to be degraded by light in a photobleaching process, limiting the number of photochemical reactions a single PS molecule can generate. Furthermore, hypoxic tumours may confer resistance to PDT, and thus treatment should be enriched with oxygen for a more successful PDT (Scherer *et al.*, 2017).

A Type IV reaction mechanism also occurring in hypoxic conditions was then proposed by Scherer and colleagues (2017). The process involves the photoisomerisation of the activated PS molecule, consequently enabling it to bind to its molecular target site, inducing cell death. This theory was used to progress

a two-photon (2P-PDT) phototherapy, which promised to be more efficient in hypoxic tumours.

2.5.3 PHOTOSENSITISERS

In PDT, the photosensitiser is of utmost importance. It is excited with visible light, and the excitation energy is transferred to the triplet oxygen present, thus converting it to singlet oxygen. The singlet oxygen is unstable and has cytotoxic effects that lead to cell death and tumour destruction *(*Khan *et al*., 2015). Photofrin®, a hematoporphyrin derivative (first generation) (Figure 2.4), was the most studied PS, but an exact chemical structure or components thereof could not be determined. Other shortcomings, such as extended periods of skin photosensitivity, required further research for improved novel PSs (second and third generation PSs). Second generation PSs are compounds that improve the Photofrin formula, such as Foscan®, a *meso*-tetrahydroxyphenylchlorine and Lutrin. Third generation photo-sensitisers are encapsulated or conjugated to nanocarriers such as polyethyleneglycol (PEG) to enhance drug delivery and selectivity (Baskaran *et al*., 2018).

For consideration as a potential PS in PDT use, a compound must meet detailed criteria. Ideal PS have the following characteristics: it should be a known, pure, and stable compound, have low toxicity in the dark but induce death post-irradiation with a specific light in the visible region. It must be absorbed, localised in target tumour tissue, and generate high quantum yields of singlet oxygen for ROS production. Finally, it must be cost-effective for commercial use (O'Connor *et al.*, 2009).

2.5.3.1 Macrocycles

Tetrapyrrole macrocyclic compounds have increased interest in PDT studies. Their ring structure can undergo functionalisation (structural modification to increase

hydrophilicity and nanoencapsulation for protection) and metallation manipulation advantageous to PDT treatment and diagnosis (Pereira and Tasso, 2021: O'Connor *et al*., 2009). Most PSs in PDT are macrocyclic tetrapyrroles, including porphyrins, phthalocyanines, chlorins, bacteriochlorins, and extended analogues due to their attractive physiochemical properties (Le *et al*., 2021).

2.5.3.1.1 Porphyrins

Porphyrin based photosensitisers are researched because of their exceptional photophysical properties, low dark-toxicities, high photostability, molar absorptivity and biocompatibility (Khan *et a*l., 2015). Porphyrins are N-heterocyclic carbenes found primarily in nature. The porphine structure contains 20 base carbon atoms with four nitrogen atoms at the inner centre, and four distinct characteristic pyrrole rings with methenyl bridges to form an aromatic ringed compound. The nitrogen atoms form a cavity wherein a metal ion can be incorporated to form metalloporphyrin compounds (Deda *et al.*, 2020). Furthermore, they absorb light in the blue light region (420nm) of the visible light spectrum, which adds a disadvantage of being incapable of penetrating deeply enough into diseased tumours. The UV-Vis spectra of porphyrins have distinct 420nm Soret band peaks and weaker 500nm and 650nm peaks which shift upon metal coordination. In addition to their qualities mentioned above, porphyrins have autofluorescent and phosphorescent qualities that allow diagnostic fluorescence tracking and biomedical imaging.

2.5.3.1.2 Phthalocyanines and Porphyrazines

Phthalocyanines and porphyrazines form part of second-generation PSs as they have kept the fluorescence, ROS generation and light absorption properties in the visible region as in porphyrins. They are known as tetradentate (binds four donor atoms to the central atom) ligands capable of forming firm Lewis adducts (Swavey and Tran, 2013). They absorb light in the 600-700nm spectra range (Pandey, 2000), can react with non-metal, metal and metalloid ions for application in PDT (Pereira

& Tasso, 2021). Phthalocyanines were inferior to porphyrins in tumour specificity, but research showed gold nanoparticles addressed the tumour targeting issue (Swavey & Tran, 2013).

2.5.3.1.3 Bacteriochlorins and Chlorins

Chlorins and bacteriochlorins are tetrapyrrolic moieties found in plants and bacteria, respectively. They differ structurally from porphyrins in that chlorins contain a reduced pyrrole, while bacteriochlorins have two reductions. Chlorins absorb within the red-light region (650-750nm), and bacteriochlorins absorb within the electromagnetic spectrum's near-infrared range (700-900nm). Bacteriochlorophyll α and chlorophyll α are common PSs. Bacteriochlorins are currently used in photodynamic inactivation (PDI) of microbials to combat multidrug resistance. Bacteriochlorin PSs accumulate in cell membranes, and irradiation induces photodamage in the microorganisms. Due to the bacteriochlorins' NIR deep penetration into tissues, they are considered promising PSs for therapeutic anticancer PDT (Pucelik *et al*., 2020).

2.5.3.2 Metal coordination into macrocycles

Macrocyclic compounds absorb light in the UV-Vis region of the spectrum. Metal –ion coordination changes the absorption spectrum and photo-physics thereof. Pereira and Tasso (2021) described the symmetry and molecular orbital distribution of the macrocycles in addition to how metallation affects the Soret, B and Q bands. Coordination of metal into phthalocyanines and porphyrazines results in a redshift in the spectrum wherein red light is absorbed, making them desirable for PDT applications. Transition metals are primarily used in PDT research to increase the triplet and singlet oxygen yields. Heavier atoms are preferred for the heavy atom effect and increasing the efficiency of the intersystem crossing process. More specifically, heavier divalent transition metals are preferred because they form stronger interactions between the metal ions and nitrogen atoms at the centre of the ring (Pucelik *et al.*, 2020)

2.5.3.3 THPP

In the '80s, Berenbaum and his counterparts (1986) sought to improve the shortcomings of Hematoporphyrin and Photofrin by studying varying porphyrins. 5,10,15,20-tetra(hydroxyphenyl)porphyrins (THPP) (Figure 2.3) showed promise of red-light absorption. THPP isomers were then produced, studied, and compared for the best PS proficiencies. *para*-THPP absorbed light at 656nm, and *meso*- & *ortho*-THPP absorbed at 648nm. *O*- & *m*-THPP were more potent PSs than *p*-THPP leading to necrotic tumour destruction. Bonnett *et al.* (1989) developed bacteriochlorin and chlorin derivatives using these isomers, which increased photonecrotic induction.

2.5.4 LIGHT IN PDT

PDT efficiency is dependent on the intensity and frequency of the light source. Therefore, excitation wavelengths must be exclusive to the type of tumour and PS selected for PDT. Tissue optics is the measurement process of the affected tissues' spatial and size distribution, including their absorption and scattering patterns (Robertson *et a*l., 2009). When working *in vivo,* tissue absorption and scattering of the light determine the depth of penetration. Visible light wavelengths offer weakened penetration and cannot be used in PDT to treat deep tumours.

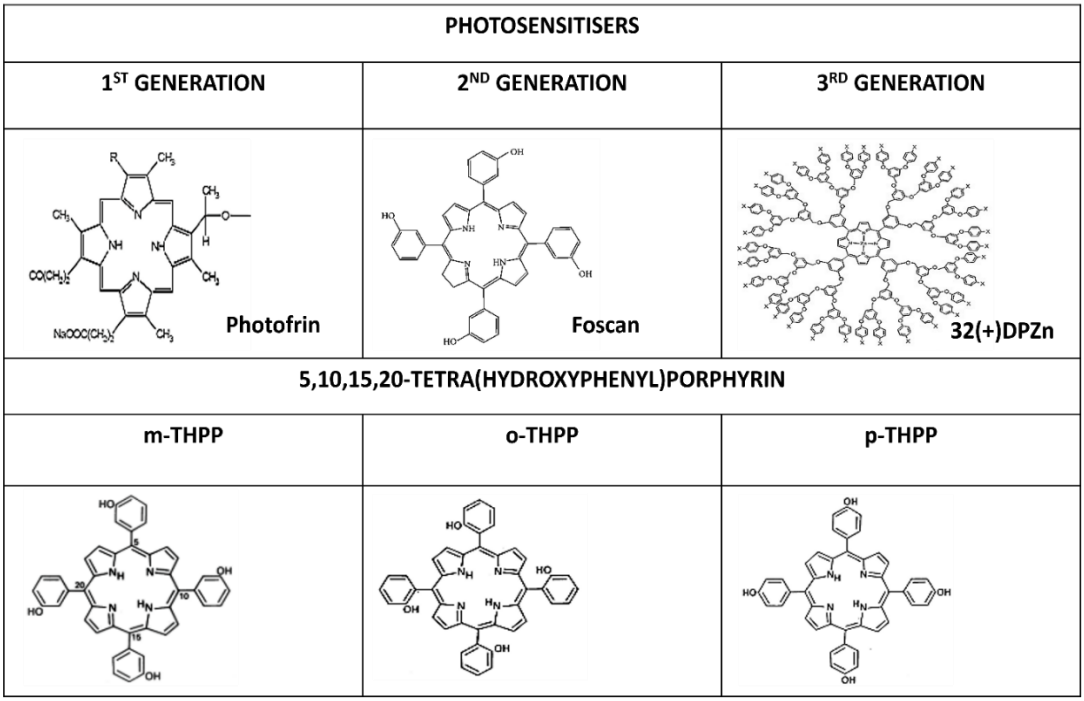

Figure 2.4 (Top) Generational development of photosensitisers. Photofrin, a Hematoporphyrin derivative, is a first-generation PS. Second generation PSs are an improvement of the first produced PSs. Third generation PSs are conjugated to biomolecules to enhance tumour selectivity. (Bottom) THPP isomers used in PDT research.

On the other hand, near-infrared light has stronger scattering but lower absorption in tissues indicating deeper penetration (Wang *et al*., 2021). In clinical settings, 600-900nm wavelengths are used, as shorter (than 600nm) wavelengths are absorbed by endogenous dyes like haemoglobin and myoglobin, while longer wavelengths fail to generate enough singlet oxygen (Nowis *et al*., 2005).

Light sources frequently used in PDT were the incoherent tungsten, fluorescent, halogen, or xenon lamps. Different laser lights offer optimal illumination due to their coherent and monochrome properties (Nowis *et al*., 2005). They include argon/dye, metal vapour, diode lasers, and non-laser light-emitting diodes (LEDs). The use of lasers has the added advantage of being able to be incorporated into fibre optics for fast, accurate and direct dosimetry to the targeted site (Mang,

2004). The amount of irradiation exposure (dosimetry) is measured in fluence (joules per centimetre squared), which is equivalent to the fluence rate multiplied by the length of exposure in time (Jacques, 2010). Cytotoxicity and the type of cell death, be it apoptosis or necrosis, is therefore directed by irradiation fluence and exposure time, wavelength and the concentration and localisation of the PS (Scherer *et al*., 2017).

2.5.5 ADVANTAGES AND DISADVANTAGES OF PDT

PDT holds many advantages over conventional cancer treatment therapies, including increased selectivity and specificity. PDT is more cost-effective than the methods mentioned above, simpler to operate, and induces fewer side effects and disfigurement to the patient (Pandey, 2000); thus can be used repeatedly and flexibly with other treatment modalities until the desired efficacy is reached (Fan and Andren-Sandberg, 2007).

The use of photosensitisers has some disadvantages since a few photosensitisers already in clinical trials have reported drawbacks, such as delayed phototoxicity and temporary excruciating pain during the light process (Pandey, 2000). Allergies in sensitive patients and limited penetration in larger cancer masses are limitations to PDT that still require development (Fan and Andren-Sandberg, 2007).

2.5.6 ADVANCES IN PDT

Further advancements of drug delivery during PDT are being made, with alternative drug carriers being studied to overcome the hydrophobicity of certain drugs. These include nanoparticles, polymer-drug conjugates, polymeric micelles and liposomes, which take advantage of the tumour's leaky neovasculature to enter into the tumour (Peng *et al*., 2009). Nanocarriers that encapsulate the photosensitising compounds offer protection, increase blood circulation time, enhance cellular uptake, and avoid multidrug resistance mechanisms, all of which help minimise the side effects, relieving the patient (Deda *et al*., 2020). Pluronic® non-ionic triblock copolymers are FDA approved nano vehicles investigated by

Sobczyński, Kristensen and Berg (2014) on THPP, TSPP, TAPD and TCPP porphyrin PSs. The use of these nano vehicles proved efficient solubilising agents of these porphyrin PSs and increased cellular uptake and phototoxicity in cancer cells. A look into mAbs conjugates to increase specificity is also underway. Antimicrobial PSs in blue light PDT are being developed to treat infections despite drug resistance (Huang *et al*., 2010).

With studies being done to advance PDT efficacy in cancer treatment, it is essential to look at the modes of cell death induced by PDT. The success of PDT lies in its cytotoxicity inducing abilities; therefore, understanding the cell death mechanisms will allow researchers to manipulate the existing processes to improve the therapy.

2.6 CELL DEATH INVOKED BY PDT

2.6.1 PDT MODE OF CELL DEATH

The PDT mode of cancer destruction can include damage to the tumour vascular system leading to ischemia, enhanced neoplasm cell recognition by the immune system or by direct induction of cancer cytotoxicity (Kessel, 2020; Huang *et al.*, 2016).

The location of the PS is vital in distinguishing the type of death initiated. PDT efficacy significantly increases when the mitochondria, lysosomes, endoplasmic reticulum (ER) and plasma membranes are targeted (Kessel, 2020). Mitochondrial localization of the PS leads to permeabilization upon irradiation by light, and ROS is produced. Once the outer mitochondrial membrane has been permeated, the cell is sentenced to apoptotic death (Velazquez *et al*., 2019). ER localization is a target for apoptotic death as well. Damage to the ER releases calcium post-PDT, which triggers caspase 12 activation and induction of cell death (Zhivotovsky & Orrenius, 2011). Lysosomal localization of the PS and consequent photodamage

can initiate apoptosis by releasing proteases that cleave Bid into a pro-apoptotic tBid portion (Kessel, 2020). tBid interactions with the mitochondria trigger apoptosis (Kessel & Oleinick, 2018). In contrast, targeting lysosomes and plasma membranes in PDT has been observed to block or interrupt the apoptotic process predisposing the tumour to necrosis (Buytaert *et al*., 2007).

Three death pathways are primarily observed in PDT are apoptosis, necrosis, and autophagy. Apoptosis was the first death pathway acknowledged in PDT. The apoptotic pathway does not elicit an inflammatory or immunological response. On the other hand, necrosis activates a fast-acting, aggressive immune response (Velazquez *et al*., 2019). Evidence has proved that these pathways have the potential to co-occur in response to PDT action (Miki *et al*., 2015).

2.6.2. APOPTOSIS

Two forms of programmed cell death exist. Apoptosis is Type I, and autophagy is Type II. Apoptosis morphological death markers include a change in DNA such as chromatin condensation and the fragmentation of chromosome structures, shrinking cells, cell membrane invagination, apoptotic body formation (Huang et al., 2016) without breaking down the plasma membrane, phosphatidylserine exposure to the outer membrane, phagocytosis by nearby cells and caspase activation (Buytaert *et al*., 2007).

Apoptosis has two molecular pathways known as the intrinsic and extrinsic pathways, both involving the activation of cysteine-dependent aspartate-specific proteases (caspases). Mitochondria are vital in triggering apoptosis as stimuli aim to permeabilize the membrane in the intrinsic pathway. Once permeabilized, inter-mitochondrial membrane apoptogenic proteins are deposited into the cytosol. At this stage, the cells are committed to undergoing cell death. Apoptogenic proteins include caspases, cytochrome *c,* Omi/HtrA2 and

Smac/Diablo, endonuclease G (Endo-G) and apoptosis-inducing factor (AIF). The mitochondrial membrane pathway also involves the activation of pro-and anti-apoptotic Bcl-2 proteins that work antagonistically (Buytaert *et al*., 2007). Bak and Bax activation from the Bcl-2 family triggers membrane permeabilization resulting in pro-apoptotic protein release, including cytochrome *c*. Meanwhile, Bcl-2 and Bcl-xL have anti-apoptotic properties that include blocking the opening of pores to release cytochrome *c* (Plaetzer *et al*., 2003).

In the extrinsic pathway, cell death is initiated by death ligands (TNF-α and TRAIL) binding to their corresponding death receptors on the cell's surface (Buytaert *et al*., 2007). The process is caused by external stimulation such as radiation, toxins and chemotherapeutics that affect the mitochondrial membrane.

Both intrinsic and extrinsic events lead to a caspase cascade wherein effector caspases (caspases -3, -6 & -7) are activated (Mroz *et al*., 2011).

2.6.2.1 Markers of apoptosis

Caspases

Caspases are cleaved and activated in both intrinsic and extrinsic pathways. In intrinsic apoptosis, intracellular stress causes the formation of an apoptosome leading to initiator caspase-9 activation, which then activates other effector caspases. Initiator caspases -8, -9 and -10 activate effector procaspases -3 and -7. Effector caspases -3, -6 and -7 are liable for initiating the hallmark apoptosis characteristics observed microscopically in dying cells (Brentnall *et al.*, 2013; Mroz *et al.*, 2011). Caspase 3 cleavage is a marker frequently used for apoptosis (Anthony *et al*., 2020). Brentnall *et al*. (2013) found caspase -3 to be the more efficient mediator of apoptotic death. In contrast, caspase -7 had a lesser effect

and instead played a supportive role by increasing ROS production and detachment from the extracellular matrix.

Cytochrome c

Release of cytochrome *c* after permeabilisation of the mitochondrial membranes is an early apoptosis marker. Translocation of cytochrome *c* is a major initiator of caspase activation. The cytochrome *c* binds to the apoptosis-inducing factor (Apaf-1) to form an apoptosome that activates caspase-9, the initiator caspase responsible for caspase-3 and -7 activation (Brentnall *et al*., 2013). Caspase -9 activation occurs in ATP or dATP presence. Cytochrome c release can be inhibited by Bcl-2 and other pro-survival proteins that work together with ER and outer mitochondria membranes to retain the integrity (Mroz *et al*., 2011).

PS externalisation

Phospholipids are present on the inner and outer sides of cell plasma membranes. Translocation of the phospholipids to the opposite sides of their original locations is mediated by scramblase, flippase and floppase enzymes. Phosphatidylserine is found on the inner surface, and externalization by the cell membrane is an early indicator of apoptotic events occurring (Mariño & Kroemer, 2013; Velazquez et al., 2019). Phosphatidylserine exposure to the outer membrane allows recognition of apoptotic cells by phagocytes for elimination. The protein Xkr8 was noted to be cleaved and activated by effector caspases. Overexpression of Xkr8 is found in events of apoptotic externalization of phosphatidylserine (Mariño & Kroemer, 2013).

The translocation of phosphatidylserine is detected flow cytometrically using a combination of FITC Annexin V and propidium iodide (PI). Uptake of PI indicates necrosis due to no membrane integrity compared to apoptotic cells that still have their membranes intact despite externalization (Suganya *et al*., 2019).

2.6.3 NECROSIS

Necrosis is a type of cell death initiated by external stimuli (Kessel & Oleinick, 2018). Necrosis following PDT treatment is caused by photodamage to the cell membranes after a supralethal PS or light irradiation dose is administered, resulting in loss of the membrane integrity, cell swelling and lysis (Kessel & Oleinick, 2018). Membrane disruption causes ATP depletion (Anthony *et al.*, 2020) and LDH release from the cells (Lange *et al*., 2019), which are significant markers for necrotic death. Furthermore, the liberation of the intracellular contents triggers an inflammatory response in the surrounding tissues (Miki *et al*., 2015). In PDT, some PSs are deliberately designed to induce necrosis instead of apoptosis by localization in the lysosomes or cell membranes (Kou *et al*., 2017). Once triggered, necrosis is an irreversible event.

Unlike apoptosis and autophagy, necrosis was thought to be an unprogrammed form of cell death. However, it was discovered that necrosis may still be activated in the absence of caspases via toll-like and death domain receptors. This regulated death is known as necroptosis (Anthony *et al*., 2020). Necroptosis shares morphological features of necrosis, but it is more regulated by distinct signal transduction pathways. External stimuli for necroptosis may include PDT, overproduction of ROS, ionization by irradiation, DNA damaging anticancer treatments or calcium overload (Fulda, 2013). Intracellularly, necroptosis is induced when mixed lineage kinase domain-like proteins (MLKLs) are phosphorylated, oligomerized and transported to the plasma membrane.

Furthermore, some receptor-interacting protein kinases 3 and -1 (RIPK3 and RIPK1) activities also induce necroptotic death (Dos Santos *et al*., 2019). Inhibition of caspases by any activity results in the formation of a protein complex containing RIPK1 and RIPK3, known as a necrosome, that propels the cells into the necroptosis pathway. The triggering of RIPK3 activity phosphorylates MLKL leading

to a necroptosis death signal (Fulda, 2013). A study done by Coupienne *et al*. (2011) on glioblastoma cells illustrated that 5-ALA PDT induced RIPK3 dependent necrosis in what we later learn as necroptosis, singlet oxygen from PDT activates necrosis, and RIPK3 is a critical factor in the process.

2.6.4 AUTOPHAGY

Autophagy is the second type of (Type II) programmed cell death whereby cells undergo self-destruction via degradation of the organelles and proteins under stress stimulation (Huang *et al*., 2016). Autophagy was observed to play a cytoprotective role mostly in PDT (Kessel, 2020), as photodamaged organelles are cloistered and reused before they can initiate an apoptotic response (Kessel, 2020). In addition, Beclin-1 production in the autophagic process has a counter-reaction to tumour growth. However, as the tumour grows, autophagy plays a role in keeping the tumour alive in an unfavourable low nutrient section of the tumour. Thus, in an advanced autophagy process whereby the cell components have been recycled, resistance to PDT may be conferred. Insufficient ROS production during PDT induces autophagy as a means for cell survival (Aniogo *et al*., 2021). Autophagy can also be deadly, depending on the administered PS dose and cell phenotype (Kessel & Oleinick, 2018).

Cells unable to trigger apoptosis turn to autophagy, mainly when lysosomes are the PDT target. The autophagy-associated protein, ATG7, is crucial in photodamage induction in lysosomes as it pokes holes in the membranes releasing apoptosis-inducing proteases (Kessel & Oleinick, 2018). Therefore, autophagy is lysosome dependent. The presence of autophagosomes is a central characteristic of autophagy. A screen for autophagy in research can include LC3-I and LC3-II proteins found in autophagosomes (Anthony *et al*., 2020). This is because LC3-I is converted to LC3-II in early-stage autophagy (Miki *et al*., 2015). LC3-II proteins get excited during photo-oxidative stress leading to the oxidation of ER subdomains

releasing CHOP or ATF4 proteins responsible for regulating autophagy-related Beclin-1, ATG5 and -12 proteins (Aniogo *et al*., 2021). A review done by Kou *et al.* (2017) reported PDT studies whereby the induced cell death was related to the activation of autophagy.

CHAPTER 3: MATERIALS AND METHODS

3.1 SYNTHESIS AND CHARACTERISATION OF CU(II)-THPP AND PD(II)-THPP METALLO-COMPLEXES

3.1.1 SYNTHESIS OF Cu(II)-THPP AND Pd(II)-THPP METALLO-COMPLEXES

p-Tetra(hydroxyphenyl)-porphine, 5,10,15,20-Tetrakis(4-hydroxyphenyl)-21H,23H-porphine (H_2THPP), copper (II) acetate and palladium (II) acetate were obtained as dry powders (Table 3.1), and 99.8% CHROMASOLV® absolute ethanol were obtained from Sigma Aldrich, USA and used for all experimental work.

Table 3.1 Summary of the compounds used in the synthesis of the PDT photosensitisers.

Compound	*Empirical formula*	*Molecular weight*	*Purity*
H_2THPP	$C_{44}H_{30}N_4O_4$	678.73 g/mol	95% dye content
Cu(II)-acetate	$C_4H_6CuO_4$	181.63 g/mol	98%
Pd(II)-acetate	$C_4H_6O_4Pd$	224.51 g/mol	99.98%

Cu(II)-THPP and Pd(II)-THPP complexes were synthesised (Figure 3.1) by reacting 1: 1.2 (w/w) ratio of H_2THPP with Cu(II)-acetate or Pd(II)-acetate metals in absolute ethanol, which had been dried over calcium hydride, passed through active silica, and stored in the presence of molecular sieves. Therefore, 50 mg H_2THPP was reacted with 16 mg Cu(II)-acetate or 19.8 mg Pd(II)-acetate respectively by placing the complexes in round bottom flasks and dissolving in 10 mL dry ethanol under agitation and >60°C heat. It was filtered using a 0.22 µm filter and left to evaporate under a vacuum at room temperature. Percentage dry mass yield for copper was 71%, and palladium was 82%. The compounds were stored in glass vials in the dark.

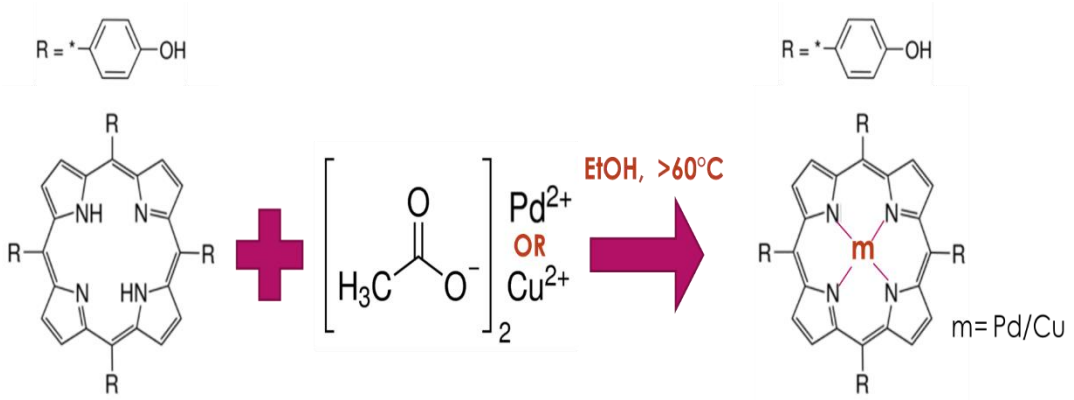

Figure 3.1 Schematic drawing of pTHPP and Cu(II)-acetate or Pd(II)-acetate reaction to produce Cu(II)-THPP or Pd(II)-THPP (structures obtained from Sigma-Aldrich).

3.1.2 PEG2000-PE ENCAPSULATION

1,2-distearoyl-sn-glycero-3-phosphoethanolamine-N-[methoxy(polyethylene glycol)-2000] (ammonium salt) (PEG2000-PE) was obtained from Avanti® Polar lipids, Inc (USA) as a dry powder and used to encapsulate the metal complexes. Dichloromethane (DCM) was obtained from SDS Votre Partenaire Chimie, and phosphate-buffered saline (PBS) was obtained as tablets from Sigma Aldrich, Germany.

From the prepared Pd(II)-THPP and Cu(II)-THPP product, 250 mg was weighed out and dissolved in 1 mL absolute ethanol. It was combined with 3.75 mg PEG2000-PE dissolved in 1 mL DCM at a 1:15 PEG2000-PE (DCM) to mTHPP (ethanol) ratio and left to react at room temperature. Following PEGylation of the compounds to enhance efficacy, the photosensitising compounds were dissolved in 1 mL 0.5X PBS solution and sonicated for 10 minutes. The complexes were stored in the dark at room temperature and used for all biological studies.

3.1.3 CHARACTERISATION OF THE CU(II)-THPP AND PD(II)-THPP METALLO-COMPLEXES

To confirm the incorporation of the metals into the H_2THPP core and ensure purity and activity of the Cu(II)-THPP and Pd(II)-THPP complexes, they were characterised using UV/Vis spectrophotometry and ^{1}H NMR spectroscopy.

3.1.3.1 Proton NMR characterisation

To confirm the binding of the Pd^{2+} and Cu^{2+} metals into the porphyrin ring, ^{1}H NMR spectroscopy was performed. Thirty (30) milligrams of the prepared Pd(II)-THPP and Cu(II)-THPP powders were dissolved in 99.5% hexadeuterodimethyl sulfoxide-d_6 (DMSO) (Sigma, USA) and analysed on a Bruker Ascend™ 500 MHz spectrometer. ^{1}H NMR spectra were analysed with the Bruker TopSpin® software.

3.1.3.2 UV/Vis spectrophotometry of the complexes

Verification of the complex's ability to absorb light around the 420 nm spectrum, UV/Vis spectrophotometric profiling was done. H_2THPP was encapsulated in PEG2000-PE as described in 3.1.2. Dilutions of 67X H_2THPP, Pd(II)-THPP and Cu(II)-THPP in 0.5X PBS were prepared. Spectral measurements were performed on the JASCO (USA) V-630 UV/Vis Spectrophotometer. The absorbance spectra were measured between 250-700 nm wavelength range.

3.2 CELL CULTURE

3.2.1 CULTURING HT-29 AND HEK-293 CELL LINES

Sterile conditions were ensured by the spraying and wiping of all surfaces and materials with 10% JIK and 70% ethanol in addition to ultraviolet treatment in the laminar. All glassware was autoclaved. Media and Hank's Balance Salt Solution (HBSS) were filter sterilized.

HT-29 (human colorectal adenocarcinoma) cell line was purchased from Cellonex (South Africa) and grown in McCoy's 5A (Modified) Medium with stable glutamine, and $NaHCO_3$ (PAN™ Biotech, Germany) supplemented with 10% foetal bovine serum [gamma-irradiated, heat-inactivated at 56°C, 30 min (Gibco™, Brazil)] and 0.6% Penicillin/streptomycin Amphotericin B (BioWhittaker®, USA) antibiotics. The HEK-293 (human embryonic kidney, CRL-1573) cell line was purchased from the American Type Culture Collection (USA) and maintained in Dulbecco's Modified Eagle's high glucose Medium ($NaHCO_3$) from Sigma Aldrich (USA) and supplemented with 0.1% Penicillin/streptomycin and 10% FBS. The cells were kept in a 37°C humidified 5% CO_2 incubator.

When the cells reached 90% confluency in the 75cm^2 NEST® flasks, they were sub-cultured by discarding old media and washed twice with 10 mL HBSS (Gibco, UK). They were trypsinized to dissociate from the flask in 5 mL of a 1% trypsin/0.1% versene (BioWhittaker, Belgium) solution and incubated for 5 minutes (HT-29) and 1 minute (HEK-293). The trypsin/versene solution was inactivated by adding 7 mL supplemented media and pelleted by centrifuging at 400xg for 4 minutes. Following resuspension in media, 200 µL of cells were returned to flasks with 20 mL supplemented media and incubated. Cells were utilised for experimentation from passages 2-5.

3.2.2 STOCKING AND STORAGE OF CELL LINES

HT-29 and HEK-293 stocks were resuspended in 90% Fetal Calf Serum (FCS) and 10% DMSO for cell culture (AppliChem, Spain) following centrifugation (section 3.2.1) and stored in the -80°C freezer until required for use.

3.3 EXPERIMENTAL CONDITIONS

3.3.1 COUNTING, SEEDING AND EXPERIMENTAL PREPARATION OF THE CELL LINES

Before experimentation, HT-29 and HEK-293 cell morphology was analysed using a Zeiss Axiovert inverted light microscopy. Cells were washed, trypsinized and

pelleted as per section 3.2.1 and resuspended in 3 mL supplemented media. A 1:1 dilution of cells to 0.4% Trypan Blue dye (Sigma Aldrich, UK) was made, and the cells were counted with an automated cell counter. Cells with 95-100% viability were seeded at 3 x 10^5 cells/mL concentration to a final concentration of 6 x 10^5 cells/mL onto NEST® 35 x 12 mm cell culture dishes. HEK-293 and HT-29 cells were given 24h and 48h respectively for adherence through incubation before experimentation.

3.3.2 CELLULAR LOCALIZATION STUDY

Visualization of uptake and localization of the photosensitizers within the cells was determined through autofluorescence studies. Seeded cells were plated on HistoBond® glass coverslips and treated with 80 µM Pd(II)-THPP-PEG2000-PE/Cu(II)-THPP-PEG2000-PE and left for 24h. The cells were washed in 1X PBS and fixed with 4% Formaldehyde (PBS, 20min, 37°C) (Sigma Aldrich, Netherlands). The cells were mounted on HistoBond® microscope slides using a 90% glycerol and 10% PBS mounting medium solution. Live-cell imaging at 400X magnification and autofluorescence was detected using the Zeiss Axioplan 2 light imaging microscope with an AxioCam HR camera. The number 15 filter of 546/12 nm band pass and Axiovision 4.7 software were used.

3.3.3 DARK TOXICITY STUDIES

Plated cells were treated with concentrations of the pegylated Pd(II)-THPP and Cu(II)-THPP ranging up to 10 µM to detect for unwanted dark toxicity in the absence of light irradiation. After 24h incubation, cell morphology was observed under an inverted light microscope, and an alamarBlue® dye reduction assay (described in section 3.4.3.1) was performed to assess cell viability.

3.3.4 IRRADIATION TOXICITY STUDY

A blue light diode laser at 405nm (Figure 3.2) rented from CSIR National Laser Centre was used to conduct PDT studies. The laser was set up, and the power output measured 120 mW and placed in a dark room. Cells were irradiated using energy dosages ranging from 0-10 J/cm^2 without THPP derivatives and incubated. Following the 24h incubation, cell viability and morphology were detected with the alamarBlue® reduction dye (described in section 3.4.3.1) and light microscopy, respectively.

Figure 3.2 Laboratory images of the 405nm blue light diode laser (provided by CSIR) used in PDT studies.

3.3.5 IC_{50} AND IC_{80} DETERMINATION FOR PD(II)-THPP AND CU(II)-THPP COMPLEXES

To determine the inhibitory concentration that would result in 50% (IC_{50}) and 20% (IC_{80}) cell viability, seeded cells were treated with Pd(II)-THPP and Cu(II)-THPP at concentrations ranging from 0-1 µM and incubated for 24 hours for cellular uptake of the photosensitizers. Old media was discarded, and new supplemented media was added. The cells were irradiated with 4 J/cm^2 energy dose and alamarBlue® reduction assay was performed after 24h incubation. Sigmoidal response curves

were plotted and analysed to determine IC_{50} and IC_{80} concentrations to be used for PDT studies.

3.3.5.1 Established PDT treatment conditions for Pd(II)-THPP

Once the IC_{50} and IC_{80} had been determined, the following treatment conditions were used for further experimentation: negative control of untreated cells, positive control that included 0.9 µM Pd(II)-THPP only and 4 J/cm^2 irradiation only, a low photosensitiser concentration PDT treatment comprising of 0.35 µM Pd(II)-THPP and 4 J/cm^2 and a high photosensitiser concentration PDT treatment of 0.9 µM Pd(II)-THPP and 4 J/cm^2.

Table 3.2 *Summary of established treatment conditions for Pd(II)-THPP*

Treatment	**Pd(II)-THPP**	**Irradiation**
Untreated Control	-	-
0.9 µM Pd(II)-THPP	0.9 µM	-
4J Irradiation	-	4 J/cm^2
0.35 µM Pd(II)-THPP PDT (IC_{50})	0.35 µM	4 J/cm^2
0.9 µM Pd(II)-THPP PDT (IC_{80})	0.9 µM	4 J/cm^2

3.4 BIOLOGICAL STUDIES

3.4.1 CELL MORPHOLOGY DETERMINATION

Live-cell samples were viewed 24 hours post-treatment to determine the morphology using the Perkin Elmer EVOS Floid® Cell Imaging System with Sony 1.3MP 1/3" ICX445 EXview camera, transmitted (relief phase) LED light and Floid® Cell Imaging Station Software at 100x magnification. Cellular morphology for dark and irradiation toxicity studies were taken with the Axiovert 25 inverted light microscope equipped with an AxioCam MRC camera and AxioVision v3.1 program.

3.4.2 PREPARATION OF TREATED CELLS FOR BIOLOGICAL STUDIES

Treated cell samples were washed in 1 mL HBSS, trypsinized with 500 µL 1% trypsin/versene solution and pelleted at 400 xg for 4 minutes. The supernatant was kept for further analysis while 600 µL of supplement media was added to the pelleted cells used for experiments.

3.4.3 INVESTIGATION INTO CELLULAR VIABILITY, CYTOTOXICITY, AND MITOCHONDRIAL ACTIVITY DETERMINATION

Assays used in the following studies included the alamarBlue® dye reduction assay kit purchased from Bio-Rad Laboratories, USA. The Celltiter-Glo® Luminescent Cell Viability Assay kit, CytoTox-ONE™ Homogenous Membrane Integrity Assay and Caspase-Glo® 3/7 were obtained from Promega Corporation, USA. The Trypan blue solution was obtained from Sigma-Aldrich, UK. The flow cytometric Muse® Oxidative Stress and Muse® Annexin V & Dead Cell kits were purchased from Millipore Merck, USA. Mitotracker® Orange CMTMRos dye was obtained from Life Technologies, USA, and anti-Cytochrome *c* (ab 154476) was purchased from Abcam Incorporated, USA. Hoechst-33258 pentahydrate was obtained from Invitrogen, USA.

The Guava® Muse® Cell Analyzer was obtained from Millipore Merck, USA installed with Muse®1.5 Analysis software. The Victor® Nivo™ Multimode plate reader with MyAssays Desktop Pro analysis software was obtained from Perkin Elmer, USA.

3.4.3.1 Cellular viability determination

To determine cellular homeostatic activity, an alamarBlue® dye reduction assay was performed. On a 96-well black opaque plate, 100 µL of the prepared treated cells were pipetted to 10 µL alamarBlue® reduction dye and incubated (2h, 37°C, dark). Fluorescence using 530/30 nm excitation and 580/20 nm emission filters was recorded on the Victor® Nivo™ Multimode plate reader.

3.4.3.2 Cell membrane integrity determination

Cell membrane integrity was tested for by treating the cells at a 1:1 ratio with the Trypan blue dye exclusion assay (0.4% Trypan Blue/ 0.81% NaCl) and counted under the Zeiss Axiovert inverted simple light microscope using a haemocytometer where live cells remained clear, and membrane compromised cells were stained blue.

3.4.3.3 Lactate dehydrogenase as an indicator for cytotoxicity

One indication of cytotoxicity is a compromised cell membrane releasing lactate dehydrogenase into surrounding media, allowing for the CytoTox-ONE™ Homogenous Membrane Integrity Assay to be used. Twenty-five (25) microliters of the treated cell-free media was added into 96-well black opaque plate. An untreated control plate was included to enumerate the possible maximum LDH release by treating the cells with 10 µL Lysis solution (10 % Triton X-100) for an hour. An equivolume of the LDH substrate from the kit was added and incubated (25°C, 12 minutes, dark). The reaction was ended with 12.5 µL Stop solution supplied in the kit and fluorescence was recorded at 530/30 nm excitation and 580/20 nm emission on the Victor® Nivo™ Multimode plate reader.

3.4.3.4 Mitochondrial activity determination

To ascertain ATP production levels and consequently mitochondrial activity within the cells, a Celltiter-Glo® Luminescent Cell Viability Assay kit was used. From the prepared cells, 25 µL was pipetted onto a 96-well plate. An equivolume of the kit's substrate solution was added to the cells and left at room temperature under constant agitation for 10 minutes in the dark. Luminescence was recorded using the 700nm blocker filter on the Victor® Nivo™ Multimode plate reader.

3.4.3.5 Mitochondrial, cytochrome c subcellular localization and nuclear change

Localization of active mitochondria and cytochrome *c* proteins was determined post treatment by labelling with the Mitotracker® Orange CMTMRos dye and anti-Cytochrome *c* (ab 154476) antibodies, respectively. Chromatin formation and sequent DNA damage was detected using Hoechst-33258 stain. Cells were plated onto 20 x 20 mm coverslips and grown over 48h to develop a cell monolayer. The cells were treated with the predetermined PDT treatment conditions. Following treatment, the cells were incubated with 100 nM Mitotracker® Orange probe for 30 minutes at 37°C. The cells were washed twice with warm 1X PBS and fixed with 4% formaldehyde for 20 minutes (37°C). After washing with PBS, cells were treated with 2 mL 0.1% Triton X-100 and placed in the fridge (4°C, 20 minutes) for permeation and then 1% BSA (Tween-20 & PBS, pH7) blocking buffer was added and incubated at room temperature for 30 minutes. 0.25 µg/mL anti-cytochrome *c* antibody (ab154476) was added and incubated for an hour at 25°C. The cells were washed three times and labelled with 1 µg/mL Hoechst-33258 (PBS) for 20 minutes and then the coverslips were mounted using mounting medium (90% glycerol: 10% PBS) onto glass microscope slide and sealed with clear nail varnish. The slides were viewed under an Axioplan 2 Imaging light microscope with AxioVision 4.7 software. An AxioCam HR camera was used with filter no 15 (Ex. 546/12 nm) to observe the Mitotracker® labelled mitochondria. Anti-Cytochrome *c* antibody-labelled proteins were viewed using Alexa 488 filter set no. 09 (Ex. 470/40 nm) and Hoechst-33258 stained nuclei were viewed using filter no. 01 (Ex. 365/12 nm). All cell pictures were taken at 400X magnification.

3.4.3.6 Reactive oxygen species production

Quantification of reactive oxygen species (superoxide anions) production in cell populations enduring oxidative stress was done following the Muse® Oxidative Stress Kit instructions. After 3h post treatment, 1 x 10^5 cells/mL were added to 500 µL 1X PBS solution and pelleted at 400xg for 4 minutes. The supernatant was discarded, and 100 µL of warm kit assay buffer was added. A prewarmed working

solution provided by the kit of 190 µL was added to 10 µL cell sample and incubated (30 minutes, 37°C). The samples were analysed on the Muse® Cell Analyzer using the Muse® Oxidative Stress programme following the kit's user guide.

3.4.3.7 Caspase 3/7 activity determination

To determine caspase 3/7 activity, a luminescent enzyme activity Caspase-Glo® 3/7 assay was used. Equivolume (25 µL) treated cells and Caspase-Glo® 3/7 reagent prepared according to manufacturer's instruction were added into a 96 well plate and incubated for an hour at 37°C. Luminescence was measured on the Victor® Nivo™ Multimode plate reader using the 700nm blocker filter.

3.4.4 INVESTIGATION OF NUCLEAR ACTIVITY AND CELL DEATH MARKERS

Assays used in the following nuclear and cell death studies were the Muse® Annexin V & Dead Cell kit obtained from Luminex Corp, USA and the Propidium Iodide (PI) Cell cycle assay kit was obtained from Sigma Aldrich, USA.

3.4.4.1 Annexin V cell death assay

Quantitative analysis of live, apoptotic, and necrotic/dead cells was done using the flow cytometric Annexin V & Dead Cell kit. Treated cells were pelleted and resuspended in 1 mL warm PBS. 1 x 10^5 cells/mL were washed in 500 µL PBS and centrifuged at 400xg for 4 minutes. The supernatant was removed. Twenty-five (25) µL of prewarmed 1X assay buffer and 25 µL of the Annexin V & Dead Cell reagent from the kit were added to the cells according to the manufacturer's instruction and incubated for 25 minutes at room temperature in the dark. After incubation, 50 µL 1X Assay buffer and 50µL cells were added into a tube, mixed by vortexing and run on the Guava® Muse® Cell Analyzer using the Annexin and Dead cell programme. A necrotic H_2O_2 control was also prepared for comparison by

treating seeded 3 x 10^5 cells/mL with 50% H_2O_2 (ACE Chem, RSA) 24 hours before analysis.

3.4.4.2 Cell cycle analysis

The flow cytometric propidium iodide (PI) dye intercalates between DNA and allows for the detection of the cell cycle phases within cells. This stain was used on the HT-29 cells post-treatment conditions. Cells were fixed by addition of 1 mL 70% ethanol and incubation (2 hours, 25°C). The cells were pelleted at 300xg for 5 minutes and after decanting the ethanol, a prepared 100 µL PI staining solution (0.1% Triton X-100, 100 µg/mL DNase-free RNase A in PBS & 20 µg/mL PI) was added and incubated for 30 minutes in the warm bath (37°C). Following incubation, 500 µL of a 1X binding buffer from the kit was added. The samples were run on a BD Accuri™ C6 flow cytometer (BD Biosciences) and analysed with BD Accuri™ C6 Software. The analysing parameters were set to run 30 000 events and the dot plots were gated to only count singlets. Corresponding histograms indicated DNA profiles and were plotted PI-A (x-axis) vs Count (y-axis).

3.5 SCREENING OF PD(II)-THPP ON NORMAL HEK-293 CELL LINE

The effects of Pd(II)-THPP were screened for cytotoxicity on the normal human embryonic kidney cell line. The cells were grown and seeded as described in 3.2.1 and 3.3.1, respectively. The cells were treated with similar conditions as the HT-29 cells: an untreated control, 0.9 µM Pd(II)-THPP only, 4J irradiation only, 0.35 µM Pd(II)-THPP PDT, 0.9 µM Pd(II)-THPP PDT and a PEG-vehicle control. Cellular morphology was observed 24 hours post-PDT treatment as described in 3.4.1, and viability was determined using the alamarBlue® reduction dye assay described in 3.4.3.1.

3.6 STATISTICAL ANALYSIS

Statistical analyses of the results was performed using Microsoft Excel. For all experiments performed, three biological replicates of HT-29 adenocarcinoma cells were used. For each biological replicate, two technical repeats were recorded and averaged (n=6). The results were then normalized to the percentage of the untreated control. Results are recorded as mean ± standard deviation. Error bars were drawn from the standard error of the mean. For the flow cytometric ROS, Annexin V, and Cell Cycle experiments, three biological repeats with one technical repeat each were conducted (n=3). The student's t-tests with two-tailed distribution were performed for statistical analysis. Groups were compared to the untreated control for significance. $P < 0.05$, $p < 0.01$ and $p < 0.001$ were used to describe the degrees of significance, with $p < 0.001$ showing greater significance.

CHAPTER 4: RESULTS

4.1 CHARACTERISATION OF CU(II)- AND PD(II)-THPP COMPLEXES

Cu(II)-acetate and Pd(II)-acetate were reacted with H_2THPP in ethanol to create Cu(II)- and Pd(II)-THPP photosensitisers. UV/Vis spectrophotometry and ^{1}H-NMR spectroscopy were performed to confirm the incorporation of the metals into the porphyrin ring structures. Porphyrin ring structures exhibit intense Soret bands in the 380-500nm and less intense Q bands within the 500-750nm range (Giovannetti, 2012). The UV/Vis spectra of Pd(II)- and Cu(II)-THPP (Figure SR1) display visible intense Soret bands in the 400-450nm range with a slight shift to the left compared to the H_2THPP as expected with the coordination of metals within the THPP core. Weaker Q bands are also noticeable in the 500-700nm range. Therefore, the presence of the Soret and Q bands confirm the absorption of 405nm blue irradiation light by the photosensitisers taken up by the HT-29 cells.

The metal coordination of Pd(II) and Cu(II) into the freebase H_2THPP core was further confirmed by ^{1}H-NMR. Freebase H_2THPP, Pd(II)-THPP and Cu(II)-THPP was dissolved in deuterated DMSO and analysed on the Bruker Ascend 500MHz spectrometer. The downfield chemical shifts on the 7-10 ppm range represent the aromatic proton signals. When comparing H_2THPP to Pd(II)-THPP and Cu(II)-THPP (Figure SR2), these signals remain, indicating that the porphyrin ring remains intact. In the upfield region at -2.83 ppm, the N-H peak present in H_2THPP disappears on the Pd(II)- and Cu(II)-THPP spectra, symbolising the incorporation of the metals into the core through the replacement of the NH protons with the metals. The disappearance of the peak is the distinguishing feature of metalloporphyrin formation (Al Neyadi *et al.*, 2019).

4.2 OPTIMISATION STUDIES

4.2.1 INTRACELLULAR LOCALISATION OF Cu(II)-THPP AND Pd(II)-THPP COMPLEXES WITHIN THE HT-29 ADENOCARCINOMA

For photodynamic therapy to be fully effective, three components need to work together to induce cytotoxicity. These are light, oxygen and a photoreactive substance. These, however, need to only react in combination but remain harmless individually. In this study, metal-incorporated porphyrin photosensitisers, Pd(II)-THPP and Cu(II)-THPP, were encapsulated with PEG2000-PE and tested for PDT efficiency.

HT-29 colorectal adenocarcinoma cells were first treated with a maximum of 80µM Pd(II)-THPP/Cu(II)-THPP to determine intracellular localisation (Figure 4.1). Following a 24-hour incubation, photosensitiser autofluorescence was visualised using fluorescence microscopy. Both photosensitisers emitted autofluorescence showing cellular uptake and concentration within the cells. The inserts magnifying the pointed cells give a clearer picture that both Pd(II)-THPP and Cu(II)-THPP are taken up into the HT-29 colorectal adenocarcinoma cells by the intense autofluorescence emitted by the photosensitisers. From the fluorescence distribution pattern within the cells, it can be deduced that both photosensitisers localise in the cytosol and the nucleus. No assays were performed to determine the exact organelles, but previous studies of porphyrin derivatives with cationic species assume mitochondrial, lysosomal and endoplasmic reticulum localisation (Sibrian-Vazquez *et al*., 2008).

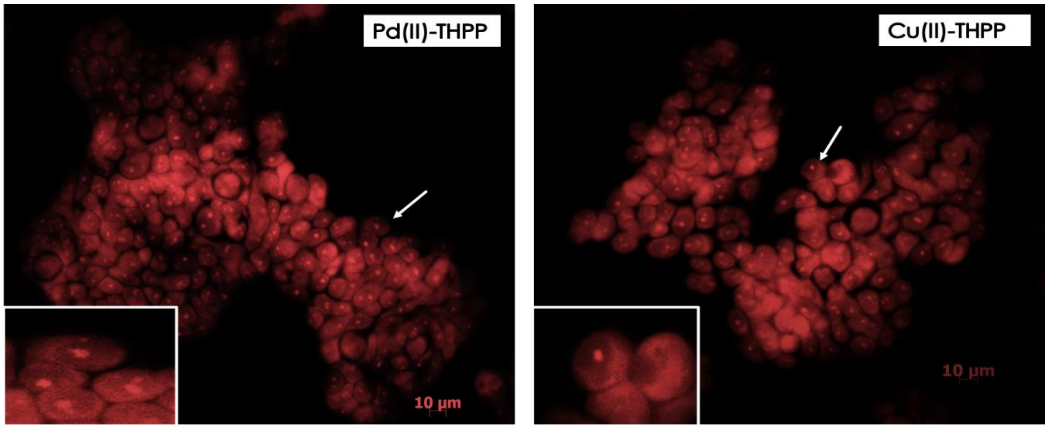

Figure 4.1 Pd(II)-THPP and Cu(II)-THPP localisation in HT-29 colorectal adenocarcinoma. Cells were treated with 80 µM photosensitiser and visualised under the AxioPlan 2 imaging light microscope with AxioVision 4.7 software and number 15 (546/12 nm) filter at 400X magnification.

4.2.2 INVESTIGATING CU(II)-THPP AND PD(II)-THPP DOSAGES FOR UNWANTED DARK TOXICITY AND IRRADIATION TOXICITY

To show that the photosensitisers and irradiation alone were indeed harmless to the HT-29 adenocarcinoma cells, dark toxicity and irradiation toxicity were investigated. Cells were treated with 2, 4, 6, 8 and 10 µM Pd(II)-THPP/ Cu(II)-THPP only and cell viability was measured with a fluorescence alamarBlue® reduction dye assay. Morphology observed under an inverted light microscope (Figure 4.2A, B) remained consistent with the untreated control cells for both Pd(II)-THPP and Cu(II)-THPP. The cells retained standard shape and confluency despite increasing photosensitiser concentrations. Cellular viability (Figure 4.2C) of Cu(II)-THPP treated cells had no significant change in comparison to the untreated control, only observing a slight increase at 2 µM averaging 139.8% and 145.2% at 4 µM, whereas Pd(II)-THPP showed significant ($p<0.001$) proliferation on all concentrations of the photosensitiser. The highest increase is seen at 6 µM, where it reached 248.6%, and 8 µM had the lower average of 234.3%.

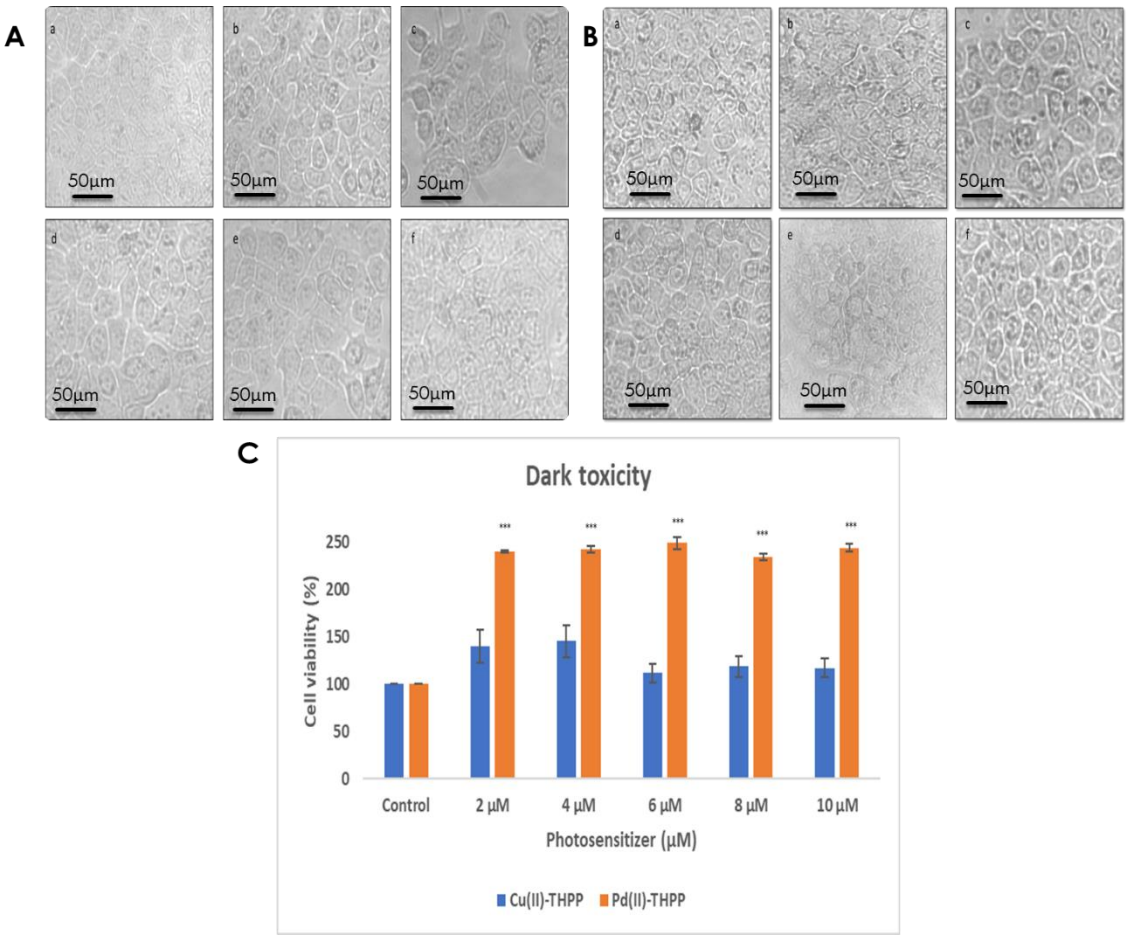

Figure 4.2 Cellular morphology study of HT-29 colorectal adenocarcinoma treated only with **A** Pd(II)-THPP and **B** Cu(II)-THPP concentrations ranging from a) 0µM (Untreated control), b) 2 µM, c) 4 µM d) 6 µM e) 8 µM and f) 10 µM. Images were taken on AxioVert 25 inverted light microscope at 20X magnification. **C** Dark toxicity of Pd(II)-THPP and Cu(II)-THPP determined using alamarBlue® dye reduction assay. (n=6, error bars are ±SEM) (***p<0.001)

Unwanted irradiation toxicity from the 405nm blue diode laser was detected by treating the cells with light energy dose concentrations of 2-10 J/cm^2. Cell viability was measured after 24 hours with alamarBlue® reduction dye assay. Morphology (Figure 4.3A) did not change compared to the untreated control. The cells remained attached and retained confluency and shape, showing healthy status. Cellular viability (Figure 4.3B) remained high but slightly decreased to 85.7%,

91.9%, 84.3%, 86.2% and 97.7% at 2,4,6,8,10 J/cm^2 respective light doses. Based on the results obtained and the intention to use a low irradiation concentration that still yields a high viability count, 4J/cm^2 was selected for further experimentation.

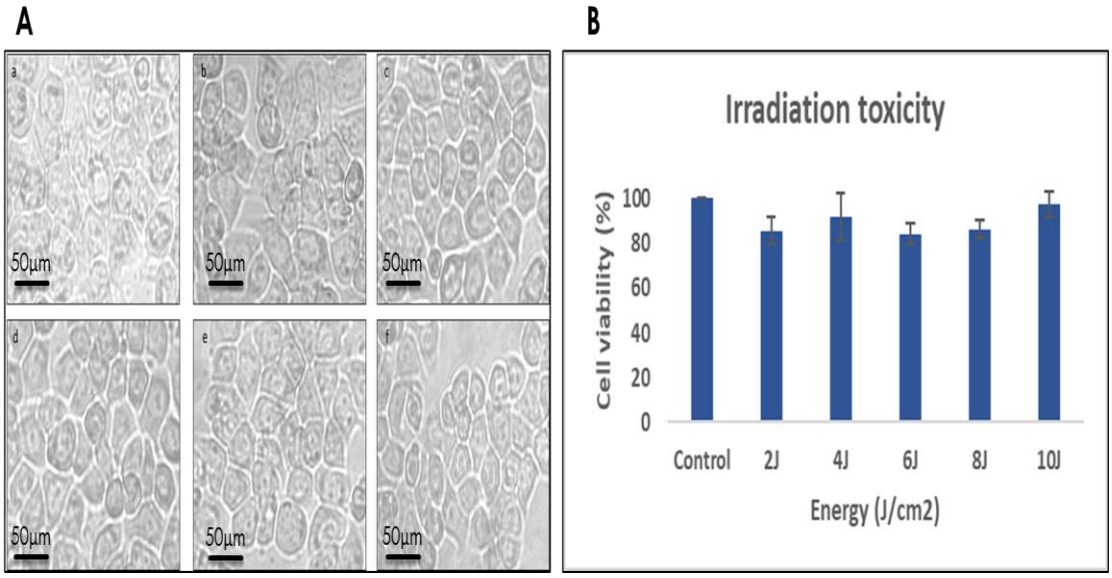

Figure 4.3 A Light microscopy images of HT-29 colorectal adenocarcinoma cells following a) no irradiation, b) 2 J irradiation, c) 4 J irradiation, d) 6J irradiation, e) 8 J irradiation, and f) 10 J irradiation with a 405nm laser at 20X magnification. **B** Viability study of irradiation toxicity 24 hours post-exposure to 405nm blue light diode laser using alamarBlue® dye reduction assay. (n=6, SEM)

Having evidence that Cu(II)-THPP/Pd(II)-THPP and irradiation are independently non-cytotoxic to HT-29 adenocarcinoma cells, the following step was to determine PDT conditions that induced cell death.

4.2.3 PD(II)-THPP IC_{50} AND IC_{80} DETERMINATION

To establish the 50% (IC_{50}) and 80% (IC_{80}) maximal inhibitory concentrations for Pd(II)-THPP, seeded HT-29 cells were treated with 0.1-1 µM concentrations and incubated overnight. Light irradiation with a 4 J/cm^2 energy dose followed. After

24 hours, an alamarBlue® reduction dye assay was done to determine mitochondrial activity. A sigmoidal dose-response curve (Figure 4.4) was then plotted, and the trendline equation was used to determine the IC_{50} and IC_{80} values. Pd(II)-THPP treated cells displayed a decline in mitochondrial activity in a dose-dependent manner. The low dose [IC_{50}] was 0.35 µM, and the high dose

[IC_{80}] was 0.9 µM at 4J/cm^2 light irradiation. Conditions are summarised in Table 4.1, which were utilised for further PDT experimentation.

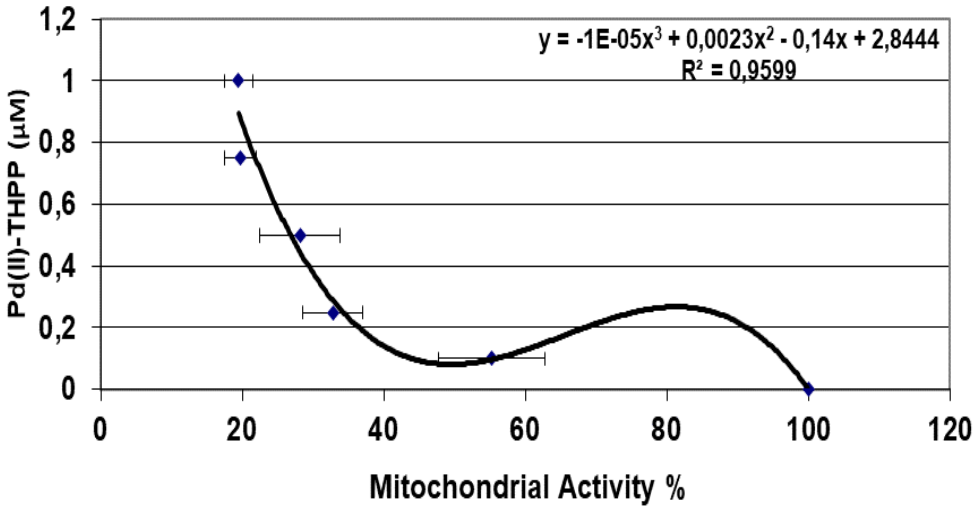

Figure 4.4 Sigmoidal polynomial curve plotted after treating HT-29 adenocarcinoma with 0.1 µM, 0.25 µM 0.5 µM 0.75 µM and 1 µM Pd(II)-THPP and 4 J/cm^2 irradiation fluency to obtain IC_{50} and IC_{80} values. (n=6, error bars ±SEM). Mitochondrial activity determined with alamarBlue® reduction dye assay.

Table 4.1 Determined treatment conditions used in Pd(II)-THPP PDT studies with low IC_{50} and high IC_{80} dose concentrations at 4 J/cm^2.

Treatment	**Pd(II)-THPP**	**Irradiation**
Control	-	-
Pd(II)-THPP	0.9 µM	-
Irradiation	-	4 J/cm^2
[IC_{50}] PDT	0.35 µM	4 J/cm^2
[IC_{80}] PDT	0.9 µM	4 J/cm^2

4.3 CU(II)-THPP IC_{50} AND IC_{80} DETERMINATION.

Once Pd(II)-THPP inhibitory conditions were established, comparative Cu(II)-THPP concentrations were determined. HT-29 colorectal adenocarcinoma cells were treated with varying increasing concentrations of Cu(II)-THPP. Following 24 hours, the cells were irradiated at 4 J/cm^2. An alamarBlue® dye reduction assay determined the mitochondrial activity within the cells to obtain [IC_{50}] and [IC_{80}] values.

After multiple attempts with varying Cu(II)-THPP concentrations, a dose-dependent trend of cellular death could not be established. Cu(II)-THPP treated cells with 4 J/cm^2 irradiation displayed stimulatory trends of increased viability. Figure 4.5 shows cells treated with 0.1, 1, 2 and 4 µM Cu(II)-THPP displayed increased viability. The sigmoidal dose-response curve equation obtained very high concentrations, which were impractical (summarised in Table 4.2). Upon conclusion that Cu(II)-THPP with irradiation does not induce cell death in HT-29 colorectal cancer cells, only Pd(II)-THPP PDT studies were continued.

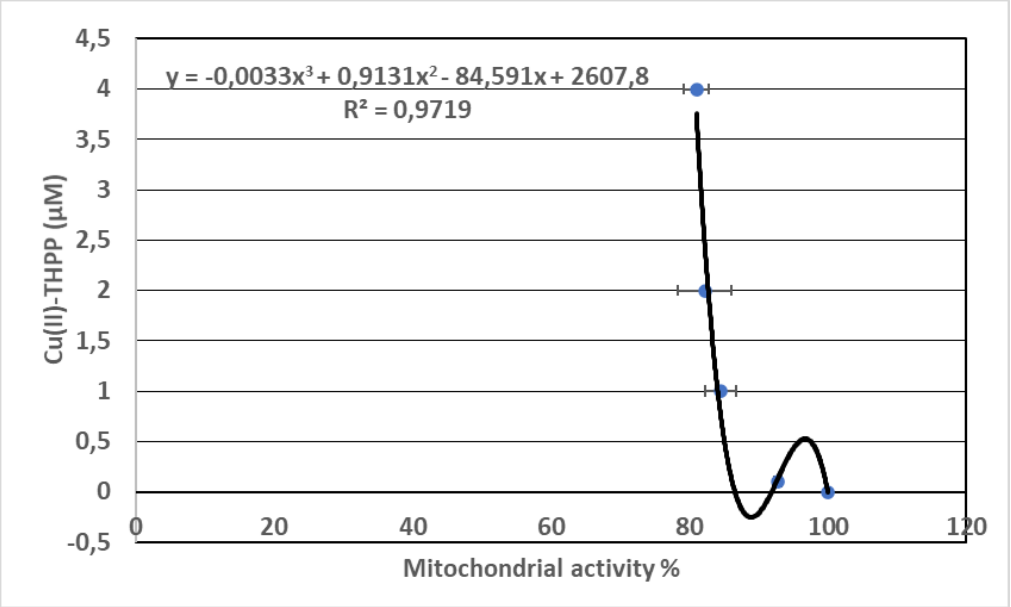

Figure 4.5 Sigmoidal polynomial curve determining Cu(II)-THPP IC_{50} and IC_{80}. Mitochondrial activity was measured with alamarBlue® reduction dye assay after treating HT-29 cells with concentrations of Cu(II)-THPP and 4 J/cm^2 irradiation fluency. (n=6, error bars drawn from SEM)

Table 4.2 Cu(II)-THPP treatment conditions determined by the sigmoidal polynomial curve equations at 4 J/cm^2 irradiation.

Treatment	**Cu(II)-THPP**	**Irradiation**
Control	-	-
Cu(II)-THPP	4638.46 µM	-
Irradiation	-	4 J/cm^2
Low [PDT]	8707.6 µM	4 J/cm^2
High [PDT]	4638.46 µM	4 J/cm^2

4.4 PHOTODYNAMIC THERAPY WITH PD(II)-THPP AS A PHOTOSENSITISER ON HT-29 ADENOCARCINOMA

4.4.1 CELLULAR VIABILITY AND MEMBRANE INTEGRITY POST PDT TREATMENT DECLINES

Photodynamic therapy was carried out *in-vitro* on HT-29 colorectal adenocarcinoma cells with Pd(II)-THPP. Treatment conditions used on the cells following maximal (IC_{50} and IC_{80}) inhibitory condition studies were determined as follows: an untreated cell control group with no Pd(II)-THPP nor irradiation, dark toxicity control of 0.9 µM Pd(II)-THPP only, an irradiation toxicity control of 4 J/cm^2 only, PDT treatments were 0.35 µM Pd(II)-THPP (IC_{50}) + 4 J/cm^2 irradiation and 0.9 µM Pd(II)-THPP (IC_{80}) + 4 J/cm^2. The cells were given 24 hour period before the experiments were performed.

Cellular morphology of PDT treated cells was visualised using the Floid® cell imaging system 24 hours post-treatment. HT-29 cells are epithelial, forming a typical tightly packed monolayer attaching to the Petri dish's surface. The control cells displayed normal confluent morphology. Cells treated with 0.9 µM Pd(II)-THPP and 4 J/cm^2 irradiation emulated the healthy untreated control cells. PDT treated cells began indicating signs of cell damage and stress. From the 0.35 µM Pd(II)-THPP PDT cells, evidence of detachment and membrane blebbing (orange arrow) could be seen. Complete detachment from the substrate and each other, swelling and rounding could be seen in 0.9 µM Pd(II)-THPP PDT cells with chromatin condensation (black arrow). In contrast, others displayed shrinkage, a combination of apoptotic and necrotic cells.

Trypan blue dye exclusion assay was employed as a means to determine cellular viability 24 hours post PDT. The percentages are presented in Figure 4.6 with standard deviation after physical heamocytometric count. The dye stains dead or membrane compromised cells while viable cells remain clear. Untreated control cells maintained high viability of 99%. Pd(II)-THPP and irradiation toxicity study

cells also had high viability of 97% and 99%, respectively, showing healthy and intact membranes. The viability of PDT treated cells decreased in a dose-dependent manner declining from 36% at 0.35 µM Pd(II)-THPP PDT to 11% at 0.9 µM Pd(II)-THPP PDT, indicating stress and compromised cell membranes.

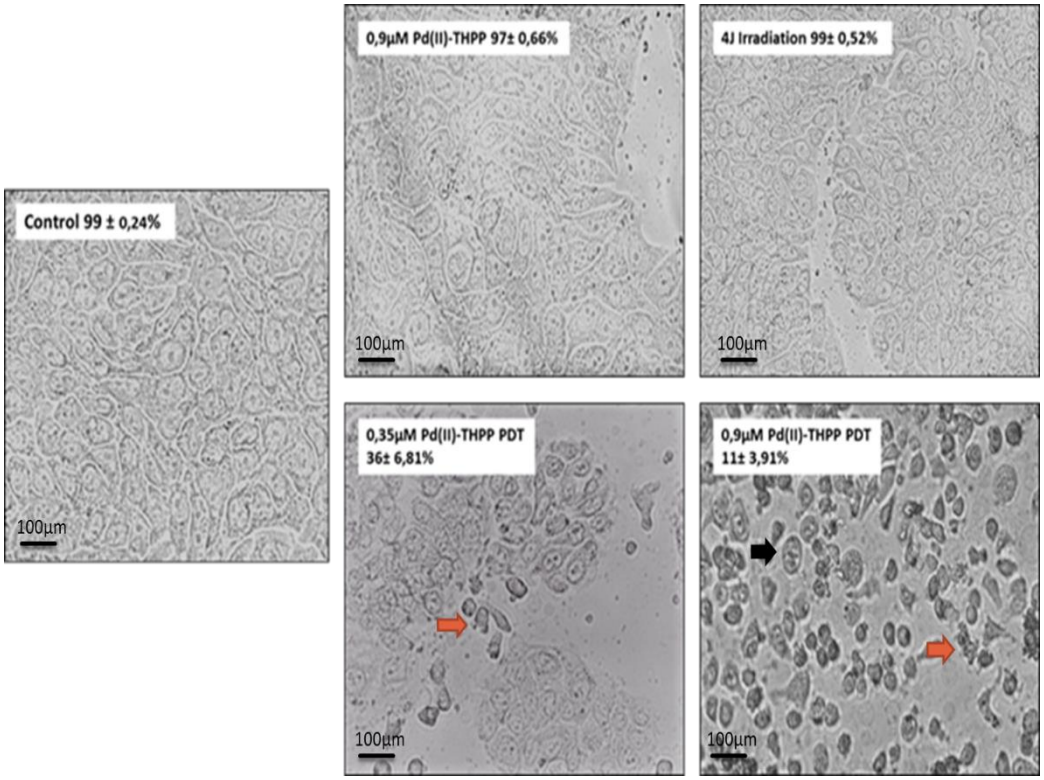

Figure 4.6 Cell morphology images of PDT treated HT-29 adenocarcinoma cells taken with the Floid® Cell Imaging System and cell viability determined using the Trypan Blue dye exclusion assay. (n=3, Mean±SD)

Cellular homeostasis and metabolic activity were determined by measuring mitochondrial activity with an alamarBlue® dye reduction assay, and membrane integrity was further examined with a CytoTox-ONE™ Homogenous Membrane Integrity Assay and Annexin V and Dead cell assay. Mitochondrial activity (Figure 4.7) was normalised to the untreated control cells. 0.9 µM Pd(II)-THPP treated cells

remained consistent with previously dark toxicity tested cells (Figure 4.2C). Viability showed a significant ($p<0.001$) stimulatory effect by the photosensitiser averaging 167.8%. In contrast, cells treated with irradiation only were comparable to control cells at 106.1% viability. PDT treated cells were stressed, and homeostasis was disrupted. Metabolic activity decreased in a dose-dependent manner for PDT treated cells. Low dose PDT had a less significant ($p<0.05$) decrease to 51.8%, whereas the high dose PDT had a more significant ($p<0.01$) decrease to 24.8% activity.

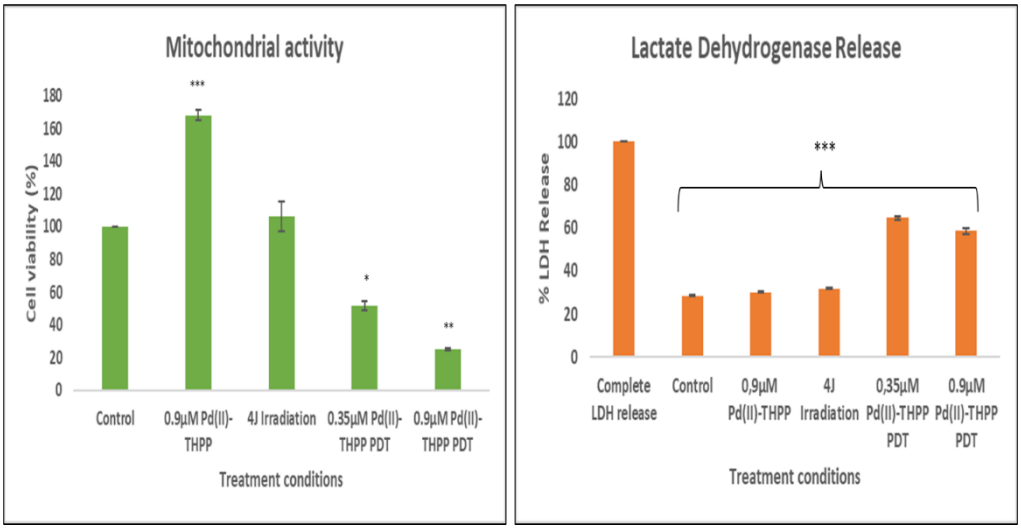

Figure 4.7 Mitochondrial activity of PDT treated HT-29 colorectal adenocarcinoma determined by the alamarBlue® dye reduction assay and the determination of Pd(II)-THPP cytotoxicity using the CytoTox-ONE™ Homogenous Membrane Integrity Assay. (P<0,05* P<0,01** P<0,001 *** n=6, SEM)

Cytosolic lactate dehydrogenase release into the media was quantified as a cytotoxicity measure (Figure 4.7). The loss of membrane integrity and consequent LDH release is a characteristic of necrotic cell death. Complete LDH release from HT-29 cells was instigated by treating the cells with 10% Triton X-100. The average percentages were normalised to complete release. All the controls (untreated

cells, Pd(II)-THPP and irradiation only) had significantly ($p<0.001$) low LDH release of 28.6%, 30.1%, and 31.8% in comparison to the LDH release control, whereas PDT treated cells had a significant ($p<0.001$) amount of cytosolic LDH detected. Low dose PDT had more LDH averaging 64.6%, and the high dose had a slightly lower percentage at 58.7%. The high LDH content in the media due to ruptured membranes confirms PDT cytotoxicity on the HT-29 adenocarcinoma.

4.4.2 PDT PRODUCES ROS CAUSING A DECREASE IN ATP AND CASPASE RELEASE

ROS production during PDT mediates cytotoxicity (Bretin et al., 2019) by inducing oxidative stress and cell death. Therefore, intracellular ROS was captured 3 hours post PDT treatment due to its short lifespan using the flow cytometric Oxidative Stress Kit (Figure 4.8). The assay reagent contains DHE (dihydroethidium) that permeates cell membranes and reacts with cytosolic superoxide anions producing ethidium bromide, which intercalates between the cell DNA. DHE fluoresces blue, but once it oxidises to ethidium bromide, it fluoresces red allowing detection (Tang *et al.*, 2007; Zanetti *et al.*, 2005). Histograms are a single representation of 3 biological repeats where M1 is the percentage of counted ROS negative activity and M2 is ROS positive activity within the cell population. The bar chart shows the calculated averages of ROS activity for each treatment. Untreated HT-29 cells and cells treated with Pd(II)-THPP and irradiation only had higher ROS negative activity (blue), averaging 95,97%, 80.59%, and 95.63%, respectively, with very little 3.98%, 19.27% and 4.03% ROS positive activity. Treatment of HT-29 cells with Pd(II)-THPP PDT produced significantly ($p<0.001$) higher ROS positive activity (red) averaging 52.19% and 61.73% in 0.35µM Pd(II)-THPP and 0.9µM Pd(II)-THPP PDT respectively, whereas ROS negative activity was at 47.3% and 37.99%.

ROS activity disrupts cellular membranes, including mitochondrial membranes and subsequent oxidative phosphorylation pathways. Intracellular respiration via ATP was quantified using a Celltiter-Glo® Luminescent Cell Viability Assay kit 24

hours after PDT treatment (Figure 4.8). The averages were normalised to the untreated control. ATP levels were considerably high in Pd(II)-THPP treated cells at 99.5% and 107.2% in 4 J/cm^2 irradiation treated cells. PDT treated HT-29 cells had significantly ($p<0.001$) lower amounts of ATP produced. Low-dose PDT produced 16.4% ATP and high-dose PDT produced 2.6% ATP. Mitochondrial activity and cellular respiration studies, therefore, correlate in confirming cell stress.

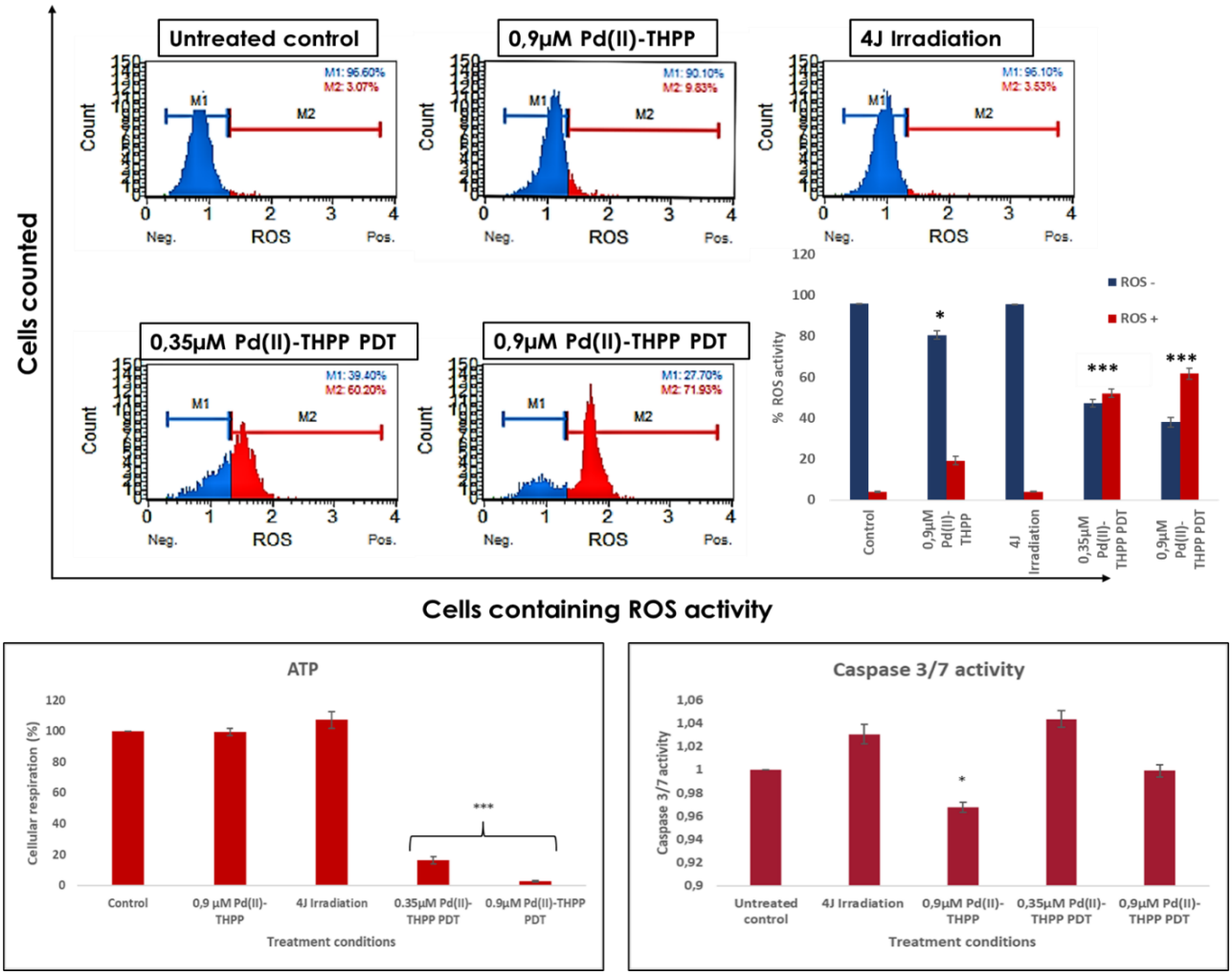

Figure 4.8 Confirmation of ROS production in PDT treated cells using the flow cytometric Muse® Oxidative Stress Kit 3 hours post-treatment and ATP quantification using the luminescence CellTiter-Glo™ Cytotoxicity Assay. Caspase 3/7 expression was quantified using

the luminescent Caspase-Glo® 3/7 assay. (P<0,05* P<0,001***, ROS activity n=3; histogram single representation, ATP, and Caspase 3/7 n=6. Error bars= SEM).

Caspases 3 and -7 are effector caspases and play critical roles in the apoptotic pathway. Active caspase 3 and -7 activity in relation to the untreated control was evaluated using the Caspase-Glo® 3/7 kit 24 hours post-PDT treatment. Quantified expression was averaged for each treatment and normalised to a ratio on the control. Figure 4.8 indicates that cells treated with 4 J/cm^2 irradiation only and low dose PDT had a positive change in caspase 3/7 expression at 1.03 and 1.04 (relative fluorescence levels of activity). Cells treated with 0.9 µM Pd(II)-THPP had minor caspase expression. 0.9 µM Pd(II)-THPP had a significant ($p<0.05$) expression level of 0.97, while high dose PDT had no change in respect to the untreated control. The small changes in caspase expression levels lead to an assumption of an alternative apoptotic pathway that excludes caspase dependence.

To visualise active mitochondria and cytochrome *c* proteins, HT-29 adenocarcinoma cells were grown over glass coverslips and treated with high 0.9 µM and low 0.35 µM Pd(II)-THPP and 4 J/cm^2 irradiation (PDT), including the negative controls. The cells were then stained with Mitotracker Orange™ CMTMRos fluorescence dye to label active intracellular mitochondria, and cytochrome *c* proteins were labelled using anti-cytochrome *c* (ab154476) antibodies. The cells were fixed onto microscope slides and visualised using the AxioPlan 2 Imaging light microscope. Figure 4.9 shows the mitochondria (red) in the cytosol surrounding the nucleus in the untreated control and 0.9 µM Pd(II)-THPP and 4 J/cm^2 irradiation controls. Both Pd(II)-THPP PDT doses show no distinct active mitochondria although stained by the dye. Cytochrome *c* proteins can be seen co-localising in the active mitochondria in all the controls by observing the yellower tones in the cell images. Pd(II)-THPP PDT induces cytochrome *c* release

from the mitochondria, indicating pro-apoptotic stimuli. A closer observation also shows some cytochrome *c* within the nuclear area.

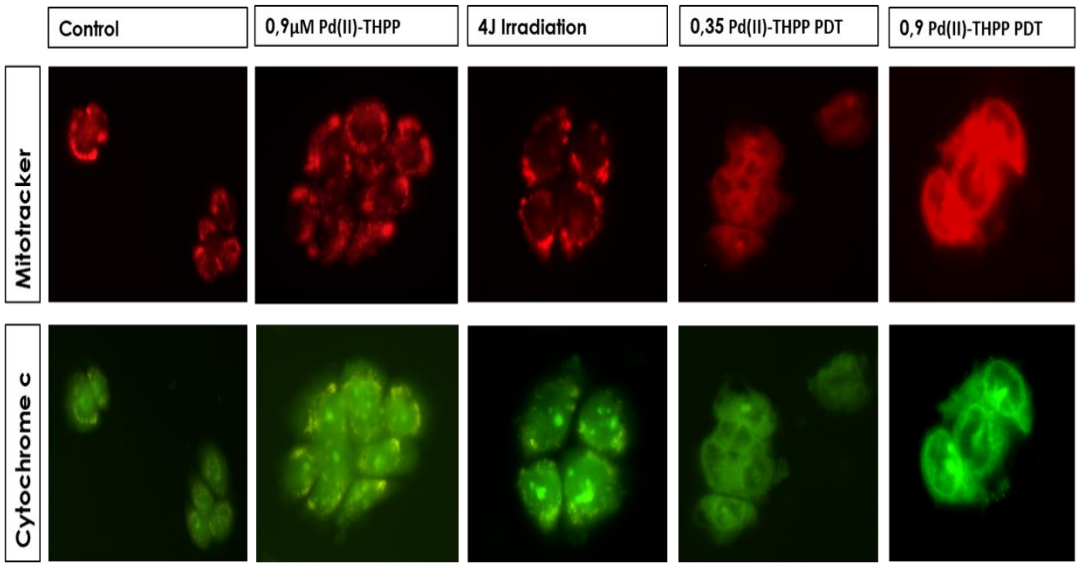

Figure 4.9 Microscopic visualisation of active mitochondria in PDT treated HT-29 adenocarcinoma labelled with Mitotracker Orange CMTMRos dye and detection of cytochrome *c* release using anti-cytochrome *c* (ab154476) labelling. Mitotracker Orange-Filter 15 Ex 546/12 nm and Cytochrome *c*- Filter 09 Ex 470/40 nm were used at 400X magnification.

4.4.3 PD(II)-THPP PDT INDUCES APOPTOSIS AND CELL CYCLE ARREST IN HT-29 COLORECTAL CELLS

Cellular markers for apoptotic stages and necrosis in HT-29 adenocarcinoma after photodynamic therapy were quantitatively analysed using the flow cytometric Muse Annexin V & Dead cell assay. Annexin-V detects and quantifies exposed phosphatidylserine on cell membranes of cells. This translocation of the phosphatidylserine to the outer surface is an early apoptosis indicator (Harmse *et al.*, 2015). The cells going through the flow cytometric analysis (Figure 4.10) were separated into four cell populations: live cells (lower left quadrant), early

apoptotic cells (lower right quadrant), late apoptosis/dead (upper right quadrant) and dead (upper left quadrant). Untreated control cells were healthy and had an average of 93.5% of live cells, with 3.1% cells in the late apoptotic stage. The 0.9 µM Pd(II)-THPP and 4 J/cm^2 irradiated cells maintained similar results to the controls averaging 91.5% and 92.9% live cells, respectively.

A smaller percentage were in the late apoptosis stage with 3.1% for 0.9 µM Pd(II)-THPP treated and 4.4% for 4 J/cm^2 irradiation treated cells. A substantial shift from the large live cell populations to most cells in the late apoptosis/ dead stage is seen in cells treated with photodynamic therapy. The shift occurs in a dose-dependent manner as cells treated with low dose (0.35 µM Pd(II)-THPP) PDT have 23.4% live cells and 69.5% cells in late apoptosis, 5.5% cells were dead while 1.6% were in early apoptosis. High dose (0.9 µM Pd(II)-THPP) PDT treated cells were 72.3% late apoptosis/dead stage and 21.7% live. A small 4.2% were dead and 1.9% in early apoptosis. A necrotic control was included of H_2O_2 treated cells which 91.1% were in the late apoptosis/ dead stage.

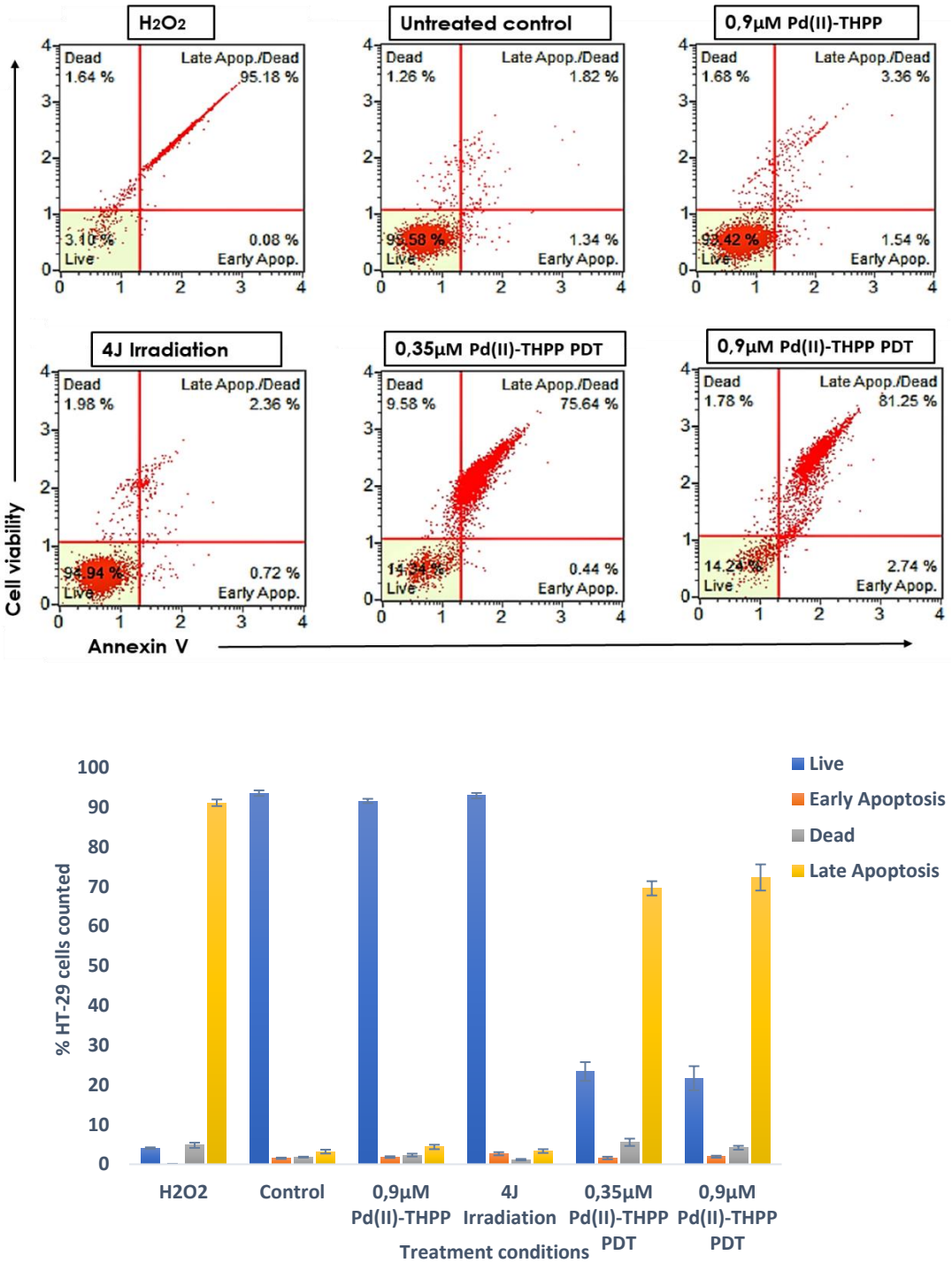

Figure 4.10 Determination of HT-29 colorectal adenocarcinoma cell stress and death stages using flow cytometric Annexin V & Dead cell assay staining 24h post-PDT treatment. (Dot plots are single representation; Percentages; n=3, mean±SEM)

The cell cycle has checkpoints that detect mistakes during DNA replication. When activated by either DNA damage or under replication, they will pause the cycle until the danger is deterred. The checkpoints are the S-phase (DNA synthesis) and M-phase (mitosis), which are separated by G1 and G2 phases (gap phase). The G0 phase (quiescence) exists when cells stop replication (Collins *et al*., 1997). The effects of photodynamic therapy with Pd(II)-THPP on the HT-29 adenocarcinoma cell cycle were evaluated 24 hours post-PDT using the flow cytometric PI stain (Figure 4.11). All control cell populations [untreated (61.1%), 0.9 μM Pd(II)-THPP (63.8%) and 4 J/cm^2 irradiation (61.7%)] were found to be in the growth G0/G1 phase while 26.4%, 23.7% and 22.3% respectively, were found in the G2/M phase. Photodynamic therapy caused cell cycle arrest and cell death as the new peak arose. Cell death occurred in a dose-dependent manner as 22.5% of 0.35 μM Pd(II)-THPP PDT treated cells were dead, and 35.3% of 0.9 μM Pd(II)-THPP PDT cells were dead.

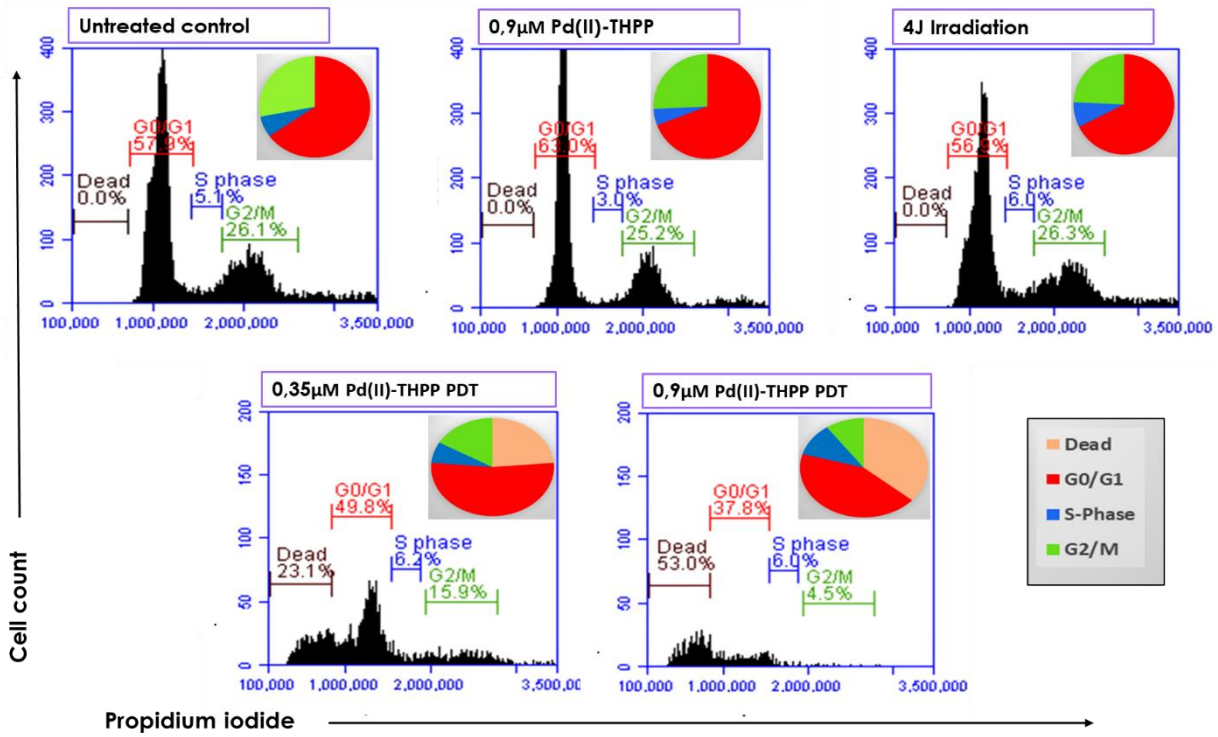

Figure 4.11 Flow cytometric DNA cell cycle analysis of PI-stained HT-29 colorectal adenocarcinoma cells. Histograms are single representations. Pie chart: mean, n=3

4.4.4 CHROMATIN CHANGES INDUCED BY PD(II)-THPP PDT INDICATE APOPTOTIC DAMAGE

The Hoechst 33258 stain and fluorescence microscopy were used to detect cellular markers for potential apoptosis or necrosis. Cells undergoing apoptosis are characterised by shrinking, nuclear chromatin condensation, margination and the formation of apoptotic bodies (Zhang *et al*., 2009). With the stain binding to DNA, chromatin changes were able to be observed (Figure 4.12). All the controls [untreated control, 0.9 µM Pd(II)-THPP and 4 J/cm^2 irradiation] maintained circular and intact DNA material found in normal healthy cells. Low and high dose Pd(II)-THPP PDT treated HT-29 cells had features of apoptosis that included shrinking in size and condensed chromatin in the nuclei indicated by the intense blue aggregated spots in figures. In some cells, karyorrhexis and marginalisation of the chromatin along the nucleoplasm diameter are vital apoptosis markers.

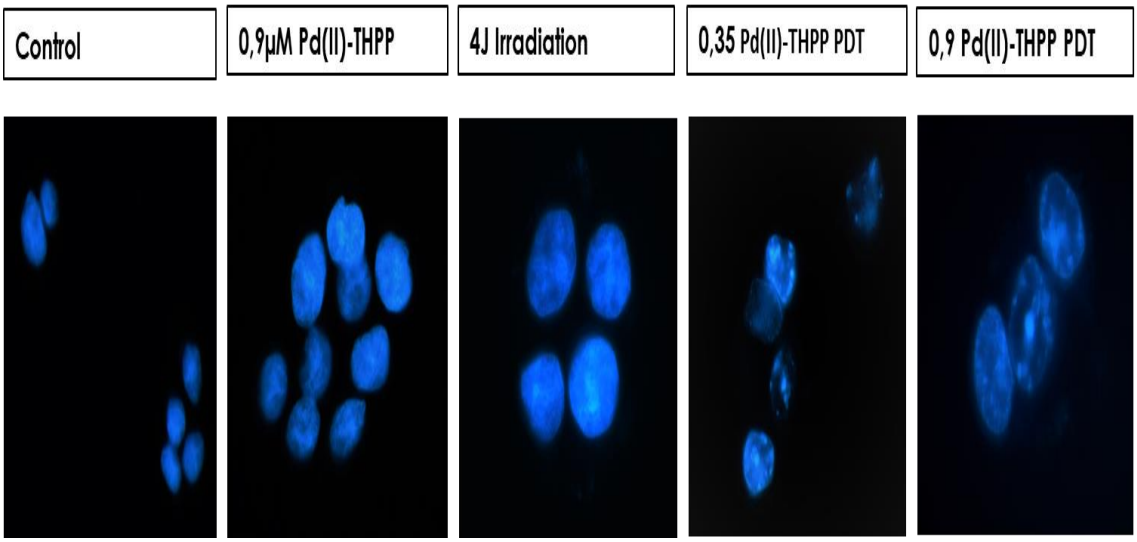

Figure 4.12 Nuclear damage determination of Pd(II)-THPP PDT treatment on HT-29 adenocarcinoma using Hoechst-33258 blue fluorescence microscopy. Cell populations included non-treated control cells, 0.9 µM Pd(II)-THPP and 4 J/cm^2 irradiation only treated cells and low 0.35 µM Pd(II)-THPP and high 0.9 µM Pd(II)-THPP PDT cells. Photos were captured using the AxioPlan 2 Imaging light microscope and no. 1 Ex. 365/12 lens filter at 400X magnification.

4.5 SCREENING THE PD(II)-THPP PHOTOSENSITISERS ON NORMAL HUMAN EMBRYONIC KIDNEY (HEK-293) CELLS.

Photodynamic therapy uses photosensitising agents intended to accumulate in cancer cells and kill the tumour when activated by a particular light. The photosensitiser delivery mechanisms are developed to limit phototoxicity to surrounding normal tissues (Kou *et al.*, 2017); however, systemic delivery of the photosensitiser may result in some tissue damage. The effects of PDT with Pd(II)-THPP encapsulated in PEG2000-PE in normal tissue were investigated using the human embryonic kidney (HEK-293) cell line.

Subcellular accumulation and localisation were determined through fluorescence microscopy. The cells were treated with 80 µM Pd(II)-THPP encapsulated in PEG2000-PE and fixed without background staining. Autofluorescence was

visualised using the Zeiss Axioplan 2 Imaging light microscope. From the microscopy image in Figure 4.13, it is evident that Pd(II)-THPP readily accumulates in normal HEK-293 cells. The insert highlights non-specific accumulation in the nucleus and cytosol. Pd(II)-THPP aggregates in some organelles as seen by intense fluorescence in the perinuclear space. No other stain was done, however, to determine exact organelle localisation.

Following confirmation of Pd(II)-THPP uptake by the HEK-293 cells, cellular morphology and homeostasis within the cells using similar treatment conditions as HT-29 cells were studied. These included an untreated cell control, 0.9 µM Pd(II)-THPP and 4 J/cm^2 blue light irradiation only, a low dose of 0.35 µM Pd(II)-THPP PDT and a high dose of 0.9 µM Pd(II)-THPP PDT. In addition, a vehicle control that was used to deliver Pd(II)-THPP into the cells was included. It comprised of 0.9 µM PEG2000-PE (3.75 mg/mL) dissolved in 0.5X PBS.

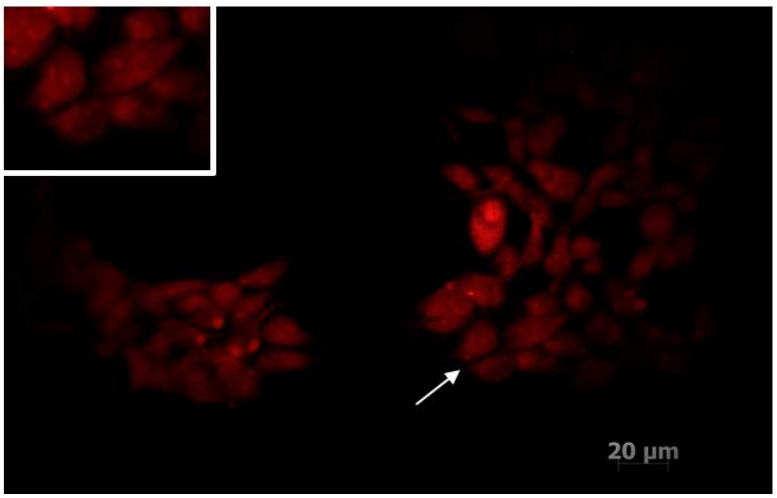

Figure 4.13 Photosensitiser uptake and localisation in HEK-293 cells. Cells were treated with 80 µM Pd(II)-THPP and incubated for 24 hours. Autofluorescence visualisation was

done on the Axioplan 2 Imaging light microscope with AxioVision 4.7 software and number 15 (546/12 nm) filter at 400X magnification.

Cellular morphology of HEK-293 cells was investigated 24 hours post-administration of 4 J/cm^2 irradiation in PDT treatment. Figure 4.14 illustrates the changes undergone by the cells after treatment. Untreated control cells show the typical irregular, spindly HEK-293 shape, and they are still attached to the culture dish indicating health status. Cells treated with 0.9 µM Pd(II)-THPP and 4 J/cm^2 irradiation only showed morphology comparable to the healthy untreated control cells. The PEG2000-PE vehicle control cells also maintained similar irregular attached morphology. PDT treatment resulted in crucial changes that signify the effect of PDT on cells. Although still attached to the culture dish, both high and low dose PDT treated cells exhibit shrinkage and more spherical shapes. In addition, the cells are clustered and appear granulated, and some apoptotic bodies appear.

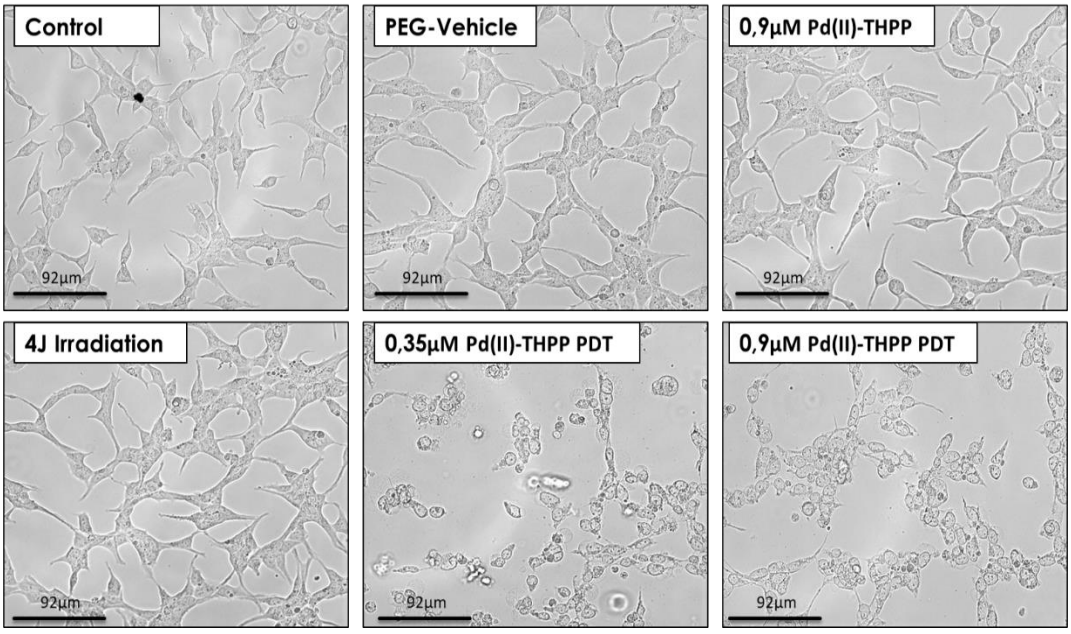

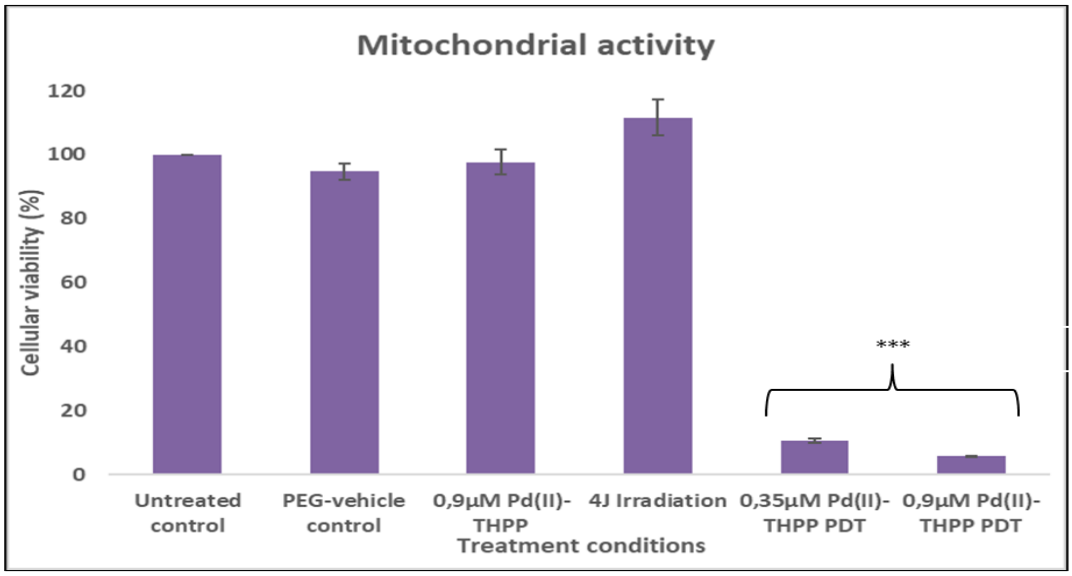

Figure 4.14 Cellular morphology of HEK-293 embryonic kidney cell line with no treatment (Control), treated with PEG2000-PE dissolved in 0.5X PBS (PEG-vehicle), 0.9 µM Pd(II)-THPP only, 4 J/cm^2 only, and PDT treated with low 0.35 µM Pd(II)-THPP and 0.9 µM Pd(II)-THPP doses. Images were taken 24 h post PDT with Floid® Cell Imaging System. Mitochondrial activity was determined using the alamarBlue® reduction dye assay. n=6, error bars are SEM, p<0.001***

Cell homeostasis via mitochondrial activity was then determined as HT-29 cells using alamarBlue®. The activity percentages were normalised and compared to the untreated control. The 4 J/cm^2 irradiation control slightly stimulated mitochondrial activity to 111.7%, which contrasts to HT-29 cells, whereas both 0.9 µM Pd(II)-THPP and PEG-vehicle controls had negligible decreases to 97.6% and 94.7% activity, respectively. Photodynamic therapy significantly (p<0.001) decreased mitochondrial activity in a dose-dependent manner. Low dose PDT obtained 10.6% mitochondrial activity and 5.8% activity for the high dose PDT. These values indicate that Pd(II)-THPP PDT doses are more cytotoxic to HEK-293 than HT-29 colorectal cells, and their suitable photosensitiser doses can be determined.

CHAPTER 5: DISCUSSION

PDT is an everchanging modality in the treatment of cancer involving a light-sensitive drug (photosensitiser), which is activated upon irradiation to produce oxidative damage-inducing ROS. Porphyrins make ideal photosensitisers due to their non-toxic, water-soluble and high tumour selectivity nature (Kulbacka *et al*., 2013) and are thus extensively studied in PDT. Our study proved that the insertion of Pd and Cu into the H_2THPP core could produce photosensitisers with comparable PDT efficiencies in HT-29 colorectal adenocarcinoma, however Cu did not produce expected results. Furthermore, we went to investigate the type of cell death induced by the functional photosensitiser and PDT treatment.

5.1 METAL INCORPORATION INTO PORPHYRINS IMPROVES BIOLOGICAL CAPABILITY

The interaction of Pd(II)-acetate and Cu(II)-acetate with H_2THPP in ethanol produced Pd(II)-THPP and Cu(II)-THPP metallo-photosensitizers. This was supported by analysis of the UV-Vis and proton NMR spectra in Figures SR1 and SR2. Coordination of metals such as Fe, Zn, Cu and Co into the porphyrin ring structure has evidenced to improve biological (Suarez *et al*., 2019), photochemical and catalytic capabilities

5.2 OPTIMAL CU(II)-THPP AND PD(II)-THPP CONDITIONS TO PERFORM PDT

5.2.1 CELLULAR UPTAKE AND LOCALISATION

One of the main determinators of PDT efficacy and selectivity is cellular uptake and localisation of the PS. Pd(II)-THPP and Cu(II)-THPP were encapsulated in PEG2000-PE to enhance delivery into the HT-29 adenocarcinoma cells. PEG encapsulation has been proved to be a safer and more efficient drug carrier system enhancing PS pharmacokinetics and tumour selectivity (Janas *et al.*, 2021; Nawalany *et al.*, 2009). Nawalany *et al.* (2012) compared PEG350, PEG2000 and

PEG5000 and liposome-encapsulated p-THPP in HCT-116 colorectal cancer and DU 145 prostate adenocarcinoma cells. Focusing on the HCT-116 cells, p-THPP encapsulated in PEG2000 accumulated more intensely in the cancer cells than in the other PEG chains. Figure 4.1 showed that Pd(II)-/Cu(II)-THPP (PEG2000-PE) was readily taken up by the HT-29 adenocarcinoma. The addition of PEG increases the lipophilicity and hydrophobicity of the PS, thus aiding the PS to penetrate the cell membranes and be taken up by the cells (Sibrian-Vazquez *et al.*, 2007). Furthermore, it increases phototoxicity during PDT (Sibrian-Vazquez *et al*., 2007; Roguin *et al*., 2019).

The distribution pattern of the PS within the HCT-116 (Nawalany *et al*., 2012) clearly showed that p-THPP did not accumulate in the nucleus. In contrast, our results show nuclear accumulation can be due to the PS concentration difference as 10 µg/mL was used on the HCT-116 and while in this study 80 µM/mL was used on the HT-29 cell line. Furthermore, incubation period as our cells were evaluated after 24 hours instead of the shorter 3-12 hours leading to the PS to diffuse into the nucleus eventually.

Subcellular localisation of the PS determines the photodamage site and type of cell death within the cells. Specific molecular probes such as Hoechst, ERTracker, MitoTracker and LysoTracker allow the detection of PS accumulation sites. Unfortunately, our uptake and localisation study only detected autofluorescence of the PS. Most research has revealed that porphyrin-based PSs localise mainly in the mitochondria, ER, lysosomes and cytoplasm, with mitochondria and lysosomes being the main targets in PDT (Velazquez *et al*., 2019).

5.2.2 PD(II)-THPP/ CU(II)-THPP IN THE DARK AND IRRADIATION ALONE DO NOT INDUCE CYTOTOXICITY

The ideal photosensitiser should not induce cytotoxicity in the dark and be excreted out of the body rapidly (Babu *et al.*, 2017). Kulbacka and colleagues (2013) studied cytotoxicity induced by the metalloporphyrins, CoTTPS and MnTMPyPCl5 on colon cancer. Their results showed the metalloporphyrins were not cytotoxic sans irradiation in the lower concentration ranges and averaged more than 100% of the control. Twenty-five (25) micromolar concentrations and upwards, however, showed greater sensitivity and cytotoxicity. In our study, Pd(II)-THPP and the lower concentration Cu(II)-THPP showed increased viability, which contradicts most studies. ABCG2 regulates the uptake of photosensitisers and is part of a family of proteins that trigger resistance to anti-cancer therapeutic agents. The interaction of ABCG2 with some porphyrins obstructs accumulation and increases proliferative capacity in the cells, enhancing overall tumour survival (Kim *et al.*, 2015; Ishikawa *et al.*, 2010). ABCG2 involvement in anti-cancer response to PDT was reviewed by Khot and his colleagues (2020). We suspect that Pd(II)-THPP induces overexpression of ABCG2 in the dark, but it is reduced as significant cytotoxicity was elicited upon irradiation. With healthy morphology and no dark toxicity induced, Pd(II)-THPP and Cu(II)-THPP were still ideal photosensitisers to use in PDT.

The application of irradiation alone should also not cause any phototoxicity to the cells. Elekonawo *et al.* (2019) irradiated HT-29 cells with light energy doses of 0, 31.5, 94.4 and 314.5 J/cm^2 and obtained similar viability ranges. The excessive light energy doses demonstrated that irradiation alone does not harm the cells. Although longer wavelengths around the red spectrum have been deemed more favourable to use in deep tissues (Wu *et al.*, 2015), our study has shown that blue light irradiation can induce PDT cell death. Kulbacka *et al.* (2013) compared 435nm and 530nm irradiation using metalloporphyrins, CoTPPS and MnTMPyPCl5 on LoVo colon adenocarcinoma and both induced phototoxicity. With the current

advances in technologies, it might even be beneficial to use blue light using a laparoscopic laser as shorter wavelengths will concentrate more on the tumour area, further minimising surrounding healthy tissue damage.

5.3 PD(II)-THPP HAS POTENT INHIBITORY CONCENTRATIONS WHILE CU(II)-THPP SHOWS RESISTANCE

Pd(II)-THPP proved potent as low photosensitiser concentrations were able to induce cytotoxicity when irradiation was applied (Figure 4.4). When HT-29 adenocarcinoma was treated with varying Cu(II)-THPP concentrations and 4J/cm^2 irradiation, they showed resistance to the treatment. Moreover, increasing the concentrations had a stimulatory effect on metabolic activity (Figure 4.5). Resistance to PDT in squamous cell carcinoma was attributed to changes in EGFR, cyclin D1 and MAP3KI expression in the genome. EGFR activates ERK, which leads to an overexpression of cyclin D1, which counters PDT action. Cyclin D1 is, therefore, the differential marker to how cells will respond to PDT. In addition, EGFR is associated with developing resistance to cytotoxic agents in some cancer, even increasing the ability to metastasise (Gilaberte *et al*., 2014). Another theory is that sublethal doses of photosensitisers increase endogenous ROS, which plays a role in cell growth. This leaves the question of whether our Cu(II)-THPP concentrations were too low in this case, and whether we should have attempted even higher concentrations? Also, if they were too low, why did Pd(II)-THPP have the opposite effect?

Spagnul *et al.* (2017) did a study comparing Cu(II)- and Pd(II)-porphyrin photosensitisers and how metal complexation influences photoactivity. Palladium forms stable complexes with porphyrins and enhances the photodynamic action of the photosensitiser due to its heavy atom effect. The effect raises the triplet state lifetime of the Pd(II)-porphyrin, increasing quantum yields of singlet oxygen which raises ROS production. In contrast, Cu(II)-porphyrin triplet state lifetime is shorter and decays back to the ground state faster, leaving less time to generate

ROS through energy transfer. Deng *et al.* (2020) supported that heavy metal atoms enhance ROS generation, thus inducing cytotoxicity during light irradiation, as seen by our results.

5.4 PHOTODYNAMIC THERAPY ON HT-29 ADENOCARCINOMA WITH PD(II)-THPP:

5.4.1 MICROSCOPIC OBSERVATION SHOWS APOPTOTIC AND NECROTIC CHARACTERISTICS

Apoptosis and necrosis are death pathways usually described in PDT-induced cell damage. The morphological characteristics of apoptosis include shrinking cell size, nuclear fragmentation, chromatin condensation and formation of apoptotic bodies. Necrotic characteristics are membrane rupture and cell swelling (Bretin *et al*., 2019). These characteristics were evident in Pd(II)-THPP PDT treated cells (Figure 4.6) and also confirmed by the Hoechst nuclear stain (Figure 4.12). The morphological changes such as cell rounding, membrane blebbing and formation of apoptotic bodies are a direct result of the produced ROS acting on the cytoskeleton. Changes in the organisation of cytoskeletal actin filaments, contractile cortex development in myosin II and actin-myosin II cortex withdrawal bring about these changes post PDT (Babu *et al*., 2017).

5.4.2 CELLULAR VIABILITY AND METABOLIC ACTIVITY DECREASED POST PDT

Porphyrin-based compounds depend upon ROS generation to induce a cytotoxic photodynamic effect, thus decreasing cellular viability. In this study, our data found that Pd(II)-THPP PDT significantly reduced cell viability in a dose-dependent manner, indicating stress within the HT-29 cells (Figure 4.6 and 4.7). In another study using the porphyrin photosensitiser, 2-TQP, a substantial yield of singlet oxygen was generated, instigating photodynamic activity in HT-29 cells. Concentrations of 3.1 µM and 6.1 µM 2-TQP were used, and viability decreased in a dose-dependent manner 24 hours post-irradiation (Costa *et al*., 2016). 2-TQP and Pd(II)-THPP have the same core structure, and it can be assumed that Pd(II)-

THPP produces highly reactive singlet oxygen and favours to accumulate in the biological membranes (mitochondrial, lysosomal and cytoplasmic), which are then destroyed upon irradiation inducing cytotoxicity. ZnPc and TAZnPC [Zn(II)tetraminephthalocyanine] decreased T98G cell viability in a dose-dependent manner (Velazquez *et al*., 2019)

5.4.3 ROS PRODUCTION DISRUPTS MITOCHONDRIAL FUNCTION INDUCING CELL DEATH

Metabolic and homeostatic control is vital in living cells. Mitochondria are the principal supporters of these control processes, which include oxidative phosphorylation and induction of apoptosis. The mitochondria's disruption and dysfunction are detrimental to the cells (Kotiadis *et al*., 2014). During oxidative phosphorylation, some ROS is produced; however, excessive ROS presence oxidises biomolecules, triggering a cascade of redox signalling pathways that result in cell death, especially apoptosis (Bretin *et al*., 2019). ROS was significantly produced post PDT with Pd(II)-THPP and disrupted the mitochondrial membrane. The presence of active mitochondria in the controls and absence thereof in the PDT treated cancer cells (Figure 4.9), and consequent decrease in produced ATP levels (Figure 4.8) provide strong evidence of ROS disruption.

Grebeňová *et al.* (2003) showed that the disruption of the mitochondrial membrane induces apoptosis. The oxidation of the ATP-synthase complex uncouples oxidative phosphorylation compromising the mitochondrial membrane, thus decreasing ATP production. PDT- induced apoptosis, however, requires ample cellular energy to initiate the apoptotic cascade. The decline in ATP may indicate necrotic cell death instead (Tsai *et al*., 2015).

Furthermore, cytochrome *c* was observed to be released from the mitochondria into the cytoplasm, where it initiates the caspase cascade by activating procaspase 9 and Apaf1 (apoptotic protease activating factor), leading to the activation of caspase 3 and -7 (Machado *et al*., 2010). Although Bax and Bcl-2 expression were not investigated in this present study, we can deduce that Bcl-2 expression was

downregulated and Bax upregulated and activated to interact with the mitochondrial membrane channel proteins to promote cytochrome *c* release (Huang *et al*., 2016). Bcl-2, pro-apoptotic-caspase 7 and 9 downregulation leads to a switch in apoptotic induction to autophagy in post-anti-cancer treatment (Wang *et al*., 2016).

More PDT studies have established that the mitochondrial caspase activation pathway is used, but inhibition of caspases or caspase-3/7 deficiency insinuate that PDT also uses a caspase-independent pathway to kill cells. The possible alternate pathway was found to be autophagy induction by phosphatidylinositol 3-kinase (PI3K) (Buytaert *et al*., 2006). The quantification of P62 and LC3B proteins involved in the autophagy signalling pathway by Shi *et al.* (2019) demonstrated that PDT does promote autophagy. P62 was down-regulated, whereas the conversion of LC3B-I to its active LC3B-II form, a marker for autophagic activity, was also detected. Lange *et al.* (2019) observed that when there is no caspase 3 activated, LC3-II levels increase. PI3K inhibition prevents the LC3B conversion and thus stops autophagy. This implies that PI3K is a significant factor in inducing autophagy during PDT.

In a more recent study, Song *et al.* (2020) showed that m-THPC-PDT activates the ROS-JNK signalling pathway to induce apoptosis and autophagy by increasing phosphorylation of JNK in colorectal cancer cells. Huang *et al.* (2016) had worked to define the relationship between apoptosis and autophagy. The results led to a conclusion of apoptosis being autophagy-dependent during PDT as it can control by stopping or initiating apoptosis. The type of PS used, concentration, cell line and PDT dose are all crucial determinants of the type of cell death, whether apoptosis, necrosis or autophagy that will be induced.

5.4.4 CELLULAR DEATH MARKERS

The purpose of PDT is to initiate cell death in the targeted tumours. The externalisation of cell membrane phosphatidylserine is an early indicator of occurring death cascade. The flow cytometric Annexin V and Dead cell assay (Figure 4.10) illustrated apoptosis and necrosis were induced by Pd(II)-THPP PDT with the late apoptotic stage being dominant. This concurs with Wu *et al.* (2015) who tested FosPeg® (mTHPC- meta(tetrahydroxyphenyl)chlorin) and obtained similar results using comparable photosensitiser concentrations (0.3 μg/mL and 0.6 μg/mL) and 3 J/cm^2 irradiation. Treatment of MG-63 osteosarcoma cells with MPPa-PDT (Huang *et al*., 2016) and ZnPcS4- PDT treated A375 melanoma cells (Naidoo *et al*., 2019) also induced a significant amount of early and late apoptosis and a small count of necrotic cells.

LDH was released into the media (Figure 4.7) because of the loss of membrane integrity induced by ROS cytotoxicity, on the other hand, illustrated necrosis to have been induced. Sulphonated zinc phthalocyanine-PDT on HeLa cells induced a dose-dependent increase in released LDH (Hodgkinson *et al*., 2017). ZnPc-PDT treated TFK-1 cells also showed an increase in LDH content while Pc32-PDT had a negligible amount present (Schmidt *et al*., 2018). LDH release can be both a primary necrosis marker or demonstrate secondary necrosis of unphagocytosed cells that had initially gone through apoptosis (Schmidt *et al*., 2018).

5.4.5 CELL CYCLE ARREST INDUCED

Markers of DNA damage were observed using the Hoechst-33258 nuclei stain (Figure 4.12), and cell cycle arrest was detected using the flow cytometric PI stain (Figure 4.11). Our findings coincide with Huang *et al.* (2016) as PDT treated cells displayed nuclear condensation, karyopyknosis and karyorrhexis. Pd(II)-THPP PDT treatment on HT-29 cells led to the formation of a new Sub-G/Dead peak where the cells are in the late apoptotic/ necrotic stage, supported by Annexin V & Dead cell results. The cell cycle is imperative for regulating proliferation and is tightly

controlled by cyclins and cyclin-dependent kinases (Anthony *et al*., 2020). The majority of PDT treated cells were arrested in the G0/G1 and Sub-G0 stages as apoptotic cells are unlikely to be actively undergoing mitosis. Development of Sub-G0 and G0/G1 arrest was seen in A-427, KYSE-70, RT-4 and SISO cell lines treated with mTHPC-PDT (Lange *et al*., 2019). Cyclin D1 regulates the conversion from G0/G1 to S phase by forming a complex with the CDK. Inhibition or downregulation of cyclin D1 by P2 Waf1/CiP1/Sd1 during PDT causes cells to remain in the G0/G1 phase (Liang *et al*., 2016) halting cell proliferation and inducing apoptosis. Sub-G0 formation by inhibition of CDK 2 and CDK1 commits cells to apoptosis or necrosis (Agarwal *et al*., 2018).

5.5 PD(II)-THPP ACCUMULATES IN NORMAL KIDNEY CELLS.

Blant and colleagues (2002) observed a high accumulation of mTHPC in the kidneys of hamsters 24h post-administration and had cleared 96 hours after being administered. This observation can lead one to conclude that PSs are removed from normal tissue through excretion after some time has passed. However, while the PS is still in the body, it can cause photo-oxidative damage upon light activation, as shown by our results. Therefore, the emphasis remains on creating PSs that accumulate only in target tumour tissues, and excess PS can be cleared by the body before irradiation by light in PDT treatment to ensure minimal damage to normal tissue.

CHAPTER 6: CONCLUSION

This study investigated novel tetra hydroxyphenyl porphyrin (THPP) photosensitisers in PDT against colorectal cancer. Pd(II) and Cu(II) metals were inserted into the freebase H_2THPP core and characterised. The effects of both PSs were tested on the HT-29 colorectal adenocarcinoma cell line to determine PDT competence and the possibility of future use in cancer therapeutics. It was hypothesised that the resultant photosensitisers would have comparable PDT efficiencies and induce cell death in the target HT-29 adenocarcinoma. Characterisation of Pd(II)- and Cu(II)-THPP showed successful incorporation of the metals into the porphyrin ring, producing biochemically active PSs with ideal absorption in the visible light region when irradiated using the blue light diode laser.

Photodynamic therapy requires light, oxygen, and a PS in combination to produce a cytotoxic response. The administration of each component individually should not induce cytotoxicity. Therefore, irradiation toxicity at 405nm and unwanted Pd(II)- and Cu(II)-THPP dark toxicity were evaluated, and we found no cytotoxicity in both components independently. Determination of the inhibitory concentrations in Pd(II)- and Cu(II)-THPP revealed a discrepancy between the photosensitisers. Pd(II)-THPP proved potent in inducing cytotoxicity at low inhibitory concentrations. Cu(II)-THPP responded inversely, producing a stimulatory effect that led to the speculation of internal resistive mechanisms to provoke such a response. Cu(II)-THPP experiments were withdrawn because of the undesirable outcome, and only Pd(II)-THPP was used further.

Comparing the efficiencies of Pd(II)-THPP and Cu(II)-THPP in HT-29 colorectal adenocarcinoma, Pd(II)-THPP was the superior PS of the two as PDT aims to induce

cell death instead of potentially growing the tumour without the means to stop it. Although Pd(II)-THPP first produced a proliferative response, significant death was induced following light irradiation. For upcoming studies, a time response study can be done to determine the ideal incubation period before irradiation so that hyperproliferation of the tissue does not occur. Furthermore, electroporation can be used as in the study Kulbacka and colleague*s* (2013) conducted to advocate quicker uptake and localisation. Cu(II)-THPP resistance to PDT in HT-29 cells has unlocked more research questions that can shed light on the resistive mechanisms triggered by PDT. In continuation of the Cu(II)-THPP PDT study, EGFR activity can be investigated using anti-EGFR to determine if it indeed plays a role in conferring resistance. In addition, the type of cell line used affects PDT response. Cu(II)-THPP PDT can be tested on other colorectal cell lines such as the CL40, CW2 and SW1417 cell lines, considered the closest models mimicking colorectal cancer tumours (Ronen *et al*., 2019).

Pd(II)-THPP PDT treated HT-29 colorectal adenocarcinoma presented signs of disrupted homeostasis by a decline in metabolic activity. Markers of apoptosis and necrosis were observed morphologically, and in DNA through microscopy, cell stress assays and flow cytometric analysis. Our results demonstrated that Pd(II)-THPP PDT induces cytotoxicity in a dose-dependent manner on the HT-29 cells. Cytochrome *c* release but lack of change in Caspase 3/7 activity raised the assumption of autophagy as the additional mode of cell death induced by Pd(II)-THPP. This study had aimed to ascertain whether apoptosis and necrosis are induced in PDT. By the evidence presented in our results, both cell death mechanisms are induced in Pd(II)-THPP PDT of HT-29 colorectal cancer with autophagy as a third mechanism. The subsequent study in Pd(II)-THPP PDT can quantify P63 and LC3B expression in HT-29 colorectal cancer post-treatment to confirm autophagy induction. Furthermore, the caspase 3/7 assay is not specific to the caspase expression. A supplementary western blot study of caspase-3 and

caspase-7 and possibly Bcl-2 and Bax expression will strengthen the evidence of apoptotic death.

PDT is a vast and growing modality with new death pathways being discovered. Since our study found caspase-independent death, a future investigation into necroptosis as a death mechanism induced by Pd(II)-THPP and looking specifically at MLKL, RIPK1 and RIPK3 expression would give more insight into all the possible death mechanisms involved in Pd(II)-THPP.

In conclusion, Pd(II)-THPP proved an ideal PS, producing ROS and phototoxicity in HT-29 colorectal adenocarcinoma when irradiated with a 405nm blue light laser. The results were comparable with other studies in PDT research, and with further refinement, Pd(II)-THPP can land on pharmaceutical shelves. With the evidence presented, PDT has the potential to be a substitute therapy to treat colorectal and other malignancies.

CHAPTER 7: REFERENCES

Abrahamse, H., & Hamblin, M. R. (2016). New photosensitizers for photodynamic therapy. *Biochemical Journal*, *473*(4), 347–364. https://doi.org/10.1042/BJ20150942

Agarwal, A., Kasinathan, A., Ganesan, R., Balasubramanian, A., Bhaskaran, J., Suresh, S., Srinivasan, R., Aravind, K. B., & Sivalingam, N. (2018). Curcumin induces apoptosis and cell cycle arrest via the activation of reactive oxygen species–independent mitochondrial apoptotic pathway in Smad4 and p53 mutated colon adenocarcinoma HT29 cells. *Nutrition Research*, *51*, 67–81. https://doi.org/10.1016/j.nutres.2017.12.011

Al Neyadi, S. S., Alzamly, A., Al-Hemyari, A., Tahir, M. I., Al-Meqbali, S., A. Ali Ahmad, M., & Bufaroosha, M. (2019). An Undergraduate Experiment Using Microwave-Assisted Synthesis of Metalloporphyrins: Characterization and Spectroscopic Investigations. *World Journal of Chemical Education*, *7*(1), 26–32. https://doi.org/10.12691/wjce-7-1-4

Aniogo, E. C., George, B. P., & Abrahamse, H. (2021). Molecular effectors of photodynamic therapy-mediated resistance to cancer cells. *International Journal of Molecular Sciences*, *22*(24). https://doi.org/10.3390/ijms222413182

Anthony, E. J., Bolitho, E. M., Bridgewater, H. E., Carter, O. W. L., Donnelly, J. M., Imberti, C., Lant, E. C., Lermyte, F., Needham, R. J., Palau, M., Sadler, P. J., Shi, H., Wang, F. X., Zhang, W. Y., & Zhang, Z. (2020). Metallodrugs are unique: Opportunities and challenges of discovery and development. *Chemical Science*, *11*(48), 12888–12917. https://doi.org/10.1039/d0sc04082g

Babu, S. P. S., Manu, P. M., Dhanya, T. J., Tapas, P., Meera, R. N., Surendran, A., Aneesh, K. A., Vadakkancheril, S. J., Ramaiah, D., Nair, S. A., & Pillai, M. R. (2017). Bis(3,5-diiodo-2,4,6-trihydroxyphenyl)squaraine photodynamic therapy disrupts redox homeostasis and induce mitochondria-mediated apoptosis in human breast

cancer cells. *Scientific Reports*, *7*(January), 1–14. https://doi.org/10.1038/srep42126

Baskaran, R., Lee, J., & Yang, S. G. (2018). Clinical development of photodynamic agents and therapeutic applications. *Biomaterials Research*, 22(25), BioMed Central Ltd. https://doi.org/10.1186/s40824-018-0140-z

Basker, R., Lee, K. A., Yeo, R., & Yeoh, K.-W. (2012). Cancer and Radiation Therapy: Current Advances and Future Directions. *International Journal of Medical Sciences*, *9*(3), 193–199. https://doi.org/doi: 10.7150

Behrens, J. (2005). The role of the Wnt signalling pathway in colorectal tumorigenesis. *Biochemical Society Transactions*, *33*(4), 672–675. https://doi.org/10.1042/BST0330672

Bennecke, M., Kriegl, L., Bajbouj, M., Retzlaff, K., Robine, S., Jung, A., Arkan, M. C., Kirchner, T., & Greten, F. R. (2010). Ink4a/Arf and oncogene-induced senescence prevent tumor progression during alternative colorectal tumorigenesis. *Cancer Cell*, *18*(2), 135–146. https://doi.org/10.1016/j.ccr.2010.06.013

Berenbaum, M. C., Akande, S. L., Bonnett, R., Kaur, H., Ioannou, S., White, R. D., & Winfield, U.J. (1986). meso-Tetra(hydroxyphenyl)porphyrins, a new class of potent tumour photosensitisers with favourable selectivity. *Br. J. Cancer*, *54*, 717–725. https://doi.org/10.1038/bjc.1986.232

Bertelsen, C. A., Neuenschwander, A. U., Jansen, J. E., Kirkegaard-Klitbo, A., Tenma, J. R., Wilhelmsen, M., Rasmussen, L. A., Jepsen, L. V., Kristensen, B., & Gögenur, I. (2016). Short-term outcomes after complete mesocolic excision compared with “conventional” colonic cancer surgery. *British Journal of Surgery*, *103*(5), 581–589. https://doi.org/10.1002/bjs.10083

Bettington, M., Walker, N., Clouston, A., Brown, I., Leggett, B., & Whitehall, V. (2013). The serrated pathway to colorectal carcinoma: Current concepts and challenges. *Histopathology*, *62*(3), 367–386. https://doi.org/10.1111/his.12055

Blant Andrejevic, S., Glanzmann, T. M., Ballini, J. P., Wagnières, G., Van den Bergh, H., & Monnier, P. (2002). Uptake and localisation of mTHPC (Foscan®) and its 14C-labelled form in normal and tumour tissues of the hamster squamous cell carcinoma model: A comparative study. *British Journal of Cancer*, *87*(12), 1470–1478. https://doi.org/10.1038/sj.bjc.6600651

Boffetta, P. and Hashibe, M. (2006). Alcohol and cancer. *The Lancet Oncology*, *7*(2), 149–159. https://doi.org/10.1016/S0140-6736(17)32868-4

Bonnett, R., White, R. D., Winfield, U.-J., & Berenbaumt, M. C. (1989). Hydroporphyrins of the meso-tetra(hydroxyphenyl)porphyrin series as tumour photosensitizers. *Biochem. J*, *261*, 277–280. doi: 10.1042/bj2610277

Brand, M., Gaylard, P., & Ramos, J. (2018). Colorectal cancer in South Africa: An assessment of disease presentation, treatment pathways and 5-year survival. *South African Medical Journal*, *108*(2), 118–122. https://doi.org/10.7196/SAMJ.2018.v108i2.12338

Bray, F., Ferlay, J., Soerjomataram, I., Siegel, R. L., Torre, L. A., & Jemal, A. (2018). Global cancer statistics 2018: GLOBOCAN estimates of incidence and mortality worldwide for 36 cancers in 185 countries. *CA: A Cancer Journal for Clinicians*, *68*(6), 394–424. https://doi.org/10.3322/caac.21492

Brentnall, M., Rodriguez-Menocal, L., Ladron De Guevara, R., Cepero, E., & Boise, L. H. (2013). Caspase-9, caspase-3 and caspase-7 have distinct roles during intrinsic apoptosis. *BMC Cell Biology*, *14*(2), 32. https://doi.org/10.11164/jjsps.8.2_248_4

Bretin, L., Pinon, A., Bouramtane, S., Ouk, C., Richard, L., Perrin, M., Chaunavel, A., & Carrion, C. (2019). Photodynamic Therapy Activity of New Human Colorectal Cancer. *Cancers*, *11*(10), 1–27. https://doi.org/10.3390%2Fcancers11101474

Broertjes, J. (2015). The Ten Hallmarks of Cancer in Cutaneous Malignant Melanoma. *UNAV Journal for Medical Students*, Vol. 1, 6-12. https://doi.org/10.15581/005.1.6-12

Buytaert, E., Callewaert, G., Hendrickx, N., Scorrano, L., Hartmann, D., Missiaen, L., Vandenheede, J. R., Heirman, I., Grooten, J., & Agostinis, P. (2006). Role of endoplasmic reticulum depletion and multidomain proapoptotic BAX and BAK proteins in shaping cell death after hypericin-mediated photodynamic therapy. *The FASEB Journal*, *20*(6), 756–758. https://doi.org/10.1096/fj.05-4305fje

Buytaert, E., Dewaele, M., & Agostinis, P. (2007). Molecular effectors of multiple cell death pathways initiated by photodynamic therapy. *Biochimica et Biophysica Acta - Reviews on Cancer*, *1776*(1), 86–107. https://doi.org/10.1016/j.bbcan.2007.07.001

CANSA (2018). Colorectal cancer signs and symptoms. https://www.cansa.org.za/colorectal-cancer-signs-symptoms/. (accessed May 2021)

Castano, A. P., Demidova, T. N., & Hamblin, M. R. (2004). Mechanisms in photodynamic therapy: Part one - Photosensitizers, photochemistry and cellular localization. *Photodiagnosis and Photodynamic Therapy*, 1(4), 279–293. Elsevier. https://doi.org/10.1016/S1572-1000(05)00007-4

Chae, Y. K., Oh, M. S., & Giles, F. J. (2018). Molecular Biomarkers of Primary and Acquired Resistance to T-Cell-Mediated Immunotherapy in Cancer: Landscape, Clinical Implications, and Future Directions. *The Oncologist*, *23*(4), 410–421. https://doi.org/10.1634/theoncologist.2017-0354

Chakraborty, S., & Rahman, T. (2012). The difficulties in cancer treatment. *Ecancermedicalscience*, *6*, 1–5. https://doi.org/10.3332/ecancer.2012.ed16

Chowdhury, S. K., & Roy, H. K. (2017). The genetics and molecular biology of colonic neoplasia: Practical implications for the clinician. In *Current Opinion in Gastroenterology*, 33(1), 47–52. Lippincott Williams and Wilkins. https://doi.org/10.1097/MOG.0000000000000323

Cogno, I. S., Gilardi, P., Comini, L., Núñez-Montoya, S. C., Cabrera, J. L., & Rivarola, V. A. (2020). Natural photosensitizers in photodynamic therapy: In vitro activity

against monolayers and spheroids of human colorectal adenocarcinoma SW480 cells. *Photodiagnosis and Photodynamic Therapy*, *31*(May), 101852. https://doi.org/10.1016/j.pdpdt.2020.101852

Collins, Kathleen. Jacks, Tyler. & Pavletich, N. P. (1997). The Cell Cycle and Cancer. *Proc. Natl. Acad. Sci*, *94*(April), 2776–2778. https://doi.org/10.1016/B978-0-12-370458-0.50014-1

Costa, L. D., De E Silva, J. A., Fonseca, S. M., Arranja, C. T., Urbano, A. M., & Sobral, A. J. F. N. (2016). Photophysical Characterization and in Vitro Phototoxicity Evaluation of 5,10,15,20-Tetra(quinolin-2-yl)porphyrin as a Potential Sensitizer for Photodynamic Therapy. *Molecules*, *21*(4), 439. https://doi.org/10.3390/molecules21040439

Coupienne, I., Fettweis, G., Rubio, N., Agostini., & Piette, J. (2011) 5-ALA-PDT induces RIP3-dependent necrosis in glioblastoma. *Photochemical & Photobiological Sciences*, 10(12), 1868-1878. https://doi.10.1039/c1pp05213f

Cunningham, D., Humblet, Y., Siena, S., Khayat, D., Bleiberg, H., Santoro, A., Bets, D., Mueser, M., Harstrick, A., Verslype, C., Chau, I., & Van Cutsem, E. (2004). Cetuximab Monotherapy and Cetuximab plus Irinotecan in Irinotecan-Refractory Metastatic Colorectal Cancer. *New England Journal of Medicine*, *351*(4), 337–345. https://doi.org/10.1056/nejmoa033025

de Leon, M. P., & Di Gregorio, C. (2001). Pathology of colorectal cancer. *Digestive and Liver Disease*, *33*(4), 372–388. https://doi.org/10.1016/S1590-8658(01)80095-5

Deda, D. K., Iglesias, B. A., Alves, E., Araki, K., & Garcia, C. R. S. (2020). Porphyrin derivative nanoformulations for therapy and antiparasitic agents. *Molecules*, *25*(9), 2080. https://doi.org/10.3390/molecules25092080

Deleemans, J. M., Chleilat, F., Reimer, R. A., Henning, J. W., Baydoun, M., Piedalue, K. A., McLennan, A., & Carlson, L. E. (2019). The chemo-gut study: Investigating the long-term effects of chemotherapy on gut microbiota, metabolic, immune,

psychological and cognitive parameters in young adult Cancer survivors; Study protocol. *BMC Cancer*, *19*(1), 1–12. https://doi.org/10.1186/s12885-019-6473-8

Deng, J., Li, H., Yang, M., & Wu, F. (2020). Palladium porphyrin complexes for photodynamic cancer therapy: Effect of porphyrin units and metal. *Photochemical and Photobiological Sciences*, *19*(7), 905–912. https://doi.org/10.1039/c9pp00363k

Dimova, D. K., & Dyson, N. J. (2005). The E2F transcriptional network: Old acquaintances with new faces. *Oncogene*, *24*(17), 2810–2826. https://doi.org/10.1038/sj.onc.1208612

Dolmans, D. E. J. G. J., Fukumura, D., & Jain, R. K. (2003). Cancer revoked: Oncogenes as therapeutic targets. *Nature Reviews Cancer*, *3*(5), 380–387. https://doi.org/10.1038/nrc1070

Dos Santos, A. F., De Almeida, D. R. Q., Terra, L. F., Baptista, M. S., & Labriola, L. (2019). Photodynamic therapy in cancer treatment - an update review. *Journal of Cancer Metastasis and Treatment*, *2019(5), 25*. https://doi.org/10.20517/2394-4722.2018.83

Elekonawo, F. M. K., Bos, D. L., Goldenberg, D. M., Boerman, O. C., & Rijpkema, M. (2019). Carcinoembryonic antigen-targeted photodynamic therapy in colorectal cancer models. *EJNMMI Research*, *9*(1), 108. https://doi.org/10.1186/s13550-019-0580-z

Fan, B-G., & Andrén-Sandberg, Å. (2007). Photodynamic Therapy for Pancreatic Cancer. *Pancreas*, 34 (4), 385-389. doi: 10.1097/mpa.0b013e3180439c50

Fearson, E.R., & Vogelstein, B. (1990). A genetic model for colorectal tumorigenesis. *Cell*, 61, 759-767. https://doi.org/10.1016/0092-8674(90)90186-i

Fulda, S. (2013). The mechanism of necroptosis in normal and cancer cells. *Cancer Biology and Therapy*, *14*(11), 999–1004. https://doi.org/10.4161/cbt.26428

Gilaberte, Y., Milla, L., Salazar, N., Vera-Alvarez, J., Kourani, O., Damian, A.,

Rivarola, V., Roca, M. J., Espada, J., González, S., & Juarranz, A. (2014). Cellular intrinsic factors involved in the resistance of squamous cell carcinoma to photodynamic therapy. *Journal of Investigative Dermatology*, *134*(9), 2428–2437. https://doi.org/10.1038/jid.2014.178

Giovannetti, R. (2012). The Use of Spectrophotometry UV-Vis for the Study of Porphyrins. In U. J. Dr. (Ed.), *Macro To Nano Spectroscopy*. InTech. https://doi.org/10.5772/38797

Grebeňová, D., Kuželová, K., Smetana, K., Pluskalová, M., Cajthamlová, H., Marinov, I., Fuchs, O., Souček, J., Jarolím, P., & Hrkal, Z. (2003). Mitochondrial and endoplasmic reticulum stress-induced apoptotic pathways are activated by 5-aminolevulinic acid-based photodynamic therapy in HL60 leukemia cells. *Journal of Photochemistry and Photobiology B: Biology*, *69*(2), 71–85. https://doi.org/10.1016/S1011-1344(02)00410-4

Gupta, G. P., & Massagué, J. (2006). Cancer Metastasis: Building a Framework. *Cell*, *127*(4), 679–695. https://doi.org/10.1016/j.cell.2006.11.001

Hanahan, D., & Weinberg. R. (2011). Hallmarks of Cancer_ The Next Generation. *Cell*, *144*(5), 646–674. https://doi.org/10.1016/j.cell.2011.02.013

Hanahan, D., & Weinberg, R. A. (2000). The Hallmarks of Cancer Review Douglas. *Cell*, *100*(7), 57–70. https://doi.org/10.1007/s00262-010-0968-0

Harmse, L., Dahan-Farkas, N., Panayides, J. L., Van Otterlo, W., & Penny, C. (2015). Aberrant apoptotic response of colorectal cancer cells to novel nucleoside analogues. *PLoS ONE*, *10*(9), e0138607. https://doi.org/10.1371/journal.pone.0138607

Hausmann, W. (1911). Die sensiblisierende Wirkung des Hematoporphyrins. *Biochem. Zeitung, 30*, 276-316. Google Scholar

Hodgkinson, N., Kruger, C. A., Mokwena, M., & Abrahamse, H. (2017). Cervical cancer cells (HeLa) response to photodynamic therapy using a zinc phthalocyanine

photosensitizer. *Journal of Photochemistry and Photobiology B: Biology*, *177*, 32–38. https://doi.org/10.1016/j.jphotobiol.2017.10.004

Hong, T. S., Clark, J. W., & Haigis, K. M. (2012). Cancers of the colon and rectum: Identical or Fraternal Twins? *Cancer Discovery*, *2*(2), 117–121. https://doi.org/10.1158/2159-8290.CD-11-0315

Hong, Y. C., Lee, K. H., Kim, W. C., Choi, S. K., Woo, Z. H., Shin, S. K., & Kim, H. (2005). Polymorphisms of XRCC1 gene, alcohol consumption and colorectal cancer. *International Journal of Cancer*, *116*(3), 428–432. https://doi.org/10.1002/ijc.21019

Horne, T. K., & Cronjé, M. J. (2017). Mechanistics and photo-energetics of macrocycles and photodynamic therapy: An overview of aspects to consider for research. *Chemical Biology and Drug Design*, *89*(2), 221–242. https://doi.org/10.1111/cbdd.12761

Huang, H., & Liu, P. (2007). Tanshinone II A attenuates atherosclerotic calcification in rat model by inhibition of oxidative stress. *Vascular Pharmacology*, *46*(6), 427–438. https://doi.org/10.1016/j.vph.2007.01.001

Huang, L., Huang, Y. Y., Mroz, P., Tegos, G. P., Zhiyentayev, T., Sharma, S. K., Lu, Z., Balasubramanian, T., Krayer, M., Ruzié, C., Yang, E., Kee, H. L., Kirmaier, C., Diers, J. R., Bocian, D. F., Holten, D., Lindsey, J. S., & Hamblin, M. R. (2010). Stable synthetic cationic bacteriochlorins as selective antimicrobial photosensitizers. *Antimicrobial Agents and Chemotherapy*, *54*(9), 3834–3841. https://doi.org/10.1128/AAC.00125-10

Huang, Q., Ou, Y. S., Tao, Y., Yin, H., & Tu, P. H. (2016). Apoptosis and autophagy induced by pyropheophorbide-α methyl ester-mediated photodynamic therapy in human osteosarcoma MG-63 cells. *Apoptosis*, *21*(6), 749–760. https://doi.org/10.1007/s10495-016-1243-4

Ishikawa, T., Nakagawa, H., Hagiya, Y., Nonoguchi, N., Miyatake, S. I., & Kuroiwa, T. (2010). Key role of human ABC transporter ABCG2 in photodynamic therapy and

photodynamic diagnosis. *Advances in Pharmacological Sciences*, *2010,* 587306. https://doi.org/10.1155/2010/587306

Jacques, S. L. (2010). How tissue optics affect dosimetry of photodynamic therapy. *Journal of Biomedical Optics*, *15*(5), 051608. https://doi.org/10.1117/1.3494561

Janas, K., Boniewska-Bernacka, E., Dyrda, G., & Słota, R. (2021). Porphyrin and phthalocyanine photosensitizers designed for targeted photodynamic therapy of colorectal cancer. *Bioorganic and Medicinal Chemistry*, *30*(December 2020), 115926. https://doi.org/10.1016/j.bmc.2020.115926

Josefsen, L. B., & Boyle, R. W. (2008). Photodynamic therapy and the development of metal-based photosensitisers. *Metal-Based Drugs,* 2008(2008), 276109. https://doi.org/10.1155/2008/276109

Katsidzira, L., Gangaidzo, I., Thomson, S., Rusakaniko, S., Matenga, J., & Ramesar, R. (2017). The shifting epidemiology of colorectal cancer in sub-Saharan Africa. *The Lancet Gastroenterology and Hepatology*, *2*(5), 377–383. https://doi.org/10.1016/S2468-1253(16)30183-2

Kawai, K., Viars, C., Arden, K., Tarin, D., Urquidi, V., & Goodison, S. (2002). Comprehensive karyotyping of the HT-29 colon adenocarcinoma cell line. *Genes Chromosomes and Cancer*, *34*(1), 1–8. https://doi.org/10.1002/gcc.10003

Kessel, D. (2020). Photodynamic therapy: apoptosis, paraptosis and beyond. *Apoptosis*, 25(9–10). 611–615. https://doi.org/10.1007/s10495-020-01634-0

Kessel, D., & Oleinick, N. L. (2018). Cell Death Pathways Associated with Photodynamic Therapy: An Update. *Photochemistry and Photobiology*, 94(2), 213–218. Blackwell Publishing Inc. https://doi.org/10.1111/php.12857

Khan, R., Idris, M., & Tuncel, D. (2015). Synthesis and investigation of singlet oxygen production efficiency of photosensitizers based on meso-phenyl-2,5-thienylene linked porphyrin oligomers and polymers. *Organic and Biomolecular Chemistry*, *13*(42), 10496–10504. https://doi.org/10.1039/c5ob01435b

Khot, M. I., Downey, C. L., Armstrong, G., Svavarsdottir, H. S., Jarral, F., Andrew, H., & Jayne, D. G. (2020). The role of ABCG2 in modulating responses to anti-cancer photodynamic therapy. *Photodiagnosis and Photodynamic Therapy*, *29*(August 2009), 101579. https://doi.org/10.1016/j.pdpdt.2019.10.014

Kim, J. H., Park, J. M., Roh, Y. J., Kim, I. W., Hasan, T., & Choi, M. G. (2015). Enhanced efficacy of photodynamic therapy by inhibiting ABCG2 in colon cancers. *BMC Cancer*, *15*(1), 1–9. https://doi.org/10.1186/s12885-015-1514-4

Kim, J. W., & Dang, C. V. (2006). Cancer's molecular sweet tooth and the warburg effect. *Cancer Research*, 66(18), 8927–8930. https://doi.org/10.1158/0008-5472.CAN-06-1501

Kotiadis, V. N., Duchen, M. R., & Osellame, L. D. (2014). Mitochondrial quality control and communications with the nucleus are important in maintaining mitochondrial function and cell health. *Biochimica et Biophysica Acta - General Subjects*, *1840*(4), 1254–1265. https://doi.org/10.1016/j.bbagen.2013.10.041

Kou, J., Dou, D., & Yang, L. (2017). Porphyrin photosensitizers in photodynamic therapy and its applications. *Oncotarget*, 8(46), 81591–81603. www.impactjournals.com/oncotarget/

Kulbacka, J., Kotulska, M., Rembiałkowska, N., Choromańska, A., Kamińska, I., Garbiec, A., Rossowska, J., Daczewska, M., Jachimska, B., & Saczko, J. (2013). Cellular stress induced by photodynamic reaction with CoTPPS and MnTMPyPCl5 in combination with electroporation in human colon adenocarcinoma cell lines (LoVo and LoVoDX). *Cell Stress and Chaperones*, *18*(6), 719–731. https://doi.org/10.1007/s12192-013-0423-1

Lai, J. H., & Law, W. L. (2012). Laparoscopic surgery for colorectal cancer. *British Medical Bulletin*, *104*(1), 61–89. https://doi.org/10.1093/bmb/lds026

Lanfranco, A. R., Castellanos, A. E., Desai, J. P., & Meyers, W. C. (2004). Robotic Surgery: A Current Perspective. *Annals of Surgery*, *239*(1), 14–21. https://doi.org/10.1097/01.sla.0000103020.19595.7d

Lange, C., Lehmann, C., Mahler, M., & Bednarski, P. J. (2019). Comparison of cellular death pathways after mTHPC-mediated photodynamic therapy (PDT) in five human cancer cell lines. *Cancers,* 11(5), 702. https://doi.org/10.3390/cancers11050702

Le, N. A., Babu, V., Kalt, M., Schneider, L., Schumer, F., & Spingler, B. (2021). Photostable Platinated Bacteriochlorins as Potent Photodynamic Agents. *Journal of Medicinal Chemistry*, *64*(10), 6792–6801. https://doi.org/10.1021/acs.jmedchem.1c00052

Liang, L., Bi, W., & Tian, Y. (2016). Cell cycle arrest induced by MPPa-PDT in MDA-MB-231 cells. *Laser Physics*, *26*(5), 055607 . https://doi.org/10.1088/1054-660X/26/5/055607

Liberti, M. V., & Locasale, J. W. (2016). The Warburg Effect: How Does it Benefit Cancer Cells? *Trends in Biochemical Sciences*, *41*(3), 211–218. https://doi.org/10.1016/j.tibs.2015.12.001

Longo, D. L. (2016). Colorectal Adenomas. *The New England and Journal of Medicine*, *374*(11), 1065–1075. https://doi.org/10.1056/NEJMra1513581

Machado, A. H. A., Moraes, K. C. M., Soares, C. P., Beltrame, M., & Da Silva, N. S. (2010). Cellular changes after photodynamic therapy on HEp-2 cells using the new ZnPcBr8 phthalocyanine. *Photomedicine and Laser Surgery*, *28*(SUPPL. 1), S143-S149. https://doi.org/10.1089/pho.2009.2561

Magwaza, S., van Hal, G., & Hoque, M. (2021). Mapping of colorectal cancer scientific landscape between South Africa and Brazil: a bibliometric analysis. *Ecancermedicalscience*, *15*, 1–19. https://doi.org/10.3332/ECANCER.2021.1216

Malki, A., Elruz, R. A., Gupta, I., Allouch, A., Vranic, S., & Al Moustafa, A. E. (2021). Molecular mechanisms of colon cancer progression and metastasis: Recent insights and advancements. *International Journal of Molecular Sciences*. 22(1), 1–24. MDPI AG. https://doi.org/10.3390/ijms22010130

Mang, T. S. (2004). Lasers and light sources for PDT: Past, present and future. *Photodiagnosis and Photodynamic Therapy*, *1*(1), 43–48. https://doi.org/10.1016/S1572-1000(04)00012-2

Manne, U., Shanmugam, C., Katkoori, V. R., Bumpers, H. L., & Grizzle, W. E. (2011). Development and progression of colorectal neoplasia. *Cancer Biomarkers*, *9*(1–6), 235–265. https://doi.org/10.3233/CBM-2011-0160

Mariño, G., & Kroemer, G. (2013). Mechanisms of apoptotic phosphatidylserine exposure. *Cell Research*, *23*(11), 1247–1248. https://doi.org/10.1038/cr.2013.115

Matsuyama, T., Kinugasa, Y., Nakajima, Y., & Kojima, K. (2018). Robotic-assisted surgery for rectal cancer: Current state and future perspective. *Annals of Gastroenterological Surgery*, *2*(6), 406–412. https://doi.org/10.1002/ags3.12202

McCabe, M., Perner, Y., Magobo, R., Mirza, S., & Penny, C. (2020). Descriptive epidemiological study of South African colorectal cancer patients at a Johannesburg Hospital Academic institution. *JGH Open*, *4*(3), 360–367. https://doi.org/10.1002/jgh3.12248

Meyer-Betz, F. (1913). Untersuchungen uber die biologische photodynamische Wirkung des Hematoporphyrins und anderer Derivative des Blut und Galenafarbstoffs. *Dtsch Arch. Klin, 112*, 476-503.

Miki, Y., Akimoto, J., Moritake, K., Hironaka, C., & Fujiwara, Y. (2015). Photodynamic therapy using talaporfin sodium induces concentration-dependent programmed necroptosis in human glioblastoma T98G cells. *Lasers in Medical Science*, *30*(6), 1739–1745. https://doi.org/10.1007/s10103-015-1783-9

Modest, D. P., Rivera, F., Bachet, J. B., de Braud, F., Pietrantonio, F., Koukakis, R., Demonty, G., & Douillard, J. Y. (2019). Panitumumab-based maintenance after oxaliplatin discontinuation in metastatic colorectal cancer: A retrospective analysis of two randomised trials. *International Journal of Cancer*, *145*(2), 576–585. https://doi.org/10.1002/ijc.32110

Mohan, G., P, Ayisha. H. T., Jijo, A. J., M, S. Devi. K., Narayanasamy, A., & Vellingiri, B. (2019). Recent advances in radiotherapy and its associated side effects in cancer — a review. *The Journal of Basic and Applied Zoology*, *80*(14). https://doi.org/10.1186/s41936-019-0083-5

Mroz, P., Yaroslavsky, A., Kharkwal, G. B., & Hamblin, M. R. (2011). Cell death pathways in photodynamic therapy of cancer. *Cancers,* 3(2), 2516–2539. https://doi.org/10.3390/cancers3022516

Murakami, T., Sakamoto, N., & Nagahara, A. (2018). Endoscopic diagnosis of sessile serrated adenoma/polyp with and without dysplasia/carcinoma. *World Journal of Gastroenterology*, *24*(29), 3250–3259. https://doi.org/10.3748/wjg.v24.i29.3250

Naidoo, C., Kruger, C. A., & Abrahamse, H. (2019). Targeted photodynamic therapy treatment of in vitro A375 metastatic melanoma cells. *Oncotarget*, *10*(58), 6079–6095. https://doi.org/10.18632/oncotarget.27221

Nawalany, K., Rusin, A., Kepczynski, M., Filipczak, P., Kumorek, M., Kozik, B., Weitman, H., Ehrenberg, B., Krawczyk, Z., & Nowakowska, M. (2012). Novel nanostructural photosensitizers for photodynamic therapy: In vitro studies. *International Journal of Pharmaceutics,* 430(1–2), 29–140. https://doi.org/10.1016/j.ijpharm.2012.04.016

Nawalany, K., Rusin, A., Kepczyński, M., Mikhailov, A., Kramer-Marek, G., Śnietura, M., Połtowicz, J., Krawczyk, Z., & Nowakowska, M. (2009). Comparison of photodynamic efficacy of tetraarylporphyrin pegylated or encapsulated in liposomes: In vitro studies. *Journal of Photochemistry and Photobiology B: Biology*, *97*(1), 8–17. https://doi.org/10.1016/j.jphotobiol.2009.07.005

Nekhlyudov, L., Aziz, N. M., Lerro, C., & Virgo, K. S. (2014). Oncologists' and primary care physicians' awareness of late and long-term effects of chemotherapy: Implications for care of the growing population of survivors. *Journal of Oncology Practice*, *10*(2), e29–e36. https://doi.org/10.1200/JOP.2013.001121

Nowis, D., Makowski, M., Stoklosa, T., Legat, M., Issat, T., & Golab, J. (2005). *Direct tumor damage mechanisms of photodynamic therapy*. *Acta biochimica Polonica*, *52*(2), 339–352. PMID: 15990919

O'Connor, A. E., Gallagher, W. M., & Byrne, A. T. (2009). Porphyrin and nonporphyrin photosensitizers in oncology: Preclinical and clinical advances in photodynamic therapy. *Photochemistry and Photobiology*, *85*(5), 1053–1074. https://doi.org/10.1111/j.1751-1097.2009.00585.x

Pandey, R. K. (2000). Recent advances in Photodynamic Therapy. *Journal of Porphyrins and Phthalocyanines*, 4(4), 368-373. https://doi.org/10.1002/(SICI)1099-1409(200006/07)4:4%3C368::AID-JPP244%3E3.0.CO;2-6

Park, J., Lee, Y. K., Park, I. K., & Hwang, S. R. (2021). Current limitations and recent progress in nanomedicine for clinically available photodynamic therapy. *Biomedicines*, *9*(1), 1–17. https://doi.org/10.3390/biomedicines9010085

Peng, C. L., Lai, P. S., Lin, F. H., Yueh-Hsiu Wu, S., & Shieh, M. J. (2009). Dual chemotherapy and photodynamic therapy in an HT-29 human colon cancer xenograft model using SN-38-loaded chlorin-core star block copolymer micelles. *Biomaterials*, *30*(21), 3614–3625. https://doi.org/10.1016/j.biomaterials.2009.03.048

Pereira, G. F. M., & Tasso, T. T. (2021). From cuvette to cells: How the central metal ion modulates the properties of phthalocyanines and porphyrazines as photosensitizers. *Inorganica Chimica Acta*, *519*, 1–11. https://doi.org/10.1016/j.ica.2021.120271

Plaetzer, K., Kiesslich, T., Verwanger, T., & Krammer, B. (2003). The modes of cell death induced by PDT: An overview. *Medical Laser Application*, *18*(1), 7–19. https://doi.org/10.1078/1615-1615-00082

Poynter, J. N., Haile, R. W., Siegmund, K. D., Campbell, P. T., Figueiredo, J. C., Limburg, P., Young, J., Le Marchand, L., Potter, J. D., Cotterchio, M., Casey, G., Hopper, J. L., Jenkins, M. A., Thibodeau, S. N., Newcomb, P. A., & Baron, J. A. (2009). Associations between smoking, alcohol consumption, and colorectal cancer, overall and by tumor microsatellite instability status. *Cancer Epidemiology Biomarkers and Prevention*, *18*(10), 2745–2750. https://doi.org/10.1158/1055-9965.EPI-09-0517

Pucelik, B., Sułek, A., & Dąbrowski, J. M. (2020). Bacteriochlorins and their metal complexes as NIR-absorbing photosensitizers: properties, mechanisms, and applications. *Coordination Chemistry Reviews*, *416*, 213340. https://doi.org/10.1016/j.ccr.2020.213340

Raab, O. (1990). Uber die Wirkung fluoresierender Stoffe auf Infusorien. *Zeitung Biol*, 39, 524-526.

Ragnhammar, P., Hafstrom L., Nygren, P., & Glimelius, B. (2001). A Systematic Overview of Chemotherapy Effects in Colorectal Cancer. *Acta Oncologica*, *40*(2–3), 282–308. https://doi.org/10.1080/02841860121543

Ribatti, D. (2017). The concept of immune surveillance against tumors. The first theories. *Oncotarget*, *8*(4), 7175–7180. https://doi.org/10.18632/oncotarget.12739

Robertson, C. A., Evans, D. H., & Abrahamse, H. (2009). Photodynamic therapy (PDT): A short review on cellular mechanisms and cancer research applications for PDT. *Journal of Photochemistry and Photobiology B: Biology*, 96(1), 1–8. https://doi.org/10.1016/j.jphotobiol.2009.04.001

Roguin, Leonor P. Chiarante, Nicolas. Garcia Vior, Maria C. Marino, J. (2019). Zinc(II) phthalocyanines as photosensitizers for antitumor photodynamic therapy. *International Journal of Biochemistry and Cell Biology*, *114*, 105575. https://doi.org/10.1016/j.biocel.2019.105575

Ronen, J., Hayat, S., & Akalin, A. (2019). Evaluation of colorectal cancer subtypes

and cell lines using deep learning. *Life Science Alliance*, *2*(6), 1–16. https://doi.org/10.26508/lsa.201900517

Rousset, M. (1986). The human colon carcinoma cell lines HT-29 and Caco-2: Two in vitro models for the study of intestinal differentiation. *Biochimie, 68*(9), 1035-1040. https://doi.org/10.1016/s0300-9084(86)80177-8

Ruddy, K. J., & Partridge, A. H. (2012). Fertility (male and female) and menopause. *Journal of Clinical Oncology*, *30*(30), 3705–3711. https://doi.org/10.1200/JCO.2012.42.1966

Scherer, K. M., Bisby, R. H., Botchway, S. W., & Parker, A. W. (2017). New Approaches to Photodynamic Therapy from Types I, II and III to Type IV Using One or More Photons. *Anti-Cancer Agents in Medicinal Chemistry*, *17*(2), 171–189. https://doi.org/10.2174/1871520616666160513131723

Schmidt, J., Kuzyniak, W., Berkholz, J., Steinemann, G., Ogbodu, R., Hoffmann, B., Nouailles, G., Gürek, A. G., Nitzsche, B., & Höpfner, M. (2018). Novel zinc- and silicon-phthalocyanines as photosensitizers for photodynamic therapy of cholangiocarcinoma. *International Journal of Molecular Medicine*, *42*(1), 534–546. https://doi.org/10.3892/ijmm.2018.3620

Shi, X., Zhang, H., Jin, W., Liu, W., Yin, H., Li, Y., & Dong, H. (2019). Metronomic photodynamic therapy with 5-aminolevulinic acid induces apoptosis and autophagy in human SW837 colorectal cancer cells. *Journal of Photochemistry and Photobiology B: Biology*, *198*(August), 111586 . https://doi.org/10.1016/j.jphotobiol.2019.111586

Sibrian-Vazquez, M. J, Jensen, T.J., Vincente, M. G. H. (2007). Synthesis and cellular studies of PEG-functionalized meso-tetraphenylporphyrins.pdf. *Journal of Photochemistry & Photobiology, B: Biology,* 86, 9–21. https://doi.org/10.1016/j.jphotobiol.2006.08.004

Sibrian-Vazquez, M., Nesterova, I. V., Jensen, T. J., & Vicente, M. G. H. (2008). Mitochondria targeting by guanidine- and biguanidine-porphyrin photosensitizers.

Bioconjugate Chemistry, *19*(3), 705–713. https://doi.org/10.1021/bc700393u

Siegel, R. L., Miller, K. D., Fuchs, H. E., & Jemal, A. (2021). Cancer Statistics, 2021. *CA: A Cancer Journal for Clinicians*, *71*(1), 7–33. https://doi.org/10.3322/caac.21654

Smith, J.J. Deane, N.G. Dhawan, P. and Beauchamp, R. D. (2008). Regulation of metastasis in colorectal adenocarcinoma: A collision between development and tumor biology. *Surgery*, *144*(3), 353–366. https://doi.org/10.1016/j.surg.2008.05.007.Regulation

Sobczyński, J., Kristensen, S., & Berg, K. (2014). The influence of Pluronics nanovehicles on dark cytotoxicity, photocytotoxicity and localization of four model photosensitizers in cancer cells. *Photochemical and Photobiological Sciences*, *13*(1), 8–22. https://doi.org/10.1039/c3pp50181g

Song, C., Xu, W., Wu, H., Wang, X., Gong, Q., Liu, C., Liu, J., & Zhou, L. (2020). Photodynamic therapy induces autophagy-mediated cell death in human colorectal cancer cells via activation of the ROS/JNK signaling pathway. *Cell Death and Disease*, *11*(10). https://doi.org/10.1038/s41419-020-03136-y

Soons, E., Bisseling, T. M., van der Post, R. S., Nagtegaal, I. D., Hazewinkel, Y., van Kouwen, M. C. A., & Siersema, P. D. (2021). The Workgroup Serrated Polyps and Polyposis (WASP) classification for optical diagnosis of colorectal diminutive polyps with iScan and the impact of the revised World Health Organization (WHO) criteria. *United European Gastroenterology Journal*, *9*(7), 819–828. https://doi.org/10.1002/ueg2.12129

Spagnul, C., Turner, L. C., Giuntini, F., Greenman, J., & Boyle, R. W. (2017). Synthesis and bactericidal properties of porphyrins immobilized in a polyacrylamide support: influence of metal complexation on photoactivity. *Journal of Materials Chemistry B*, *5*(9), 1834–1845. https://doi.org/10.1039/c6tb03198f

Stanculeanu, D. L., Zob, D., Lazescu, A., Bunghez, R., & Anghel, R. (2016).

Development of new immunotherapy treatments in different cancer types. *Journal of Medicine and Life*, *9*(3), 240–248. PMID: 27974927; PMCID: PMC5154307.

Suarez, E. D., Lima, F. C. D. A., Dias, P. M., Constantino, V. R. L., & Petrilli, H. M. (2019). Theoretical UV-Vis spectra of tetracationic porphyrin: effects of environment on electronic spectral properties. *Journal of Molecular Modeling*, *25*(9), 264. https://doi.org/10.1007/s00894-019-4149-6

Suganya, M., Gnanamangai, B. M., Ravindran, B., Chang, S. W., Selvaraj, A., Govindasamy, C., Elsadek, M. F., & Ponmurugan, P. (2019). Antitumor effect of proanthocyanidin induced apoptosis in human colorectal cancer (HT-29) cells and its molecular docking studies. *BMC Chemistry*, *13*(3). https://doi.org/10.1186/s13065-019-0525-7

Sung, H., Ferlay, J., Siegel, R. L., Laversanne, M., Soerjomataram, I., Jemal, A., & Bray, F. (2021). Global cancer statistics 2020: GLOBOCAN estimates of incidence and mortality worldwide for 36 cancers in 185 countries. *CA: A Cancer Journal for Clinicians*, *0*(0), 1–41. https://doi.org/10.3322/caac.21660

Swavey, S., & Tran, M. (2013). Porphyrin and Phthalocyanine Photosensitizers as PDT Agents: A New Modality for the Treatment of Melanoma. *Recent Advances in the Biology, Therapy and Management of Melanoma,* 253–282. InTech. https://doi.org/10.5772/54940

Tam, S. Y., & Wu, V. W. C. (2019). A review on the special radiotherapy techniques of colorectal cancer. *Frontiers in Oncology*, *9*(APR), 1–9. https://doi.org/10.3389/fonc.2019.00208

Tamas, K., Walenkamp, A. M. E., de Vries, E. G. E., van Vugt, M. A. T. M., Beets-Tan, R. G., van Etten, B., de Groot, D. J. A., & Hospers, G. A. P. (2015). Rectal and colon cancer: Not just a different anatomic site. *Cancer Treatment Reviews*, *41*(8), 671–679. https://doi.org/10.1016/j.ctrv.2015.06.007

Tang, F., Wu, X., Wang, T., Wang, P., Li, R., Zhang, H., Gao, J., Chen, S., Bao, L.,

Thrumurthy, S. G., Thrumurthy, S. S. D., Gilbert, C. E., Ross, P., & Haji, A. (n.d.). Colorectal adenocarcinoma: Risks, prevention and diagnosis. *BMJ (Clinical research ed)*, *354,* i3590. https://doi.org/10.1136/bmj.i3590

Tricker, A. R., & Preussmann, R. (1991). Carcinogenic N-nitrosamines in the diet: occurrence, formation, mechanisms and carcinogenic potential. *Mutation Research,* 259(3-4), 277-89. https://doi.org/10.1016/0165-1218(91)90123-4

Tsai, S. R., Yin, R., Huang, Y. Y., Sheu, B. C., Lee, S. C., & Hamblin, M. R. (2015). Low-level light therapy potentiates NPe6-mediated photodynamic therapy in a human osteosarcoma cell line via increased ATP. *Photodiagnosis and Photodynamic Therapy*, *12*(1), 123–130. https://doi.org/10.1016/j.pdpdt.2014.10.009

Vargas, A. J., & Thompson, P. A. (2012). Diet and nutrient factors in colorectal cancer risk. *Nutrition in Clinical Practice,* 27(5), 613–623) https://doi.org/10.1177/0884533612454885

Velazquez, F. N., Miretti, M., Baumgartner, M. T., Caputto, B. L., Tempesti, T. C., & Prucca, C. G. (2019). Effectiveness of ZnPc and of an amine derivative to inactivate Glioblastoma cells by Photodynamic Therapy: an in vitro comparative study. *Scientific Reports*, *9*(1), 1–15. https://doi.org/10.1038/s41598-019-39390-0

Viglietta, V., Shi, F., Hu, Q. Y., Ren, Y., Keilty, J., Wolff, H., McCarthy, R., Kropp, J., Weber, P., & Soglia, J. (2020). Phase 1 study to evaluate safety, tolerability and pharmacokinetics of a novel intra-tympanic administered thiosulfate to prevent cisplatin-induced hearing loss in cancer patients. *Investigational New Drugs*, *38*(5), 1463–1471. https://doi.org/10.1007/s10637-020-00918-1

von Kleist, S., Chany, E., Burtin, P., King, M., & Fogh, J. (1975). Immunohistology of the antigenic pattern of a continuous cell line from a human colon tumor. *Journal of the National Cancer Institute*, *55*(3), 555–560. https://doi.org/10.1093/jnci/55.3.555

von Tappeiner, H., & Jesionek, A. (1903). Therapeutische versuche mit fluoreszierender stoffen. *Muench M. Wochenschr*, 47, 2042-2044.

von Tappeiner, H., & Jodblauer, H. (1907). Die sensiblisierende Wirkung fluoreszerender Substanzer Gesammte Untersuchungen uber die photodynamische Erscheinerung. *Voger FC Leipzig*, 210.

Wang, H., Li, L., Wang, P., Wang, X., Zhang, K., & Liu, Q. (2016). Comparison of photodynamic treatment produced cell damage between human breast cancer cell MCF-7 and its multidrug resistance cell. *Photodiagnosis and Photodynamic Therapy*, *16*, 1–8. https://doi.org/10.1016/j.pdpdt.2016.07.004

Wang, Z., Peng, H., Shi, W., Gan, L., Zhong, L., He, J., Xie, L., Wu, P., Zhao, Y., Deng, Z., Tang, H., & Huang, Y. (2021). Application of photodynamic therapy in cancer: Challenges and advancements. *Biocell*, *45*(3), 489–500. https://doi.org/10.32604/BIOCELL.2021.014439

Weber, P. A., Merola, S., Wasielewski, A., Ballantyne, G. H., & Delaney, C. P. (2002). Telerobotic-assisted laparoscopic right and sigmoid colectomies for benign disease. *Diseases of the Colon and Rectum*, *45*(12), 1689–1696. https://doi.org/10.1007/s10350-004-7261-2

Wu, R. W. K., Chu, E. S. M., Huang, Z., Olivo, M. C., Ip, D. C. W., & Yow, C. M. N. (2015). An in vitro investigation of photodynamic efficacy of FosPeg ® on human colon cancer cells. *Journal of Innovative Optical Health Sciences*, *8*(5), 1–8. https://doi.org/10.1142/S1793545815500273

Yan, H. H., Pickup, M., Pang, Y., Gorska, A. E., Li, Z., Chytil, A., Geng, Y., Gray, J. W., Moses, H. L., & Yang, L. (2010). Gr-1+CD11b+ myeloid cells tip the balance of immune protection to tumor promotion in the premetastatic lung. *Cancer Research*, *70*(15), 6139–6149. https://doi.org/10.1158/0008-5472.CAN-10-0706

Yang, L., Pang, Y., & Moses, H. L. (2010). TGF-β and immune cells: an important regulatory axis in the tumor microenvironment and progression. *Trends in Immunology*, *31*(6), 220–227. https://doi.org/10.1016/j.it.2010.04.002

Yokota, J. (2000). Tumor progression and metastatis. *Carcinogenesis, 21*(3), 497-503. https://doi.org/10.1093/carcin/21.3.497

Younis, M., Thangavelu, S., Anand, V., Sujeetha, P., Sangeetha, T., Kaviya, M., Bharathi, K., & Anand, A. V. (2021). Molecular Heterogeneity in Colorectal Cancer: Insights from Genetic Profiling Medical Genetics and Clinical Biochemistry View project Molecular Heterogeneity in Colorectal Cancer: Insights from Genetic Profiling. *Journal of Advanced Applied Scientific Research*, *3*, 6–15. https://www.researchgate.net/publication/354619775

Yu, Z., & Li, W. (2006). Induction of apoptosis by puerarin in colon cancer HT-29 cells. *Journal of the National Cancer Institute*, *238*(1), 53–60. https://doi.org/10.1016/j.canlet.2005.06.022

Zampino, M. G., Magni, E., Santoro, L., Zorzino, L., Dell'Orto, P., Sonzogni, A., Fazio, N., Monfardini, L., Chiappa, A., Biffi, R., & De Braud, F. (2008). Epidermal growth factor receptor serum (sEGFR) level may predict response in patients with EGFR positive advanced colorectal cancer treated with gefitinib? *Cancer Chemotherapy and Pharmacology*, *63*(1), 139–148. https://doi.org/10.1007/s00280-008-0722-x

Zanetti, M., d'Uscio, L. V., Peterson, T. E., Katusic, Z. S., & O'Brien, T. (2005). Analysis of superoxide anion production in tissue. *Methods in Molecular Medicine*, *108*(2), 65–72. https://doi.org/10.1385/1-59259-850-1:065

Zbakh, H., Zubía, E., de Los Reyes, C., Calderón-Montaño, J. M., & Motilva, V. (2020). Anticancer Activities of Meroterpenoids Isolated from the Brown Alga Cystoseira usneoides against the Human Colon Cancer Cells HT-29. *Foods*, *9*(3), 300. https://doi.org/10.3390/foods9030300

Zhang, X., Ge, Y. L., & Tian, R. H. (2009). The knockdown of c-myc expression by RNAi inhibits cell proliferation in human colon cancer HT-29 cells in vitro and in vivo. *Cellular and Molecular Biology Letters*, *14*(2), 305–318. https://doi.org/10.2478/s11658-009-0001-9

Zhang, Y., & Zhang, Z. (2020). The history and advances in cancer immunotherapy: understanding the characteristics of tumor-infiltrating immune cells and their therapeutic implications. *Cellular and Molecular Immunology*, *17*(8), 807–821.

https://doi.org/10.1038/s41423-020-0488-6

Zhivotovsky, B., & Orrenius, S. (2011). Calcium and cell death mechanisms: A perspective from the cell death community. *Cell Calcium*, *50*(3), 211–221. https://doi.org/10.1016/j.ceca.2011.03.003

ANNEXURE

SUPPLEMENTARY RESULTS I

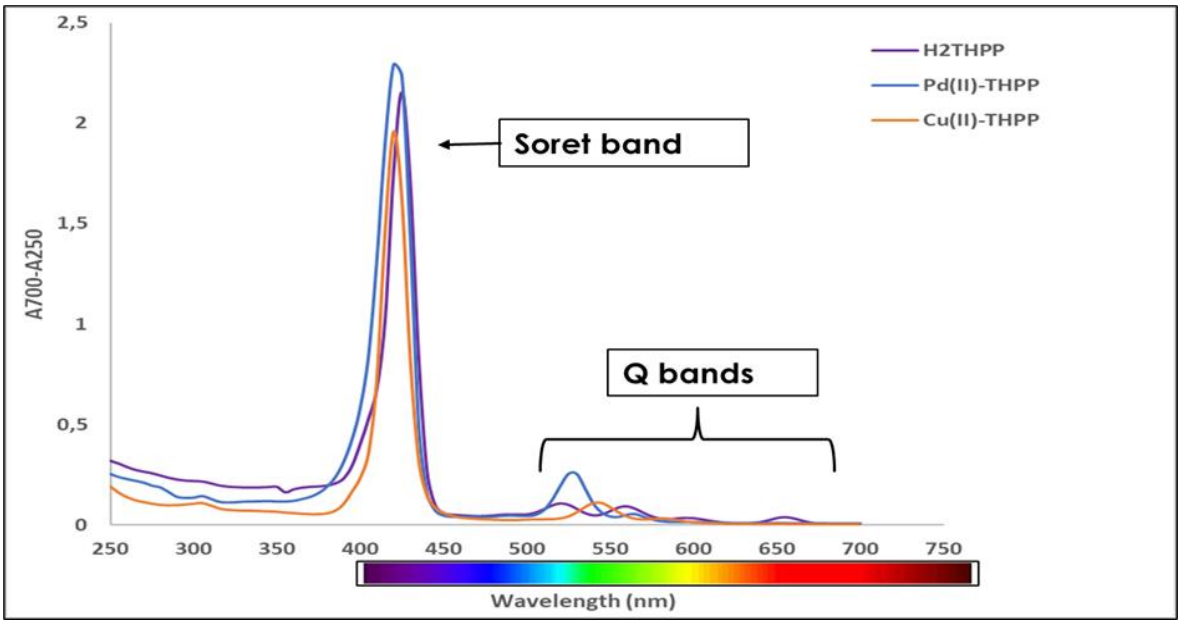

Figure SR1 UV/Vis absorbance spectra of PEG2000-PE encapsulated H2THPP, Pd(II)-THPP and Cu(II)-THPP complexes dissolved in 0.5X PBS. Absorbance was recorded on a Jasco V-630 Spectrophotometer.

SUPPLEMENTARY RESULTS 2

A

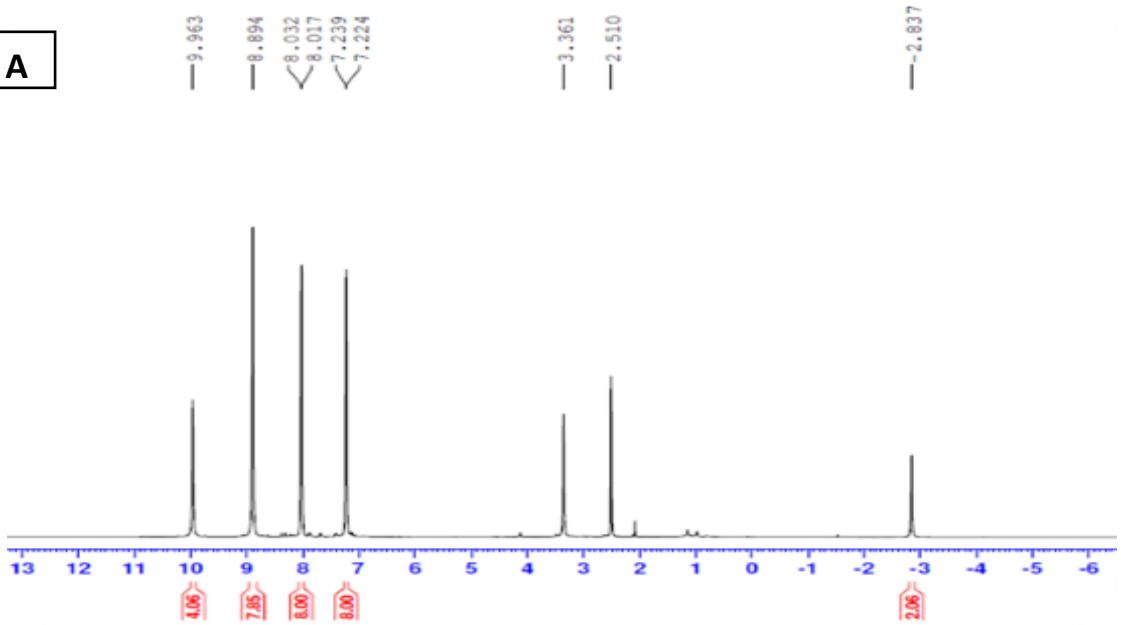

B

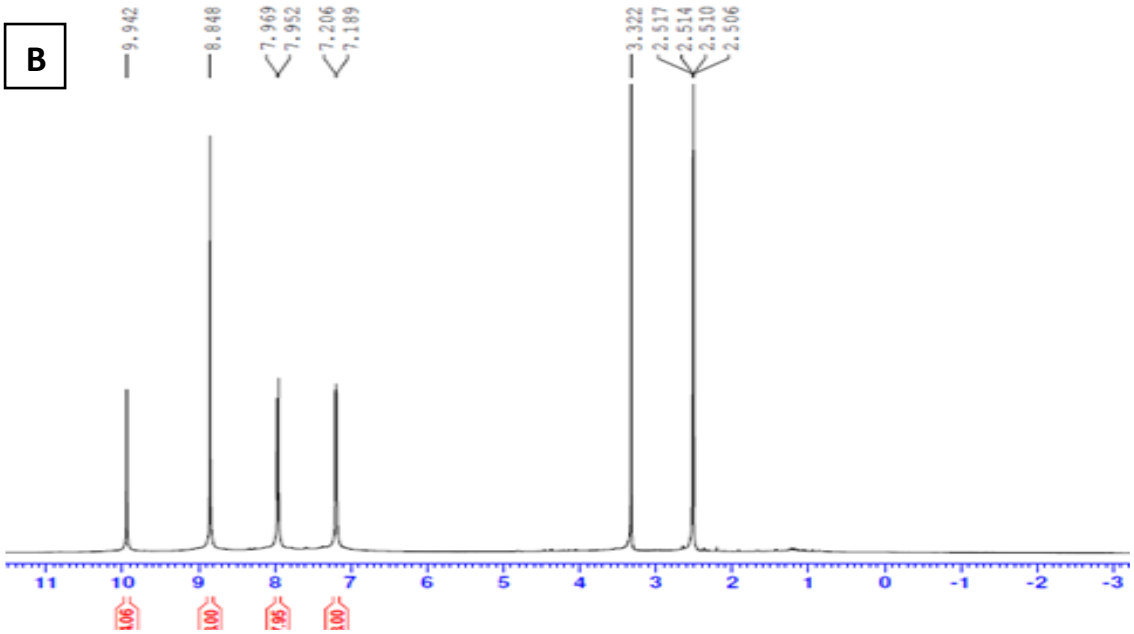

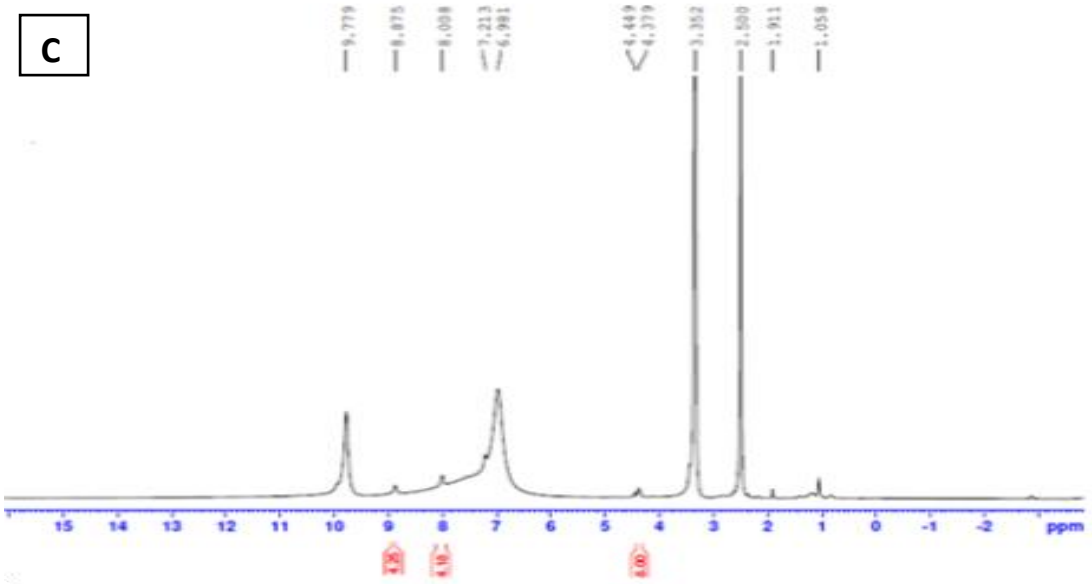

Figure SR2 Proton NMR spectra of **A** H_2THPP, **B** Pd(II)-THPP and **C** Cu(II)-THPP. H_2THPP was dissolved in deuterated DMSO and run. Pd(II)-acetate and Cu(II)-acetate were reacted with H_2THPP in 99.8% ethanol. 30mg dry powder was dissolved in deuterated DMSO and analysed on a Bruker Ascend 500MHz spectrometer.